
Electronic Thesis and Dissertation Repository

11-16-2015 12:00 AM

Development of an in-vitro passive and active motion Simulator for the investigation of wrist function and Kinematics

Duncan J. Iglesias
The University of Western Ontario

Supervisor
Dr. James Johnson
The University of Western Ontario

Graduate Program in Biomedical Engineering
A thesis submitted in partial fulfillment of the requirements for the degree in Master of Engineering Science
© Duncan J. Iglesias 2015

Follow this and additional works at: <https://ir.lib.uwo.ca/etd>



Part of the [Biomechanical Engineering Commons](#), and the [Biomedical Engineering and Bioengineering Commons](#)

Recommended Citation

Iglesias, Duncan J., "Development of an in-vitro passive and active motion Simulator for the investigation of wrist function and Kinematics" (2015). *Electronic Thesis and Dissertation Repository*. 3443.
<https://ir.lib.uwo.ca/etd/3443>

This Dissertation/Thesis is brought to you for free and open access by Scholarship@Western. It has been accepted for inclusion in Electronic Thesis and Dissertation Repository by an authorized administrator of Scholarship@Western. For more information, please contact wlsadmin@uwo.ca.

DEVELOPMENT OF AN IN-VITRO ACTIVE MOTION SIMULATOR
FOR THE INVESTIGATION OF WRIST FUNCTION AND KINEMATICS

by

Duncan Iglesias

Graduate Program in Biomedical Engineering

A thesis submitted in partial fulfillment
of the requirements for the degree of
Masters of Engineering Science

The School of Graduate and Postdoctoral Studies
The University of Western Ontario
London, Ontario, Canada

© Duncan James Iglesias 2016

Abstract

This thesis outlines the design and development of an active motion simulator for the investigation of wrist kinematics in multiple gravity loaded positions. Using optical trackers on the third metacarpal, radius, and ulna, the position of the wrist was monitored in real time without introducing material incompatibilities as present for electromagnetic tracking systems. Performance of the system was performed using a series of five cadaver upper limbs that compared the ability to produce repeatable trials using unrestrained active motion techniques over passive manipulation methods. Comparisons to achieve static positions as well as motion trials in flexion-extension and radial-ulnar deviation planes proved the superior performance of computer controlled motion over that of passive manipulation. Investigation into the application of tendon portioning to model *in-vivo* conditions more accurately suggest that they may improve overall quality of motion.

Keywords: Active Motion Simulator, Wrist Kinematics, Reparative Surgery Assessment, Muscle Portioning, Gravitational Effects

Co-Authorship Statement

Chapter 1: Introduction

Duncan Iglesias - sole author

Chapter 2: Design & Development

Duncan Iglesias - developed platform & control system, study design, data collection, statistical analysis, wrote manuscript

Josh Giles - technical assistance

Jason Lockhart - apparatus design, data collection

James Johnson - study design, reviewed manuscript

Graham King - study design, specimen preparation, reviewed manuscript

Chapter 3: Gravitational Effects

Duncan Iglesias - developed controller, study design, data collection, statistical analysis, wrote manuscript

Jason Lockhart - apparatus design, data collection

James Johnson - study design, reviewed manuscript

Graham King - study design, specimen preparation, reviewed manuscript

Chapter 4: Tendon Portioning

Duncan Iglesias - developed controller, study design, data collection, statistical analysis, wrote manuscript

Jason Lockhart - data collection

James Johnson - study design, reviewed manuscript

Graham King - study design, specimen preparation, reviewed manuscript

Chapter 5: Discussion & Conclusions

Duncan Iglesias - sole author

Acknowledgments

I would like to start by thanking my supervisors, Dr. J. Johnson & Dr. G. King, for the incredible opportunity to work at the Hand & Upper Limb Centre (HULC) and to be part of the first class research that is coming out of this lab. Thank you for your unwavering support throughout the entire process, the freedom to explore my own avenues, and the confidence you put in right from the very start. The skills I have gained during my time as a masters student are by far the most valuable to date. Dr. King, thank you for all the early mornings you donated to help with specimen preparation on testing days. It was a pleasure being able to work so closely with such a skilled surgeon and experience the ease of which you operate.

To Mark, without you I never would have pursued my masters at Western University in Biomedical Engineering. The connection you made between Dr. Johnson and myself was truly life changing; I can not imagine where I would have been right now if you had not suggested that I take over for you at the HULC. It was only fitting that I adopted your wrist simulator project, the 'Masamulator', and carried on with the research that you, Dr. Bradon, and Dr. Masao were so involved with. Best of luck to you in your hybrid career of engineering and physiotherapy.

To my sister and her ever growing family on the farm, you acted as my private rehab allowing me to escape away to hang by the pool and play with cows when overwhelmed with school. Russel and Oliver are two beautiful little boys and I am excited for the third one coming this December! Stefan is pretty cool too. Thank you to my parents for your food and beverage donations over the past two years, it kept me going when the only thing left in my cupboards were red solo cups.

Jason Lockhart, thank you for all your hard work this past summer. Many of the images and data in this thesis I can thank you for. You put many long hours into organizing data and creating bone models not to mention the passive guide rail and automated LED array that you prototyped from scratch for me. Josh Giles, you set me up from the start and showed me the ropes with the fundamentals of motor communication with the SmartMotors and were always

available to answer questions over G-Mail chat. Jordan O'Brien, you were there through many hours of troubleshooting and offered an excellent insight into many of the systems in our lab that were ultimately incorporated into my thesis.

Thank you to all the students and researchers from 'the Tank' who were always willing to donate their time to help me during back to back 21-hour test days and then still have the energy to play a round of tennis during lunch at Doidge Park. I may be a fun guy, but you are all way 'funner'. I will be sure to return the favour the best I can.

Matt Stokes, you constantly motivated me to work harder than ever before and approach technical challenges in manners outside the norm. Many countless hours were spent at 'Tech House' mulling ideas over on the wall of white boards or solving our most recent thesis stumpers between Halo sessions. I have truly valued our friendship over these past two years, and I wish you the best of luck with your career down in California, I will be sure to keep tabs.

Finally, to Emilie Brent for being such an understanding girlfriend and having unlimited patience for when I went missing for days on end during periods of intense deadlines, overloaded testing schedules, conferences, and those random side projects that stole my attention more than I had originally anticipated. You were always right there when I reemerged and were ready to listen to whatever rant or idea that was currently occupying my mind, and no matter how technical or in depth I got you always showed the utmost interest in what I had to say. You are my psychiatrist, my partner in crime, and my best friend. I truly cherish what we have together.

Contents

Abstract	ii
Co-Authorship Statement	iii
Acknowledgments	iv
List of Figures	xii
List of Tables	xv
1 Introduction	1
1.1 Anatomy of the Wrist & Hand	2
1.1.1 Osteology	2
1.1.1.1 Radius	2
1.1.1.2 Ulna	4
1.1.1.3 Carpal Bones	6
1.1.1.4 Metacarpals	6
1.1.1.5 Phalanges	7
1.1.2 Ligaments	8
1.1.2.1 Radiocarpal Ligaments	8
1.1.2.2 Ulnocarpal Ligaments	8
1.1.2.3 Distal Radioulnar Ligaments	9
1.1.2.4 Intercarpal Ligaments	9
1.1.2.5 Carpometacarpal Ligaments	9
1.1.3 Joint Capsules	11
1.1.3.1 Distal Radioulnar Joint (DRUJ)	11
1.1.3.2 Radiocarpal Joint	11
1.1.3.3 Intercarpal Joint	11
1.1.3.4 Carpometacarpal Joint	12
1.1.4 Myology	13
1.1.4.1 Volar Compartment	15
1.1.4.2 Dorsal Compartment	15
1.1.4.3 Forearm Rotators	16
1.2 Wrist Kinematics & Biomechanics	17
1.2.1 Range of Motion	17
1.2.1.1 Flexion-Extension Motion	17

1.2.1.2	Radial-Ulnar Deviation	18
1.2.1.3	Pronation-Supination Motion	18
1.2.2	Joint Geometry	19
1.2.3	Antagonistic Muscle Pairs	20
1.2.4	Cross Sectional Area	21
1.2.5	Moment Arms	21
1.2.6	Kinematic Chains	21
1.3	Euler Angles	22
1.4	Coordinate Transformations	24
1.4.1	Transformation Matrix	24
1.4.2	Transformation Chain	25
1.5	Body Segment Coordinate Systems	26
1.6	Methods of Tracking	32
1.6.1	Goniometer	32
1.6.2	Inertial Measurement Units	33
1.6.3	Image Based Tracking	34
1.6.4	Electromagnetic Tracking Systems	36
1.6.5	Optical Tracking Systems	37
1.7	Clinical Complications	39
1.7.1	Traumatic Injuries	39
1.7.2	Degenerative Disease	40
1.7.3	Bracing Methods	40
1.8	Biomechanical Testing & Simulation of Motion Pathways	41
1.8.1	<i>In-Silico</i> Simulations	42
1.8.2	<i>In-Vitro</i> Simulators	43
1.8.2.1	Passive Motion Simulators	43
1.8.2.2	Active Motion Simulators	45
1.9	Thesis Rationale	48
1.10	Objectives & Hypotheses	49
1.11	Thesis Overview	50
	Chapter One References	50
2	Design, Development, & Validation	56
2.1	Introduction	57
2.2	Methods	59
2.2.1	Simulator Development	59
2.2.1.1	Platform Design	59
2.2.1.2	Motor Manifold	60
2.2.1.3	Force Transducers	60
2.2.1.4	Cable Guide Rail	62
2.2.1.5	Humeral Clamp	63
2.2.1.6	Ulnar Support Tower	64
2.2.1.7	Passive Guide Rail	65
2.2.2	Control Algorithm Development	66
2.2.2.1	Force Controller Development	66

2.2.2.2	Position Controller Development	67
2.2.3	Clinical Evaluation of the Active Motion Simulator	69
2.2.3.1	Motion Trials	70
2.2.3.2	Static Position Trials	70
2.2.3.3	Center of Rotation Algorithm	71
2.2.4	Outcome Variables & Statistical Analysis	71
2.3	Results	72
2.3.1	Repeatability of Motion Profiles	72
2.3.1.1	FEM Motion Trials	73
2.3.1.2	RUD Motion Trials	74
2.3.1.3	Static Trials	75
2.3.2	Center of Rotation Repeatability	76
2.3.3	Repeatability of Tendon Forces	77
2.3.3.1	Static Trials	77
2.3.3.2	Motion Trials	78
2.4	Discussion	81
2.5	Conclusions	84
	Chapter Two References	84
3	Gravitational Effects on Kinematics	87
3.1	Introduction	88
3.2	Methods	90
3.2.1	Specimen Preparation	90
3.2.2	Data Collection	90
3.2.3	Outcome Variables & Statistical Analysis	91
3.3	Results	92
3.3.1	Repeatability of Motion Profiles	92
3.3.1.1	In-Plane Motions	93
3.3.1.2	Out-of-Plane Motions	96
3.3.2	Center of Rotation Repeatability	99
3.3.3	Repeatability of Tendon Forces	99
3.3.3.1	Static Trials	100
3.3.3.2	Motion Trials	101
3.4	Discussion	103
3.5	Conclusions	106
	Chapter Three References	106
4	Muscle Portioning	109
4.1	Introduction	110
4.2	Methods	112
4.3	Results	114
4.3.1	Repeatability of Motion Trials	114
4.3.1.1	In-Plane Motion Profiles	114
4.3.1.2	Non-Planar Deviations	117
4.3.2	Repeatability of Tendon Forces	118

4.4	Discussion	119
4.4.1	Effects of Portioning on the Motion Profile	119
4.4.2	Effects of Portioning on Magnitude of Forces	120
4.4.3	Developing Tendon Portioning Ratios	120
4.5	Conclusions	121
	Chapter Four References	122
5	Discussion & Conclusion	124
5.1	Summary	125
5.2	Strengths & Limitations	127
5.3	Current & Future Directions	128
	Chapter Five References	128
A	Establishing Bone Coordinate Systems	131
A.1	Local Reference Frame: Ulna	132
A.2	Local Reference Frame: Radius	133
A.3	Local Reference Frame: Metacarpal	134
A.4	Applying Local Transforms	135
B	Force Transducer Calibration	136
B.1	Validation of a Load Cell	136
B.2	Force Transducer Calibration	137
C	Simulator Mechanical Drawings	138
D	Open Source Code & License Agreement	154
D.1	BSD License	155
D.2	3D Circle Fitting MATLAB Algorithm	156
D.3	3D Sphere Fitting MATLAB Algorithm	159
E	The Effects of Tissue Degradation on System Performance: An 18 Hour Test	161
F	Bone Tracker Design	162
G	Curriculum Vitae	164

List of Figures

1.1	Radius	3
1.2	Ulna	5
1.3	Carpal Bones & Metacarpals	7
1.4	Ligaments of the Wrist and Hand	10
1.5	Joints of the Wrist	12
1.6	Muscles of the Wrist	14
1.7	Range of Wrist Motion: Flexion-Extension	17
1.8	Range of Wrist Motion: Radial-Ulnar Deviation	18
1.9	Range of Wrist Motion: Pronation-Supination	18
1.10	Antagonistic Muscle Pairs	20
1.11	Euler Rotations of a Coordinate System	22
1.12	Radial Coordinate System (ISB)	29
1.13	Ulnar Coordinate System (ISB)	30
1.14	Metacarpal Coordinate System (ISB)	31
1.15	Goniometer	32
1.16	Inertial Measuring Unit	33
1.17	Image Based Tracking: Human Model	34
1.18	Image Based Tracking: Model Matching	35
1.19	Electromagnetic Tracking System	36
1.20	Optical Tracking	37
1.21	Open Reduction & Internal Fixation: Colles Fracture	39
1.22	Full Wrist Arthroplasty	40
1.23	Stewart Platform	43
1.24	Pneumatic Array	44
1.25	Dunning's Active Simulator	46
1.26	Werner's Active Simulator	47
2.1	Simulator Platform	59
2.2	Motor Manifold & Transducer Placement	61
2.3	Cable Guide Blocks	62
2.4	Humeral Clamp	63
2.5	Ulna Support Tower	64
2.6	Passive Guide Rail	65
2.7	Force-Motor Position PID Controller	67
2.8	Position-Force PID Controller	68
2.9	Krackow Suture Technique	69

2.10	3D Circle Fit	71
2.11	Repeatability Between Manipulation Methods	72
2.12	Repeatability of Motion: FEM Trials	73
2.13	Repeatability of Motion: RUD Trials	74
2.14	Repeatability of Position: Static Trials	75
2.15	FEM Tendon Forces	79
2.16	RUD Tendon Forces	80
3.1	Center of Mass Shift in Neutral Gravity Loaded Position	89
3.2	Repeatability of Motion Trials	92
3.3	Repeatability of Motion Profiles: FEM Plane	94
3.4	Repeatability of Motion Profiles: RUD Plane	95
3.5	Repeatability of Motion Profiles: Non-Planar FEM	97
3.6	Repeatability of Motion Profiles: Non-Planar RUD	98
4.1	Repeatability of Motion Profiles: In-Plane Extension	115
4.2	Repeatability of Motion Profiles: In-Plane Flexion	116
4.3	Equal Loading vs. PCSA Portioning: Non-Planar Profile	117
4.4	Equal Loading vs. PCSA Portioning: Forces	118
A.1	ISB Coordinate System: Ulna	132
A.2	ISB Coordinate System: Radius	133
A.3	ISB Coordinate System: Metacarpal	134
B.1	Load Cell Calibration	136
F.1	Optical Tracker Mounts	163

List of Tables

1.1	Types of Joints	19
2.1	Center of Rotation of Motion Trials	76
2.2	Static Forces	77
2.3	Average Peak Active Tendon Forces	78
3.1	Center of Rotation of Motion Trials	99
3.2	Static Forces	100
3.3	Average Peak Active Tendon Forces	102
3.4	Neutral Static Position	105
4.1	Portioning of Wrist Muscles	113

Chapter 1

Introduction

***OVERVIEW:** This chapter begins with a review of the basic anatomy and biomechanics of the wrist and forearm then continues with an overview of common joint simulation methods and a comparative discussion of active and passive in-vitro joint manipulation techniques. Previously implemented in-vitro simulators have successfully reproduced motion using cadaveric specimens but their platforms lack versatility for a range of kinematic investigations that stem from material incompatibilities, spatial tracking methods, and control limitations. This chapter concludes with a discussion of the rationale for developing an active wrist and forearm motion simulator that permits studies to be performed with the arm in multiple orientations.*

1.1 Anatomy of the Wrist & Hand

An understanding of the anatomy of the wrist is crucial when studying wrist joint motion. The following section will discuss the three main tissue structures of the wrist; osteology (bony structure), ligaments, and myology (musculature).

1.1.1 Osteology

The wrist is comprised of 27 bones that articulate with the distal forearm to provide the rigid structure necessary for everyday tasks [1]. Bones have two layers of tissues, a dense outer layer known as cortical bone and a porous core known as cancellous bone [2], and are categorized as long bones or irregular bones of which only long and short bones reside in the hand and wrist. Long bones have three recognizable regions including both the proximal and distal ends (epiphysis) that articulate with adjacent bones, and a shaft (diaphysis) [3]. Short bones are equally wide as they are long to form a cube like structure for providing support and stability with little relative movement [4].

1.1.1.1 Radius

The radius is the shorter of the two parallel long bones (Figure 1.1) that make up the forearm and is located on the lateral side of the ulna when positioned in the anatomic position [5]. The proximal end of the radius is cylindrical forming the radial head with a concave surface that articulates with the capitellum of the distal humerus allowing for axial rotation of the forearm. The radius narrows distally to form the radial neck that gives way to the shaft of the bone. A rough projection on the medial, anterior surface of the proximal radius, known as the radial tuberosity, is the insertion for the biceps brachii tendon responsible for supination [1]. The shaft bows laterally along the length presenting three surfaces; dorsal border, volar border, and medial border. The distal radius has of two articulating surfaces; the ulnar notch on the medial side that interfaces with the ulna, and a smooth concave groove on the distal surface to articulate with the lunate and scaphoid of the carpus. A conical projection on the lateral side of the distal radius is termed the radial styloid process.



Figure 1.1: *The radius is lateral bone of the forearm adjacent to the ulna. A: Proximal Radial Head, B: Radial Styloid Process, C: Radioscaphoid Fossa, D: Radiolunate Fossa*

1.1.1.2 Ulna

The ulna is the longer of the two parallel long bones (Figure 1.2) that make up the forearm and is located medial to the radius when in the neutral anatomical position [1]. Similar to the radius the ulna has three segments; the proximal end, the shaft and the distal end. A major difference from the radius is that the ulna converges to a smaller head distally while the radius diverges to a larger metaphysis. The proximal end forms a cup-like projection that articulates with the trochlea of the distal humerus consists of three parts: the olecranon process, semilunar notch, and coronoid process. The olecranon process is the most proximal edge of the projection with an anteroinferior concave surface forming the upper portion of the semilunar notch. The coronoid process is the distal portion of the semilunar notch with a smooth anterosuperior surface to close the cup-like structure of the semilunar notch. The semilunar notch is the concave curvature residing between these projections creating a hinge joint structure to articulate with the trochlea of the humerus. A concave groove on the lateral side of the proximal extremity, known as the radial notch, articulates with the radial head to allow rotation about the ulna during supination and pronation. The distal end of the ulna contains two distinct eminences; a round articulating surface on the lateral side to articulate with the distal radius, and the ulnar styloid process projecting distally on the medial side.

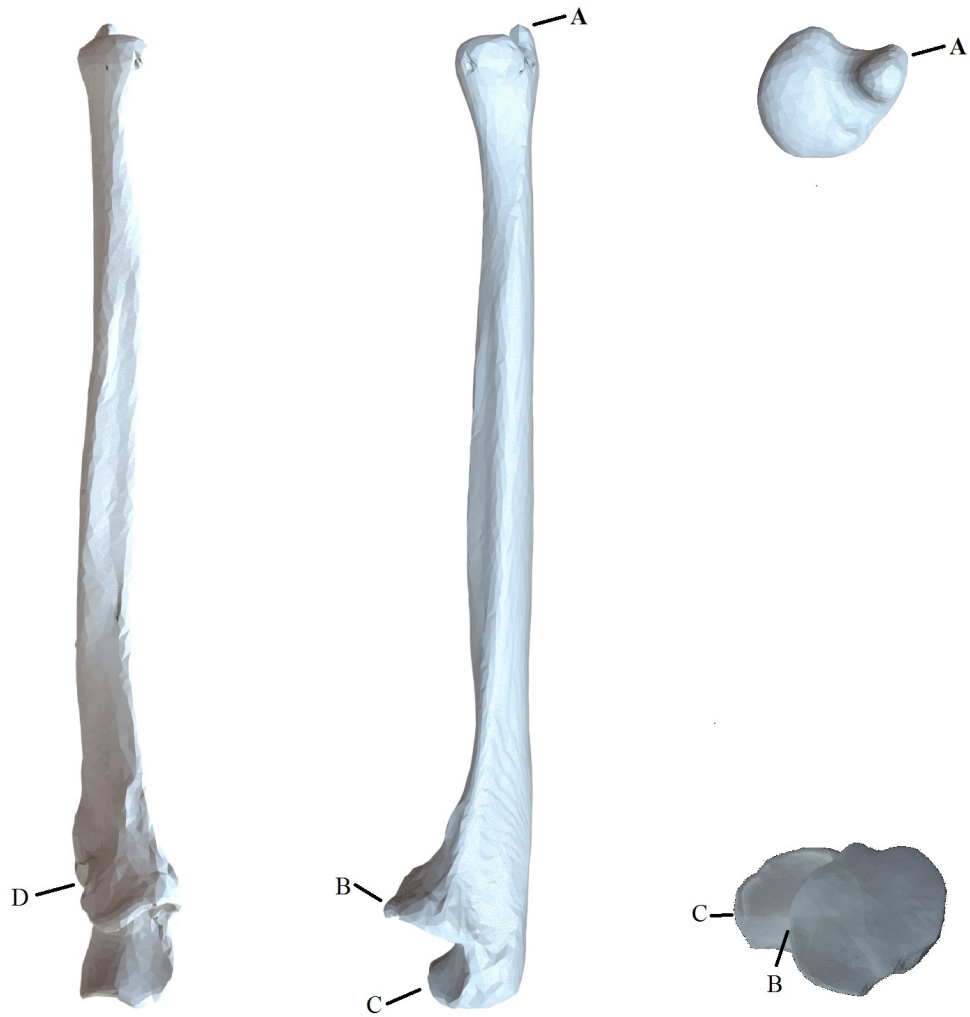


Figure 1.2: *The ulna is the medial bone of the forearm. A: Ulnar Styloid Process, B: Coronoid Process, C: Olecranon Process, D: Radial Notch*

1.1.1.3 Carpal Bones

There are eight short bones arranged into two rows of four that make up the carpal bones of the hand (ossa carpi). The proximal row from the lateral side moving medially is composed of the scaphoid, lunate, triquetrum, and pisiform while the distal row naming in the same direction is composed of the trapezium, trapezoid, capitate, and hamate. For the purpose of this thesis only three carpal bones will be discussed in detail: the scaphoid, the lunate, and the capitate (Figure 1.3). The cube-like structure of the carpal bones present six surfaces on each bone of which the volar and dorsal surfaces are intended for the attachment of ligaments and tendons while the remaining four surfaces articulate with the surrounding bones.

The scaphoid is the largest and most lateral carpal bone in the proximal row with five articulations; the distal radius, trapezium, trapezoid, capitate, and lunate. The proximal surface is convex in shape to articulate with the concave groove on the distal radius. The lunate has a deep crescent-like form and has four articulations: scaphoid, hamate, triquetrum, and distal radius. The proximal surface of the lunate is convex to articulate with the concave distal radius while the distal surface is concave to articulate with the capitate. These two bones are the primary means of axial load transfer from the forearm to the hand as they bridge the distal radius to the remaining carpal bones [6]. The capitate is the largest of the carpal bones and moves in concert with the third metacarpal during flexion-extension.

1.1.1.4 Metacarpals

The metacarpals are five long bones (Figure 1.3) that provide the structure of the palm of the hand [6]. The naming convention starts medially moving laterally assigning the thumb as the first metacarpal and the small finger as the fifth metacarpal. The proximal metacarpal is concave and articulates with the respective carpal bone(s) in the distal row of the wrist. The distal metacarpals are convex and articulate with the proximal phalanges. The shaft of each metacarpal has three surfaces; medial, lateral, and dorsal. The medial and lateral surfaces are concave while the dorsal surfaces are relatively flat allowing for insertion of the extensor tendons.

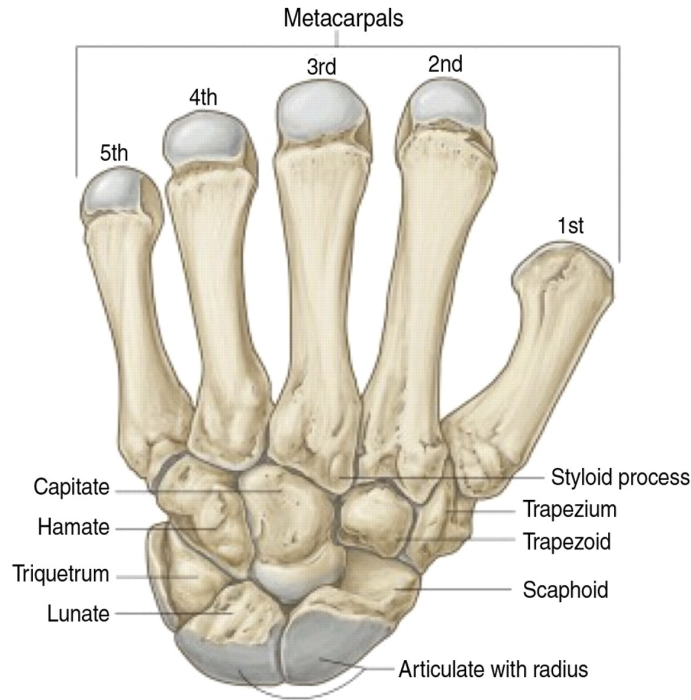


Figure 1.3: The five metacarpal bones of the hand (left) with their relative position to the distal row of carpals; (proximal row) scaphoid, lunate, triquetrum, pisiform and (distal row) trapezium, trapezoid, capitate, hamate [7]

1.1.1.5 Phalanges

The phalanges are the remaining 14 bones that make up the digits. Each digit contains three phalanges named after their respective position; proximal, middle, and distal with an exception to the thumb which only contains a proximal and distal phalanx [6]. These structures are not involved with the motions of the wrist, rather they allow for the insertion of tendons from the muscles responsible for the flexion and extension of the digits to provide grip strength.

1.1.2 Ligaments

Ligaments are fibrous connective tissues composed of collagenous fibers that act to bind bones together across an articulation to provide joint stability [8]. The ligaments in the hand and wrist are categorized into intrinsic and extrinsic groups on both the volar and dorsal sides as seen in (Figure 1.4). Intrinsic ligaments originate and insert on adjacent carpal bones to provide a rigid framework for the wrist. Extrinsic ligaments bridge the carpal bones with either multiple carpal bones, the proximal metacarpals, or the distal radius and ulna. Ligaments are conventionally named with the bone of origin as the prefix and end with the bone of insertion. They are also placed into broader categories that describe a group of ligaments such as: *radiocarpal*, *ulnocarpal*, *distal radioulnar*, *intercarpal*, and *carpometacarpal* ligaments.

1.1.2.1 Radiocarpal Ligaments

There are four extrinsic radiocarpal ligaments on the palmar surface of the wrist that originate from the distal lateral surface of the radial styloid and span medially into the adjacent carpals: *radioscaphocapitate*, *long radiolunate*, *short radiolunate*, and *radioscapholunate* [9]. These ligaments bridge the radius to the adjacent carpal bones to provide stability to the wrist during extension. On the dorsal surface of the wrist there is only the *radiocarpal* ligament that originates from the medial dorsal surface of the radial tubercle and inserts into the proximal tubercles of the lunate and triquetrum to provide lateral support to the wrist during flexion [8].

1.1.2.2 Ulnocarpal Ligaments

The ulnocarpal ligaments are extrinsic and only present on the volar side of the wrist. The *ulnolunate* ligament originates from the base the ulnar styloid process and inserts into the proximal lunate. The *ulnocapitate* ligament originates from the fovea of the ulnar head and inserts into the proximal capitate. These ligaments provide medial support to the wrist during extension.

1.1.2.3 Distal Radioulnar Ligaments

The distal radioulnar ligaments are responsible for maintaining the congruity between the ulnar head and the ulnar notch of the radius, the distal radioulnar joint (DRUJ), during pronation and supination [10]. The *distal palmer radioulnar* ligament originates from the anterior surface of the ulnar notch on the radius and inserts on the anterior head of the ulnar head. The *distal dorsal radioulnar* ligament originates from the posterior surface of the ulnar notch on the radius and inserts into the posterior surface of the ulnar head.

1.1.2.4 Intercarpal Ligaments

The intercarpal ligaments are intrinsic to the wrist that maintain congruity between and provide rigid attachments that only allow slight movements between adjacent carpals. The ligaments are named with respect to the affected carpals and labeled as follows: *scaphotrapezial*, *scaphotrapezoidal*, *scapholunate*, *scaphocapitate*, *triquetrocapitate*, *lunotriquetral*, *trapezotrapezoid*, *capitotrapezoid*, *capitohamate*, and *triquetrohamate*.

1.1.2.5 Carpometacarpal Ligaments

The carpometacarpal ligaments are responsible for attaching the proximal metacarpal to the distal row of carpal bones on both the volar and dorsal side of the hand to maintain the stability of the carpometacarpal articulation.

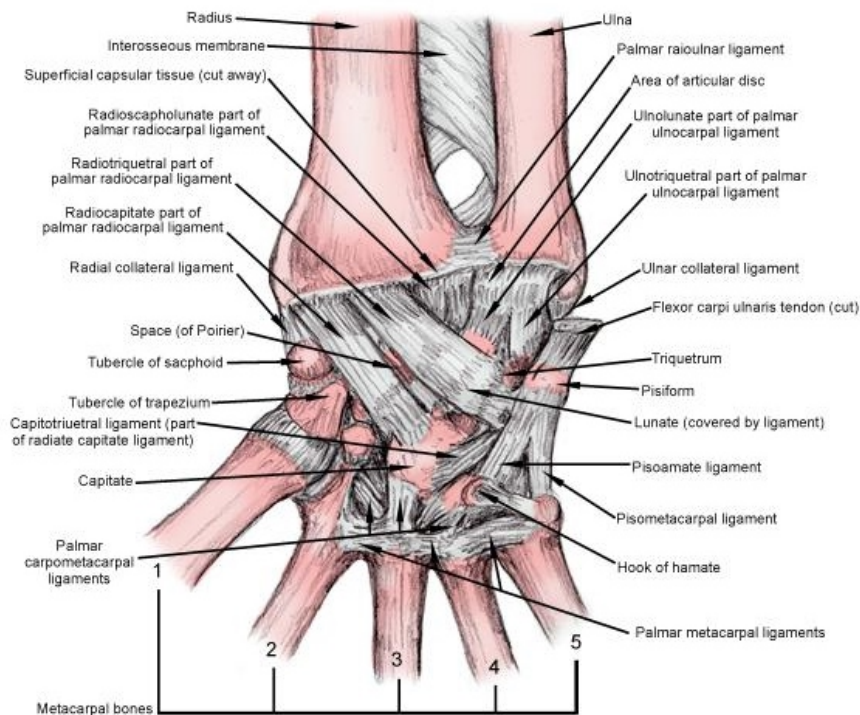
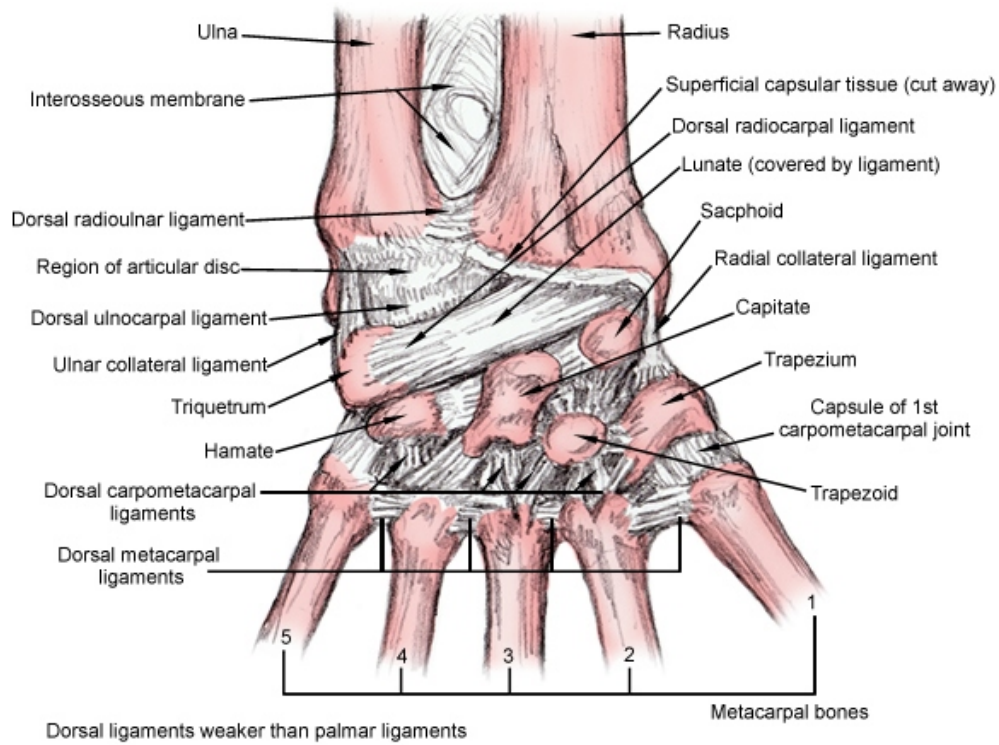


Figure 1.4: Ligaments of the right wrist and hand for the dorsal [top] and volar [bottom] views showing their origins and insertions [11]

1.1.3 Joint Capsules

The wrist is composed of an array of synovial joints and are classified into the *distal radioulnar joint* (DRUJ), *radiocarpal joint*, *intercarpal joint*, and the *carpometacarpal joints* of which only the first three will be discussed. Articular cartilage covers the surfaces of the fifteen bones that bridge the distal forearm to the hand; distal radius and ulna, eight carpal bones, and the proximal metacarpals. Articular cartilage is a low friction, avascular tissue that allows joints to track smoothly during motion. However, this tissue is not present on either the dorsal or volar surfaces as these are occupied by ligament attachments and are non-articular portions.

1.1.3.1 Distal Radioulnar Joint (DRUJ)

The DRUJ is the articulation between the ulnar notch of the radius and the medial ulnar head [12]. The dorsal and volar radioulnar ligaments maintain joint congruency during pronation and supination [10]. A fibrocartilaginous ligament known as the *articular disk* attaches the radius to the ulna to allow for a more evenly distributed force between the bones and directs the synovial fluid in the joint to areas of higher friction.

1.1.3.2 Radiocarpal Joint

The *radiocarpal joint* is responsible for the transfer of force between the hand and distal forearm primarily through the articulation of the lunate and scaphoid with the distal radius [12]. The joint is composed of the distal radius, scaphoid, lunate, triquetrum, and the radioulnar disk and to allow the wrist to achieve flexion, extension, radial and ulnar deviation [13].

1.1.3.3 Intercarpal Joint

The articulations between the carpal bones which are held together by the palmar and dorsal intercarpal ligaments form the *intercarpal joints*. Articulating cartilage found on their surfaces allow for rotation and translation during wrist motion. The intercarpal articulations form the midcarpal joint between the proximal and distal rows of carpal bones and contribute to flexion-extension and radioulnar motions of the wrist.

1.1.3.4 Carpometacarpal Joint

The *carpometacarpal joints* are the articulations between the metacarpal bases and the corresponding carpal bone in the distal row including the trapezium, trapezoid, capitate, and hamate. These are ellipsoid joints that allow for slight movements in flexion/extension as well as abduction/adduction allowing flexibility in the palm of the hand.

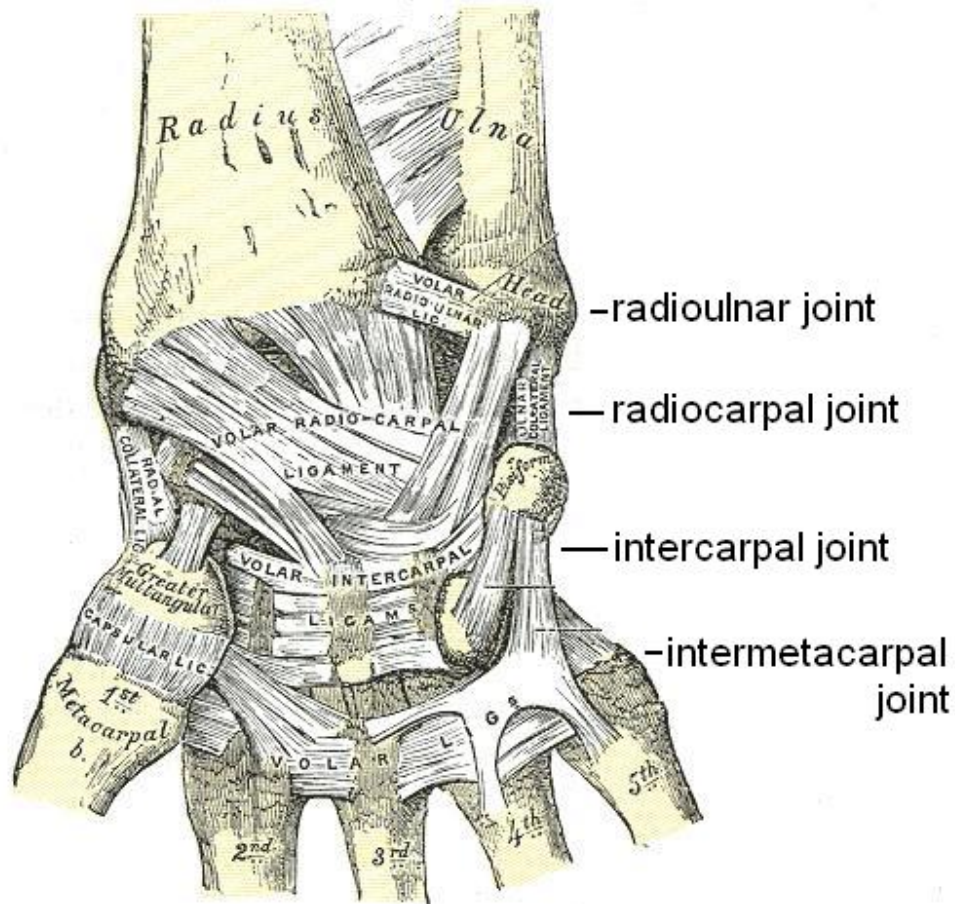


Figure 1.5: The joints of the wrist including the distal radioulnar, radiocarpal, intercarpal, and carpometacarpal joints [11]

1.1.4 Myology

Human muscle is classified into three types of tissue: smooth, cardiac, and skeletal of which only the later will be discussed. Skeletal muscle is a contractile soft tissue that spans across joints and attaches to bone through tough, fibrous connective tissue known as tendons [14]. Muscles fibers within the muscle belly actively generate tension across a joint by contracting in length producing a moment arm to effectively manipulate the position of the joint. The amount of force generated depends on the size, type, and insertion length from the joint center of the muscle. Tendons are responsible for anchoring the muscle belly to the bone and do not actively change length, although they may experience slight changes in length due to their viscoelastic nature.

Since muscles can only produce contractile forces to shorten the muscle, they coordinate with muscles influencing joint motion in the opposite direction to form antagonistic pairs. Typically, a single muscle is not entirely responsible for the motion around the joint; rather a group of synergistic muscles aid in the motion with the muscle applying the largest load classified as the primary mover [15].

The six main muscles responsible for the motion of the wrist are the *extensor carpi radialis brevis (ECRB)*, *extensor carpi radialis longus (ECRL)*, *extensor carpi ulnaris (ECU)*, *flexor carpi radialis (FCR)*, *flexor carpi ulnaris (FCU)*, and *abductor pollicis longus (APL)* [16] (Figure 1.6). These muscles are extrinsic to the wrist as they originate from medial and lateral epicondyles of the distal humerus, with exception to the APL, and their muscle bellies reside in the proximal forearm [14, 15]. Pronation and supination of the wrist are primarily controlled via the *biceps brachii* and *pronator quadratus* respectively through their insertions on the proximal radius and ulna [14].

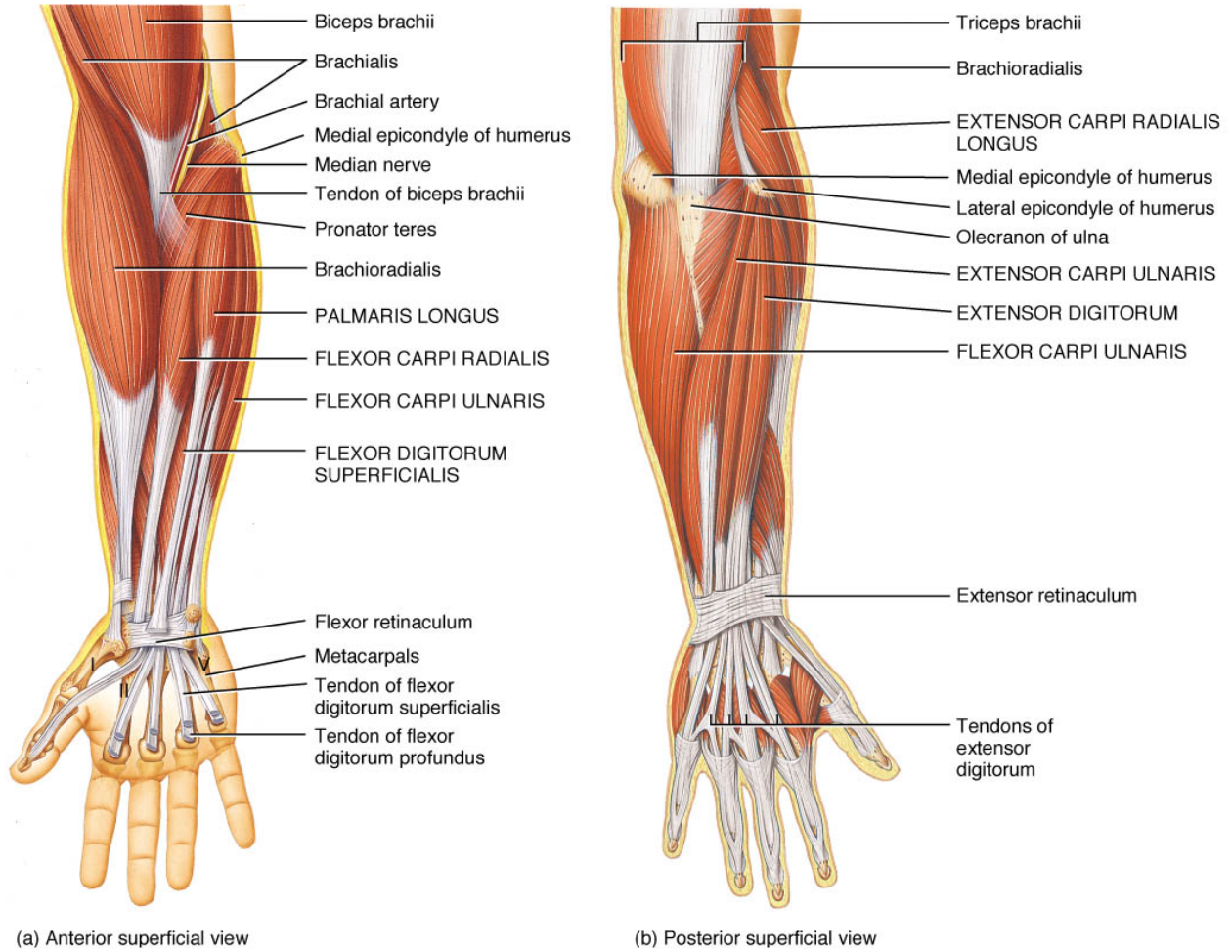


Figure 1.6: *Muscles of the right upper extremity for both the volar [left] and dorsal [right] compartments [17]*

1.1.4.1 Volar Compartment

These muscles reside in the ventral forearm and assist one another with flexion as well as ulnar and radial deviation of the wrist.

The *FCU* is the primary flexor muscle and is a synergist to ulnar deviation acting to stabilize the wrist during finger extension. The muscle originates from the medial epicondyle of the humerus and inserts into the dorsal surfaces of the pisiform, hamate, and the proximal end of metacarpal V [15].

The *FCR* is a powerful synergist muscle that aids in both wrist flexion and radial deviation [16]. The muscle originates from the medial epicondyle of the humerus and inserts into the base of metacarpals II & III.

The *APL* is the primary abductor of the wrist and extends the thumb. Unlike the other flexor muscles, the *APL* originates from the posterior aspect of the radius and ulna instead of the medial epicondyle of humerus and inserts into the base of metacarpal I and the trapezium.

1.1.4.2 Dorsal Compartment

The muscles in the dorsal forearm assist with wrist extension as well as adduction and abduction. The extensor muscles are antagonists to the flexors.

The *ECU* is the primary muscle for both wrist extension and adduction. The muscle originates from the lateral epicondyle of the humerus and inserts into the base of the small finger to oppose the *FCU* that inserts on the ventral side.

The *ECRL* is synergist muscle that assists in wrist extension as well as abduction. The muscle originates from the lateral epicondyle of the humerus and inserts into the base the index finger to oppose the *FCR*.

The *ECRB* is a synergist muscle in wrist extension and abduction and stabilizes the wrist during finger flexion. The muscle originates from the lateral epicondyle of the humerus and inserts into the base of the long finger to oppose the *FCR*.

1.1.4.3 Forearm Rotators

The *biceps brachii* and *supinator* are the primary supinator muscles and the *pronator teres* and *pronator quadratus* are the primary pronators of the forearm.

The *biceps brachii* is the primary supinator of the forearm and is a synergistic muscle for elbow flexion. The muscle has two proximal heads that originate from the supraglenoid tubercle and the coracoid process of scapula and converges to a single head that inserts into the radial tuberosity in the proximal forearm.

The *supinator* is a synergistic muscle that assists the *biceps brachii* with supination of the forearm. The muscle originates on the lateral epicondyle of the humerus and the proximal ulna and inserts into the proximal shaft of the radius.

The *pronator teres* originates from the medial epicondyle of the humerus and the proximal ulna and inserts onto the lateral midshaft of the radius.

The *pronator quadratus* is a synergistic muscle that assists the *pronator teres* with pronation of the forearm. It spans from the anterior distal shaft of the ulna to the radius [15].

1.2 Wrist Kinematics & Biomechanics

1.2.1 Range of Motion

When describing the motions of the wrist joint it is important to understand the anatomical neutral position in which all range of motion such as flexion-extension, radioulnar deviation, and pronation-supination are defined. The neutral position of the wrist is defined as the third metacarpal relative to the distal forearm [18, 19]. Neutral forearm rotation is defined as the palm of the hand parallel with the humerus with the elbow at 90 degrees of flexion; not to be confused with the neutral anatomical position of the body where the palm of the hand is facing anteriorly.

1.2.1.1 Flexion-Extension Motion

Flexion-extension motion (FEM) of the wrist (Figure 1.7) has a center of rotation based around the centroid of the capitate in the sagittal plane. Range of FEM is approximately 160 degrees depending on several factors including age and gender. Full extension of the wrist averages 70 degrees from neutral with the radiocarpal joint contributing to 67% of the paired motion with the midcarpal joint. In full flexion the wrist averages to 90 degrees from neutral with the radiocarpal joint sharing 40% of the motion and the midcarpal joint sharing 60%. Wrist extension is restricted by the combination of the palmer ligaments and the dorsal surface of the distal radius while flexion is only limited by the dorsal radiocarpal ligaments [20].

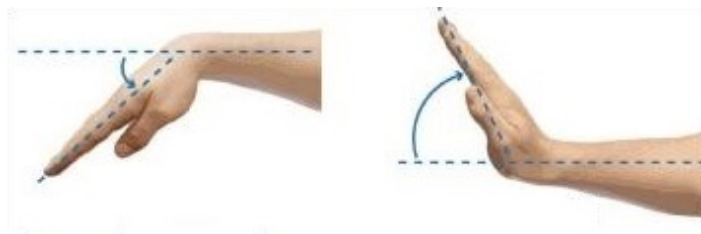


Figure 1.7: Motion of the wrist in flexion (left) & extension (right) [21]

1.2.1.2 Radial-Ulnar Deviation

Radioulnar deviation (RUD) of the wrist (Figure 1.8) has an approximate range of 60 degrees with the center of rotation acting about the capitate-scapoid articulation [20]. The wrist averages 25 degrees radially from neutral with 60% from the midcarpal joint and 35 degrees of ulnar deviation with 86% of the motion from the radiocarpal joint. Major limitations to motion result from carpal impaction with the radial styloid and tightening of the ulnar collateral ligaments in radial deviation, and the radial collateral ligaments in ulnar deviation.

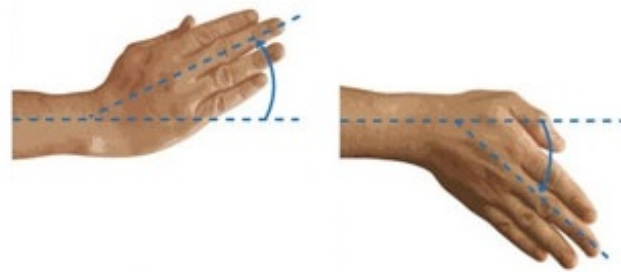


Figure 1.8: Motion of the wrist in radial (left) & ulnar (right) deviation [21]

1.2.1.3 Pronation-Supination Motion

Pronation and supination of the forearm (Figure 1.9) is the rotation in the transverse plane of the radius about the ulna following the longitudinal axis drawn between the radial and ulnar heads. Forearm rotation averages to 155 degrees with 70 degrees from neutral in pronation and 85 degrees in supination. The radioulnar ligaments are the primary limitation to supination while pronation is limited by the crossing of the radius and ulnar shafts.

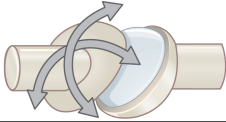
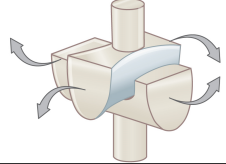
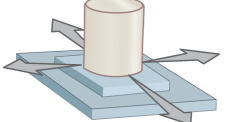
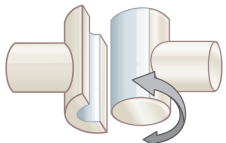
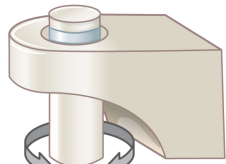
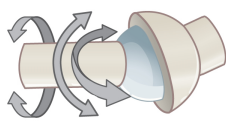


Figure 1.9: Motion of the wrist in pronation (left) & supination (right) [21]

1.2.2 Joint Geometry

Joints are classified by their shape and mobility as either condyloid, saddle, planar, hinge, pivot, or ball-and-socket (Table 1.1). The geometry of the articulating surfaces between the bones determines the congruency within the joint; a more rounded surface will have a greater contact area and inherently be more stable as the joint naturally will remain engaged when under tension provided from supporting tissues such as ligaments and tendons [22].

Table 1.1: Types of joints and their degrees of freedom (DOF) with a example of each [23]

	DOF	Example	
Condyloid	3	Wrist	
Saddle	2	Thumb	
Planar	2	Finger	
Hinge	1	Elbow	
Pivot	1	Vertebrae	
Ball & Socket	3	Shoulder	

1.2.3 Antagonistic Muscle Pairs

Muscles function as unidirectional actuators producing purely tensile forces through the contraction of the muscle length when stimulated by a motor neuron [20]. As a result muscles may only induce motion in one direction and must coordinate their contractions in antagonistic pairs to effectively provide and control motion [16, 24]. These antagonist pairs allow for holding static positions, controlling rate of angular rotation, and applying continuous muscle tone to maintain joint congruency [14]. Typically, a single muscle is not entirely responsible for the motion around the joint rather a group of synergist muscles aid in the motion with the muscle applying the largest load classified as the primary mover [15].

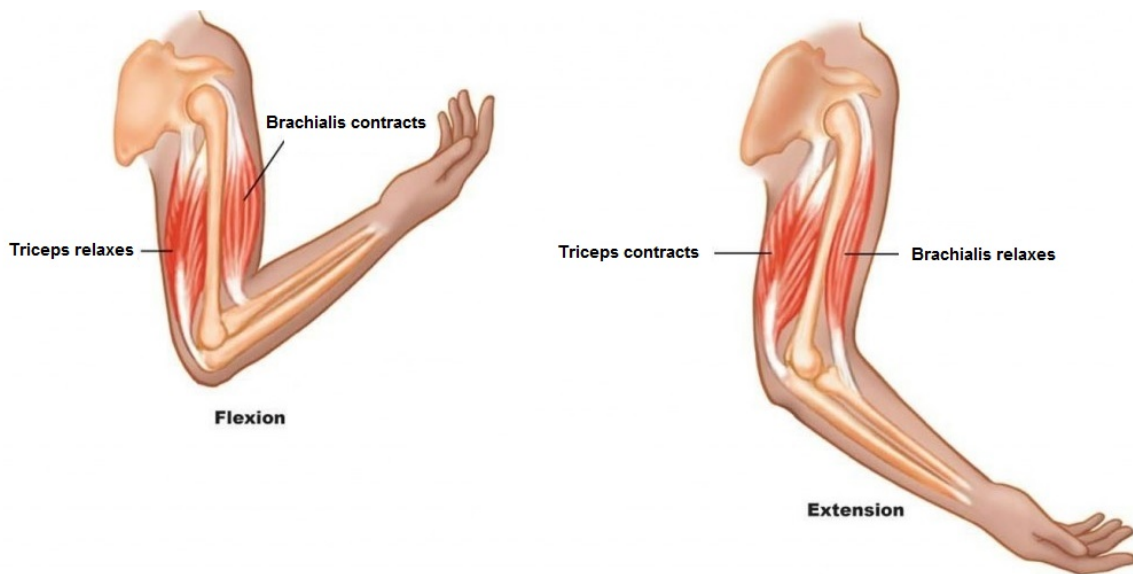


Figure 1.10: Antagonistic muscle pairs for the elbow; the brachialis activates while the triceps relax to induce elbow flexion [left] and the biceps relax while the triceps activate to induce elbow extension [right] [25]

1.2.4 Cross Sectional Area

The cross sectional area of a muscle plays an important role in the amount of force it is capable of producing [19]. The *physiological cross sectional area* PCSA is the area of the cross section that is perpendicular to the muscle fibers at the largest point and is not to be confused with the *anatomical cross sectional area* (ACSA) which is the cross sectional area of the muscle perpendicular to the longitudinal axis. For non-pennate muscles the fibers are parallel to the longitudinal axis of the muscle therefore PCSA and ACSA are coincident. The size of cross sectional area is directly proportional to the strength as larger muscles will have more fibers to produce contractile force. For instance, the maximum peak flexion force for the wrist is approximately 70% greater than that of extension primarily due to the flexor muscle group (FCU, FCR, & APL) containing a larger PCSA than the extensor muscle group (ECRB, ECRL, & ECU) [26].

1.2.5 Moment Arms

A moment arm is the perpendicular distance of tendon insertion from the center of a joint which transforms force into moment to produce motion. The flexor muscle groups of the wrist are significantly larger than those of the extensor muscle group, which combined with the larger PCSA of the flexors results in the increased strength in flexion over extension [27]. During wrist flexion moments average to 12.2 ± 3.7 Nm, peaking at 40 degrees from neutral while extension moments are only 7.1 ± 2.1 Nm, remaining relatively constant between 30° and 70° from neutral. Abduction and adduction moments average 11.0 ± 2.0 Nm and 9.5 ± 2.2 Nm respectively with no peak moments due to the limited motion [19].

1.2.6 Kinematic Chains

The upper limb is represented as an open chain linkage system composed of three rigid bodies: upper arm, forearm, and hand. The dynamics of each component is that of its own motion plus the sum of every proximal body in the link. For instance, the dynamics of the hand is the sum of all three links while the dynamics of the forearm are only the sum of the forearm itself and the upper arm as it is proximal to the forearm in the linkage [28].

1.3 Euler Angles

Euler angles describe the pose of local coordinate systems of rigid bodies in Euclidean space with respect to the global reference frame (Figure 1.11). These angles describe a sequence of three elemental rotations around the axes of a coordinate system from which any orientation in space may be reached. Rotations may either be intrinsic or extrinsic depending on which coordinate system the rotations are based around.

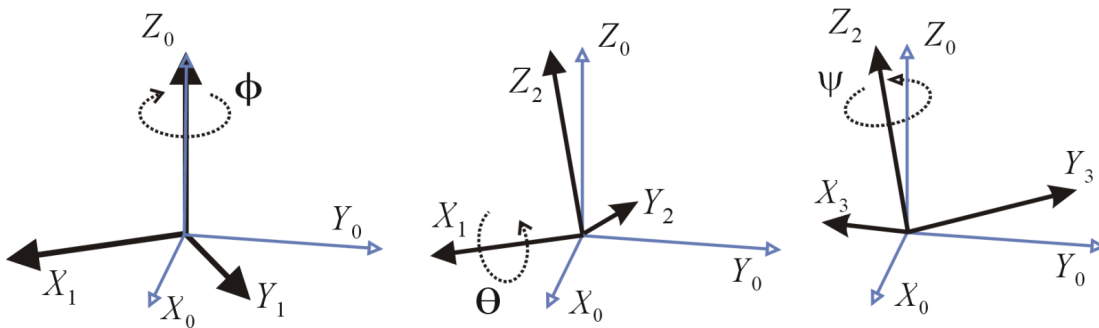


Figure 1.11: Euler rotations, Z-X-Z, showing a rotation about Z_0 axis (left), X_1 axis (middle), and Z_2 axis (right) [29]

Extrinsic rotations are around the axes of the global reference frame X-Y-Z and may occur in any order as long as a rotation about the same axis is not immediately repeated. Intrinsic rotations are around the local coordinate system axes which produce a new set of axes denoted by a single or double apostrophe for each rotation. For instance, an intrinsic rotation about the x-axis produces a y' and z' -axis, followed by a rotation about the y' -axis produces an x'' and z'' -axis. The order of rotations is important to ensure translations arrive at their intended position. Euler angles use θ theta, ϕ phi, and ψ psi to track the rotations of the rigid bodies in Euclidean space and will be used in this thesis for tracking wrist position.

Using the three Euler angles, a 3x3 rotation matrix that describes the orientation of the rotated coordinate system with respect to the initial can be constructed (Equation 1.1).

$$X = \begin{bmatrix} 1 & 0 & 0 \\ 0 & \cos(\theta) & -\sin(\theta) \\ 0 & \sin(\theta) & \cos(\theta) \end{bmatrix}$$

$$Y = \begin{bmatrix} \cos(\phi) & 0 & \sin(\phi) \\ 0 & 1 & 0 \\ -\sin(\phi) & 0 & \cos(\phi) \end{bmatrix}$$

$$Z = \begin{bmatrix} \cos(\psi) & -\sin(\psi) & 0 \\ \sin(\psi) & \cos(\psi) & 0 \\ 0 & 0 & 1 \end{bmatrix}$$

$$R = ZYX \quad (1.1)$$

Otherwise expressed as:

$$R = \begin{bmatrix} x_i & x_j & x_k \\ y_i & y_j & y_k \\ z_i & z_j & z_k \end{bmatrix} = \begin{bmatrix} r_{11} & r_{12} & r_{13} \\ r_{21} & r_{22} & r_{23} \\ r_{31} & r_{32} & r_{33} \end{bmatrix} \quad (1.2)$$

Likewise, the rotation matrix can be decomposed (Equation 1.3) to provide the three Euler angles of the local coordinate system with respect to the reference frame at that specific instant of time [30]:

$$\begin{aligned} \theta &= \text{atan2}(r_{32}, r_{33}) \\ \phi &= \text{atan2}\left(-r_{31}, \sqrt{r_{32}^2, r_{33}^2}\right) \\ \psi &= \text{atan2}(r_{21}, r_{11}) \end{aligned} \quad (1.3)$$

1.4 Coordinate Transformations

1.4.1 Transformation Matrix

Raw data collected from the tracking system provides pose, position and orientation of the bones of interest with respect to the global frame. The 6 DOF of each local frame which includes the Cartesian coordinates and the axial rotations are represented by a transformation matrix T (Equation 1.4) which is a 4x4 (16 element) array of real numbers composed of a 3x3 (9 element) rotation matrix R , a 3x1 (3 element) translation matrix P , and an arbitrary 1x4 (4 element) row $[0,0,0,1]$ to maintain orthogonal properties when transposed [31].

$$R = \begin{bmatrix} x_i & x_j & x_k \\ y_i & y_j & y_k \\ z_i & z_j & z_k \end{bmatrix} \quad P = \begin{bmatrix} P_x \\ P_y \\ P_z \end{bmatrix} \quad w = \begin{bmatrix} 0 & 0 & 0 & 1 \end{bmatrix}$$

$$T = \begin{bmatrix} x_i & x_j & x_k & P_x \\ y_i & y_j & y_k & P_y \\ z_i & z_j & z_k & P_z \\ 0 & 0 & 0 & 1 \end{bmatrix} \quad (1.4)$$

The rotation matrix holds the orthonormal direction vectors (x,y,z) and the unit direction vectors of the body's local coordinate system relative to the reference coordinate system. These direction vectors are organized so each column represents the orientation of the body relative to the reference frame and the rows represent the orientation of the reference frame relative to the body which is important to ensure that the transpose of the rotation matrix is equal to its inverse. The translation matrix states the origin of the local coordinate system in relation to the reference frame but does not describe any orientation characteristics. The last row $[0,0,0,1]$ acts to make the transformation matrix square to ensure that the vectors are represented in homogeneous coordinates. Homogeneous coordinates are a system of coordinates used in projective geometry due to their simplicity when compared with Cartesian coordinates that are used in Euclidean geometry.

1.4.2 Transformation Chain

A transformation chain is an equation that explains the steps undergone to change the frame of reference from one object with respect to another, commonly used to shift the frame of reference onto a rigid body of interest and away from the global. Tracking wrist motion requires the relative movements of the third metacarpal with respect to the radius, ${}^R{}^MCT$, but the incoming data relates the motion of each bone with respect to the global frame. The transforms of each rigid body can be multiplied in sequence to alter the data with respect to another object of interest, thus creating a transformation chain.

By multiplying the transform of the third metacarpal relative to the global frame, ${}^G{}^MCT$, by the inverse transform of the radius relative to the global frame, ${}^R{}^G T$, it would read as the third metacarpal with respect to the global frame with respect to the radius (Equation 1.5). The common global frames effectively cancel out to remain with just ${}^R{}^MCT$.

$$\begin{aligned} {}^R{}^MCT &= {}^G{}^MCT [{}^R{}^G T]^{-1} \\ {}^R{}^MCT &= {}^G{}^MCT {}^R{}^G T \end{aligned} \quad (1.5)$$

Where the superscript represents the dependent (distal) body and the subscript represents the independent (proximal) body under consideration. The same equation is relevant for relating the radial data to the ulna (Equation 1.6).

$$\begin{aligned} {}^R{}^U T &= {}^G{}^U T [{}^R{}^G T]^{-1} \\ {}^R{}^U T &= {}^G{}^U T {}^R{}^G T \end{aligned} \quad (1.6)$$

1.5 Body Segment Coordinate Systems

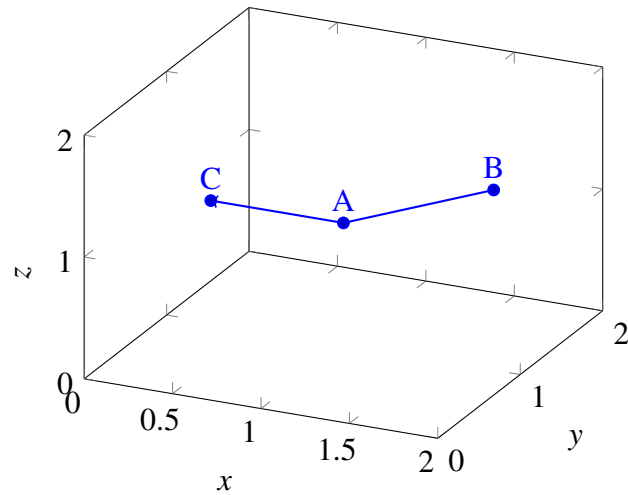
A vector space is created from a set of mutually perpendicular vectors of magnitude one, known as an orthonormal basis, and is the underlying component of coordinate systems. The *International Society of Biomechanics* (ISB) set a standard of identifying *joint coordinate systems* (JCS) for each bone to further improve communications between researchers in this field [18]. *Local coordinate systems* (LCS) are established for bones based on bony landmarks to allow for tracking the three Cartesian coordinates and three axial rotations relative to the more proximal or *global coordinate system* (GCS). For the purpose of tracking wrist joint position the bones of interest are the ulna, radius, and third metacarpal since the carpal bone motions are not generally considered in the research community. Pronation and supination of the forearm may be tracked by determining the position of the radius relative to the ulna while the flexion-extension and radioulnar deviation may be tracked by determining the position of the third metacarpal relative to the radius.

From three bony landmarks, P_A - P_B - P_C , an orthonormal coordinate system can be established which will ultimately characterize the position and orientation, otherwise known as the pose, of the each bone or segment being described [18]. Two vectors, v_1 and v_2 , are created from the landmarks with P_A as the origin.

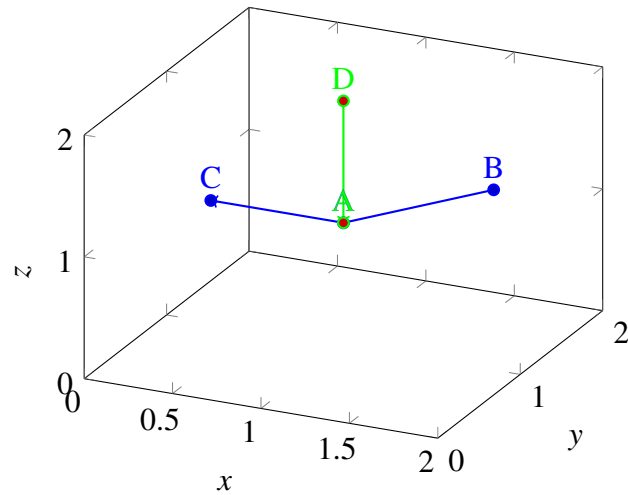
$$\begin{aligned} P_A &= (P_{Ax}, P_{Ay}, P_{Az}) \\ P_B &= (P_{Bx}, P_{By}, P_{Bz}) \\ P_C &= (P_{Cx}, P_{Cy}, P_{Cz}) \end{aligned} \quad (1.7)$$

Two vectors, v_1 and v_2 , are created from subtracting each point from the origin.

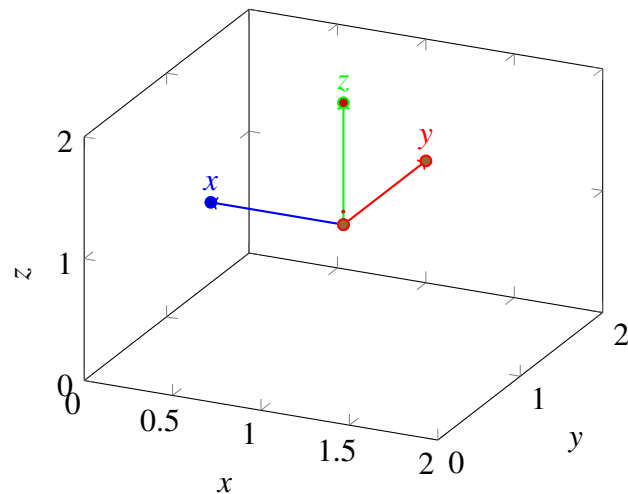
$$\begin{aligned} v_1 &= (P_{Bx} - P_{Ax}, P_{By} - P_{Ay}, P_{Bz} - P_{Az}) \\ v_2 &= (P_{Cx} - P_{Ax}, P_{Cy} - P_{Ay}, P_{Cz} - P_{Az}) \end{aligned} \quad (1.8)$$



The cross product of $v_1 \times v_2$ creates a mutually perpendicular vector, v_3 , to the A-B-C plane.



A vector cross product of $v_3 \times v_1$ is the third mutually perpendicular vector, v_4 .



These vectors are normalized to a unit length of one to complete the set of orthonormal vectors that comprise the local coordinate system of the bony body segment. The magnitude of each vector is calculated as follows:

$$\begin{aligned} |P_A| &= \sqrt{P_{Ax}^2 + P_{Ay}^2 + P_{Az}^2} \\ |P_B| &= \sqrt{P_{Bx}^2 + P_{By}^2 + P_{Bz}^2} \\ |P_C| &= \sqrt{P_{Cx}^2 + P_{Cy}^2 + P_{Cz}^2} \end{aligned} \quad (1.9)$$

Where each element in the vector is divided by the magnitude to normalize it to a unit length.

$$\begin{aligned} \hat{P}_{Ax} &= P_{Ax} / |P_A| & \hat{P}_{Bx} &= P_{Bx} / |P_B| & \hat{P}_{Cx} &= P_{Cx} / |P_C| \\ \hat{P}_{Ay} &= P_{Ay} / |P_A| & \hat{P}_{By} &= P_{By} / |P_B| & \hat{P}_{Cy} &= P_{By} / |P_C| \\ \hat{P}_{Az} &= P_{Az} / |P_A| & \hat{P}_{Bz} &= P_{Bz} / |P_B| & \hat{P}_{Cz} &= P_{Bz} / |P_C| \end{aligned} \quad (1.10)$$

The unit vectors are arranged into a 3×3 rotation matrix to provide a description of orientation of the local coordinate system with the origin set as point P_A .

$$R = \begin{bmatrix} \hat{P}_{Ax} & \hat{P}_{Bx} & \hat{P}_{Cx} \\ \hat{P}_{Ay} & \hat{P}_{By} & \hat{P}_{Cy} \\ \hat{P}_{Az} & \hat{P}_{Bz} & \hat{P}_{Cz} \end{bmatrix} \quad P = [P_{Ax} \ P_{Ay} \ P_{Az}]^T \quad (1.11)$$

The rotation and the positional matrices are combined to create a 4×4 transformation matrix.

$$T = \begin{bmatrix} \hat{P}_{Ax} & \hat{P}_{Bx} & \hat{P}_{Cx} & P_{Ax} \\ \hat{P}_{Ay} & \hat{P}_{By} & \hat{P}_{Cy} & P_{Ay} \\ \hat{P}_{Az} & \hat{P}_{Bz} & \hat{P}_{Cz} & P_{Az} \\ 0 & 0 & 0 & 1 \end{bmatrix} \quad (1.12)$$

The ISB created an agreed upon list of anatomical landmarks commonly used to establish local coordinate systems to track the bones of the upper limb. Specific coordinate systems for the carpal bones are neglected as their motion will be considered as a single unit during tracking of the wrist.

The radial coordinate system, $X_r Y_r Z_r$, has its origin, O_r , midway along the principle axis of inertia that spans from the ridge between the radioscaphoid and radiolunate fossae to the center of depression of the radial head (Figure 1.12). In the transverse plane this will place O_r at approximately the center of the diaphysis. For a right arm the Y_r axis points proximally along the longitudinal axis, the Z_r axis points laterally (radially), and the X_r axis points in the volar direction. For a left arm the Y_r axis points distally along the longitudinal axis, the Z_r axis points medially (ulnar), and the X_r axis points dorsally (Appendix A).

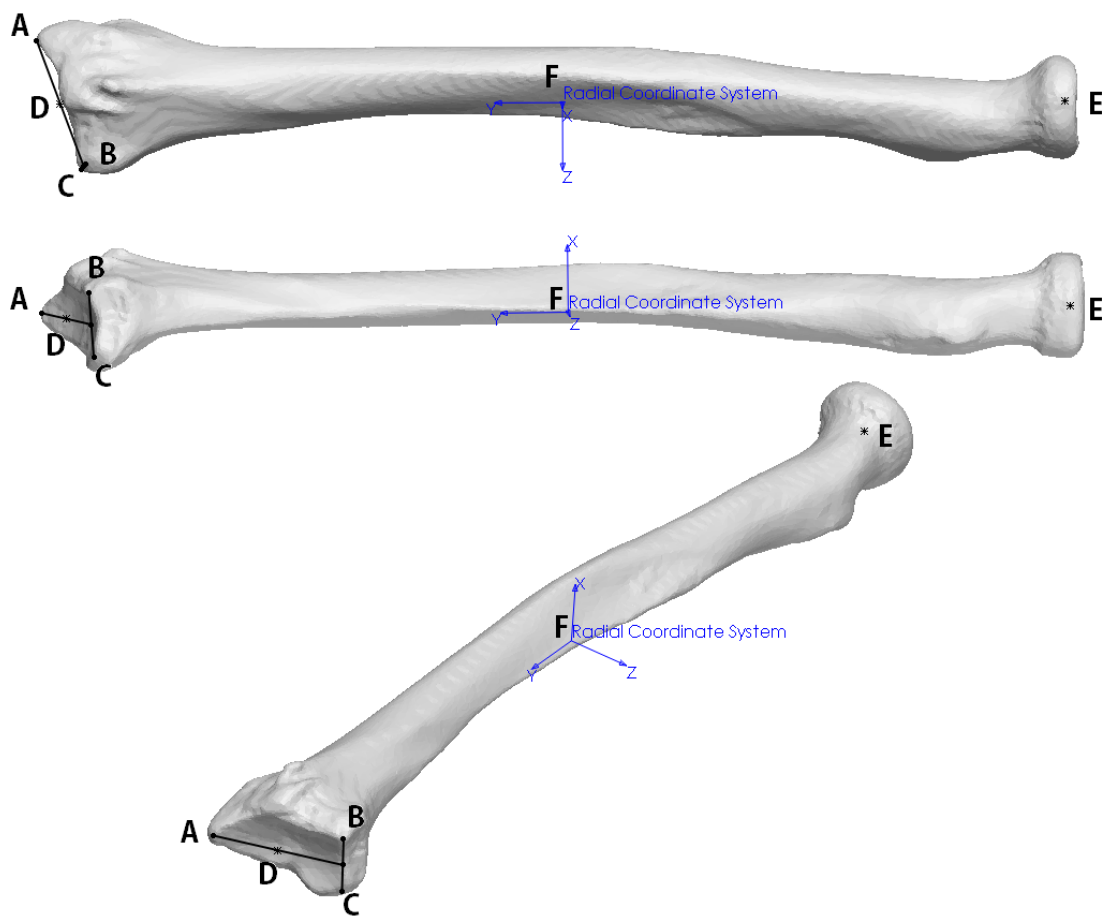


Figure 1.12: Construction of an ISB radial coordinate system for a left arm. *A: Radial Styloid Process, B: Dorsal Radioulnar Aspect, C: Volar Radioulnar Aspect, E: Radial Dish Center, F: Origin*

The ulnar coordinate system, $X_u Y_u Z_u$, has its origin, O_u , midway along the principle axis of inertia defined by the center of the dome depression on the distal head and the coronoid process at the proximal end (Figure 1.13). In the transverse plane this will place O_u at approximately the center of the diaphysis. For a right arm the Y_u axis points proximally along the longitudinal axis, the Z_u axis points laterally (radially), and the X_u axis points in the volar direction. For a left arm the Y_u axis points distally along the longitudinal axis, the Z_u axis points medially (ulnar), and the X_u axis points dorsally (Appendix A).

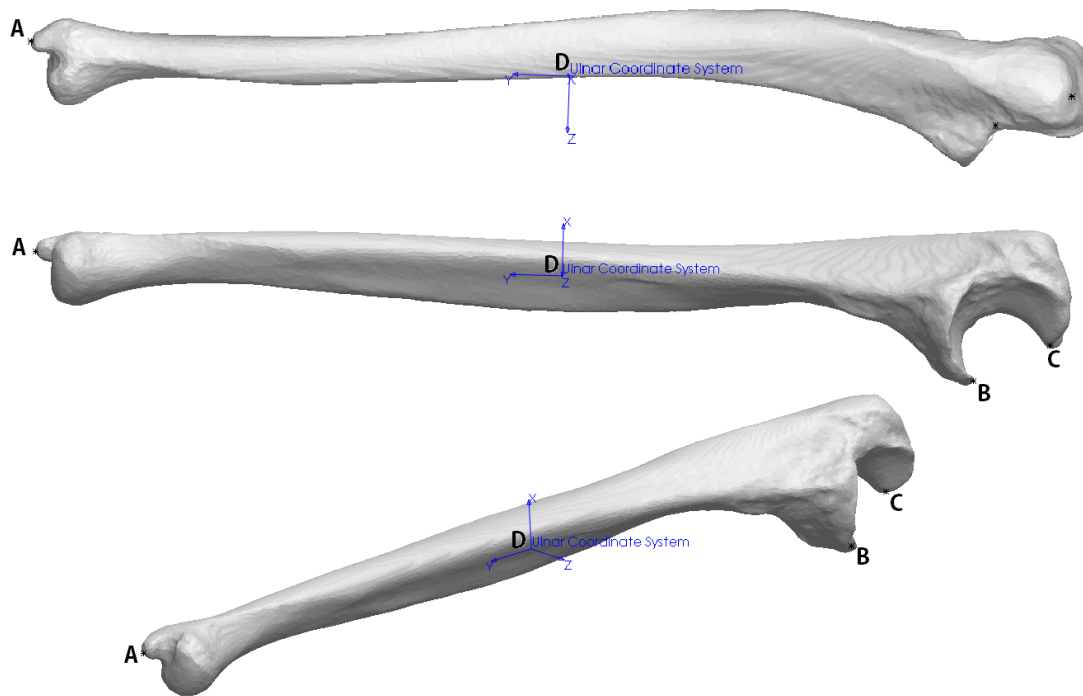


Figure 1.13: The construction of an ISB ulnar coordinate system for a left arm. **A:** Radial Styloid Process, **B:** Coronoid Process, **C:** Olecranon Process, **D:** Origin

The third metacarpal coordinate system, $X_m Y_m Z_m$, has its origin, O_m , midway between the distal and proximal extremities at approximately the center of the diaphysis in the transverse plane. For a right arm the Y_m axis points proximally along the longitudinal axis, the Z_m axis points laterally (radially), and the X_m axis points in the volar direction. For a left arm the Y_m axis points distally along the longitudinal axis, the Z_m axis points medially (ulnar), and the X_m axis points dorsally (Appendix A).

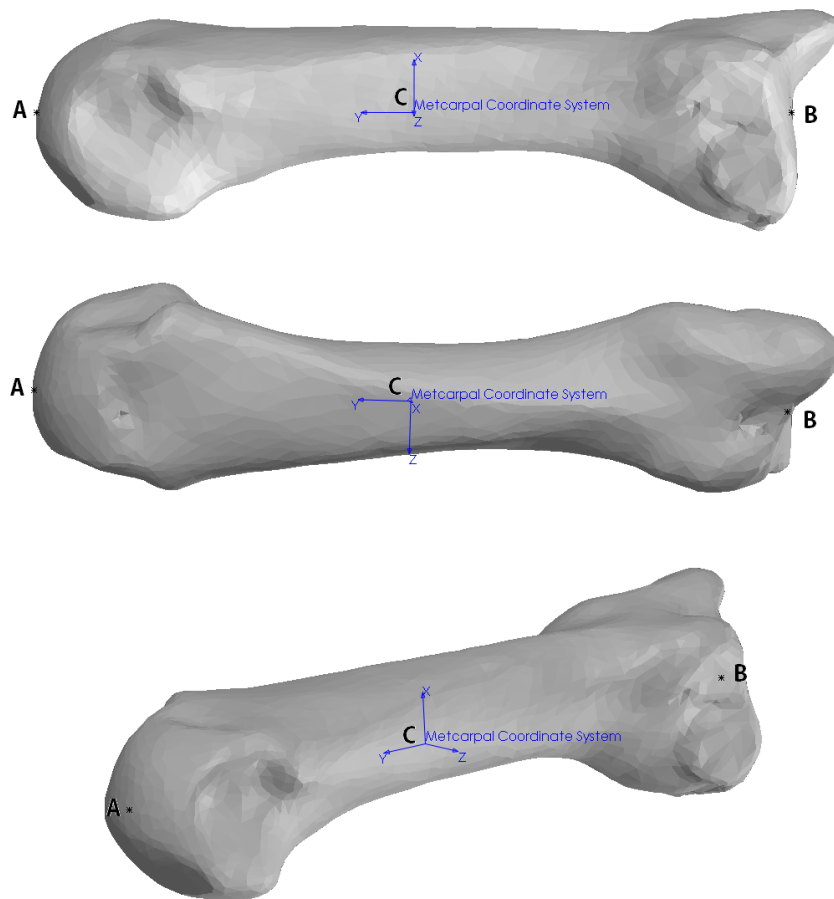


Figure 1.14: *The construction of an ISB metacarpal coordinate system for a left arm. A: Distal Head, B: Proximal Head, C: Origin*

1.6 Methods of Tracking

With ever increasing technology there are a variety of methods currently adopted for measuring *in vitro* joint kinematics of which most predominately include, but are not limited to, goniometers, inertial sensors, image based tracking, electromagnetic tracking, and optical tracking.

1.6.1 Goniometer

Goniometers measure the flexibility of a joint by comparing the angle of two bones relative to one another using either an over joint or lateral method [32]. The over joint method aligns the dial to either the inner or outer surface of the joint to measure the angle while the lateral method places the dial (Figure 1.15) adjacent to the joint with the center of rotation of the dial aligned with that of the joint [33]. This method allows for a simple means to measure joint angle for *in vitro* specimens since calibration is not required for the instrument. The drawbacks are that the center of motion for some joints shifts during flexion/extension and the substantial estimation errors of the position of the joint segments by the operator [34].

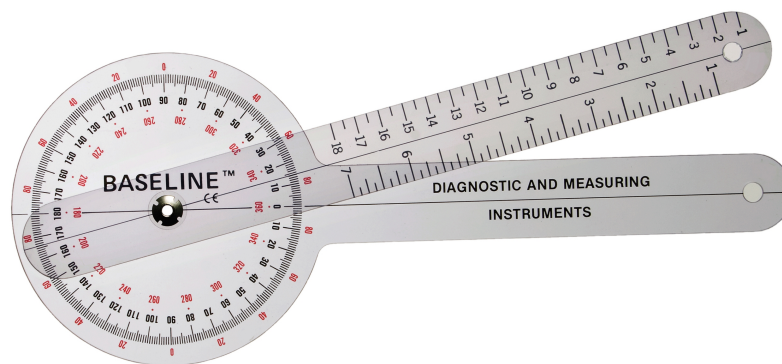


Figure 1.15: An instrument for the measurement of angles [35]

1.6.2 Inertial Measurement Units

Inertial measurement units (IMU) are relatively small compared to the other tracking methods and are composed of accelerometers and gyroscopes to measure translation and rotation for each of the three axis (Figure 1.16). Through forward kinematics the position of each segment being tracked may be interpreted from the kinematic information received from each IMU. This method is excellent for interpreting impact forces and changes in rotational energy of body segments while being able to estimate change in position. The drawbacks are that the IMUs are sensitive to drift error due to signal noise which may result in up to approximately 10 to 25 degrees per minute of use if not calibrated correctly [36]. Since the upper extremities of the human body are modeled as open kinematic chains the results in the motion of a link will be that of itself as well as every proximal link before it requiring complex equations to deduce the individual link motion when analyzing multi-linkage systems.

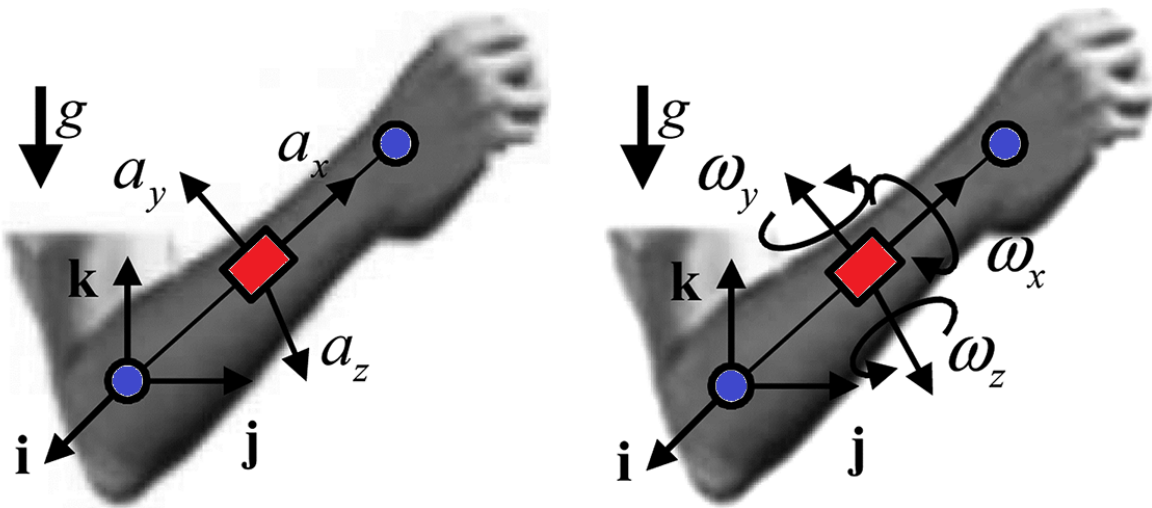


Figure 1.16: A 9DOF digital IMU sensor [red rectangle] with a 3DOF accelerometer to measure acceleration (a_x, a_y, a_z) [left], a 3DOF gyroscope to measure rotation (w_x, w_y, w_z), and a 3DOF magnetometer to measure magnetic north for a body segment between two points [blue circles] [37]

1.6.3 Image Based Tracking

Image based tracking, or video tracking, is the process of programmatically stitching together a sequence of images from a video source to recognize and track the motion of an object of interest between frames and determine the behaviours exhibited [38]. *Edge matching* between sequential frames is a technique that detects boundaries of sharp changes in values, otherwise known as contrast, between adjacent pixels and outlines that region. For instance, a bouncing white ball in a well-lit black room would provide the best contrast for tracking.

Using this method for tracking human motion becomes a Gaussian problem that uses a probability distribution of possible relative poses from an image along with a predefined skeletal model (Figure 1.17) to predict the most likely outcome [39]. The shortfalls of tracking human motion using a single camera arise from the loss of image depth and scale, reflective ambiguities where multiple poses produce similar images, and lost observations due to occlusions of limbs during motion [40].

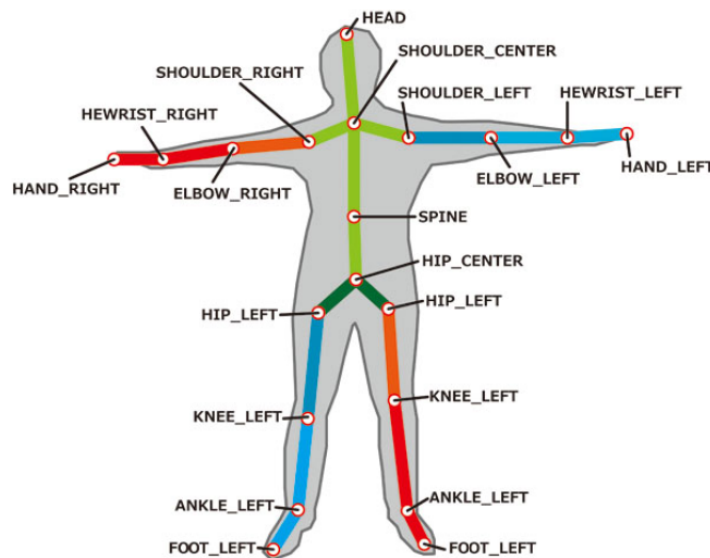


Figure 1.17: Image based tracking attempts to map an object from an image to a known rigid body, such as the human skeletal model, to provide feedback of position and pose [41]

New developments in technology have led to the introduction of the Microsoft Kinect (Microsoft Corp., WA), which was initially intended as a hands free controller interface for the Microsoft XBox 360 gaming console that recognizes gestures from the user using two cameras and an infrared sensor to reconstruct a 3D representation of all objects in the frame of view. Matching this information to a skeletal model can provide a more accurate estimate of pose and position of individual body segments that a singular camera could achieve [41]. These methods are excellent for general motion of limbs for investigating gait, however they are limited by the assumption of bone positions based on skin markers and are unable to provide any insight to the kinematics of the underlying skeletal system.



Figure 1.18: Microsoft XBox Kinetic used for mapping the human skeletal model to the user in the frame of reference [42]

1.6.4 Electromagnetic Tracking Systems

Electromagnetic Tracking Systems (EMTS) are commonly used in invasive surgery as the method does not require a direct line of sight between the source and sensor [43]. This method uses induction coils to generate a magnetic field from a tracker which is read by the sensor to determine the pose and attitude of the tracker. By sequentially activating three coils within the tracker the sensor can record the disturbance in the surrounding magnetic field to obtain a 5 DOF reading of the tracker [44]. By introducing multiple trackers to the system each can effectively become a sensor during their latency period thus increasing the system accuracy to 6 DOF. The major drawback to this method is that the use of ferromagnetic materials such as cobalt-chromium and titanium distort the magnetic fields and drastically degrade the positional accuracy of the system [45]. Special design considerations are needed as conventional fasteners and medical tooling may not be used.

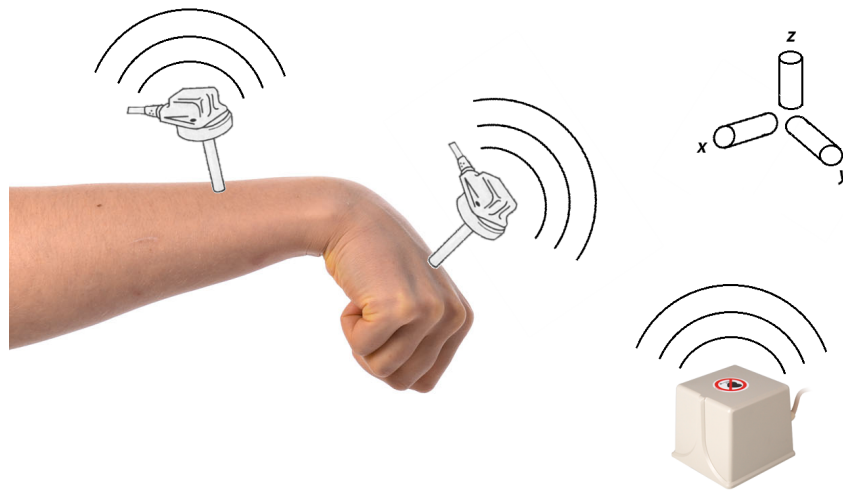


Figure 1.19: *Electromagnetic sensors induce a magnetic field in three directions (x,y,z) that is interpreted by a detector for orientation and strength to obtain the estimated position of the trackers in 3D space*

1.6.5 Optical Tracking Systems

Optical tracking systems use an array of at least two infrared cameras Figure 1.20 to triangulate the global Cartesian coordinates of the markers within the field of view [45]. Passive markers are commonly spheres or surfaces that reflect infrared light emitted from the camera and are the more mobile option as there are no wires or power sources required (META Motion). However, there is error associated with artifacts from other potential unwanted reflective surfaces in the field of view of the camera which have to be filtered from the data. Passive markers are relatively large to ensure they are detected by the camera resulting in the system having to estimate the marker centroid producing a floating center point. Active markers contain light emitting diodes (LEDs) that emit their own infrared light requiring a power source from either a battery or the terminal [44]. The intensity of light from an LED allows the point of recognition to be much smaller than a passive marker lowering the relative error from a floating center. Furthermore the LEDs can be activated in succession with respect to the other markers to allow for an ordered marker array which can aid in trouble shooting.

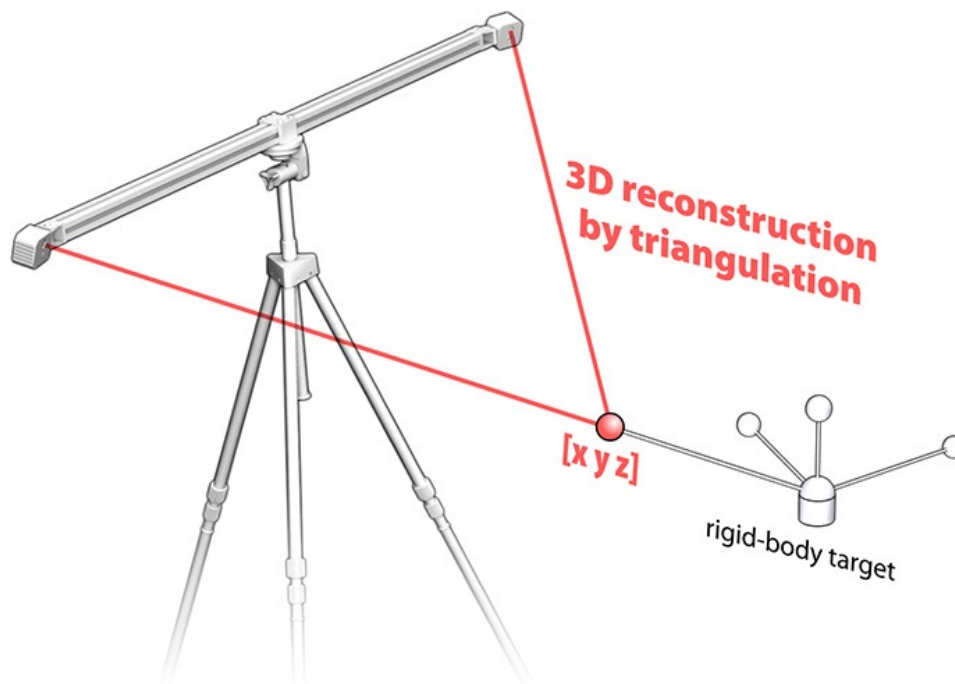


Figure 1.20: An array of cameras may determine the location of infrared LEDs [red circle] that can provide the position and orientation of a rigid body in space [46]

From the point array obtained by both optical and electromagnetic trackers, the joint motion can be determined using inverse kinematics to give the pose and attitude of the bones relative to one another [47]. The Cartesian coordinates of markers can be assigned to specific bones and important bony landmarks to create relevant body segment coordinate systems within a computer program to later analyze. Markers defined relative to anatomical landmarks of the bone assist in joint angle calculations. A stylus is a tracker with a predefined tip length, or rigid body, assigned to it and is used to digitize landmarks of the bone segments to align the trackers coordinate systems with their respective bones.

1.7 Clinical Complications

Wrist pain is a debilitating health issue that can be classified as either mechanical, neurological, or systemic and can decrease overall quality of life and independence of those affected. It may be the result from sustaining a traumatic injury or the onset of a degenerative disease [48].

1.7.1 Traumatic Injuries

Upper limb injuries are most commonly the result of a trip or fall where the wrist is extended as a protective mechanism and may result in bone fractures or injury to ligaments causing sprains [49, 50]. The most common injury is *Colles Fracture* (Figure 1.21) which occurs at the distal radius and requires casting, pin fixation, *external fixation* or *open reduction & internal fixation* to maintain the normal bone position [6, 51, 52]. Soft tissue injuries may sprain or tear ligaments and in severe cases result in joint dislocations. These injuries may increase laxity between adjacent bones potentially influencing the range of motion and altering normal carpal motion.

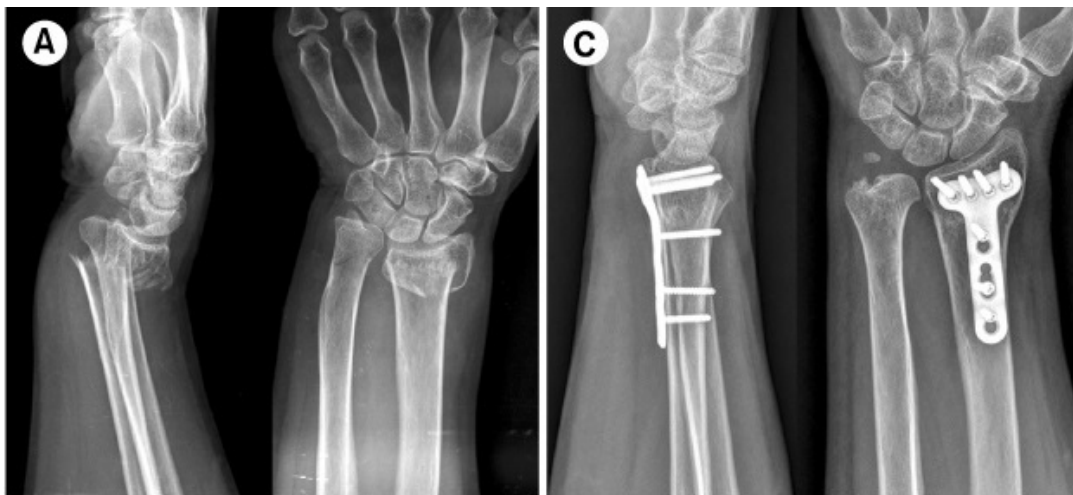


Figure 1.21: *Uncorrected Colles fracture (left) and an internal fixation method (right)* [53]

1.7.2 Degenerative Disease

Degenerative diseases may result from wear and tear or a past injury and can reduce the healthy layer of articular cartilage present in the joint causing painful bone on bone articulation. In the event of extreme degradation, wrist fusion may be employed to alleviate pain, however the loss of wrist motion is functionally disabling. Wrist arthroplasty may be performed to restore wrist function, however relative to the experience with the hip, knee and shoulder these devices have a higher failure rate and have yet to be optimized. Hemi-arthroplasty replaces a single side with the adjacent surface still the native tissue, and a full-arthroplasty replaces the full joint (Figure 1.22).

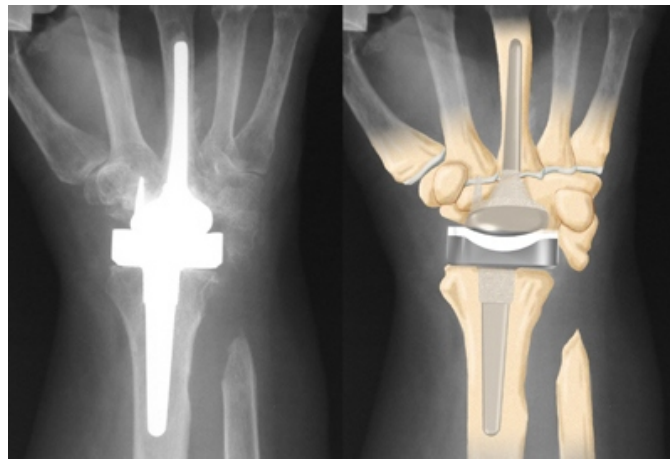


Figure 1.22: Total wrist arthroplasty restoring motion to the joint [54]

1.7.3 Bracing Methods

Bracing is commonly used immobilize the joint during a period of recovery after sustaining an injury or reparative surgery. They are also used in high intensity sports to prevent injury. In sports, dynamic bracing provides athletes with the required mobility but restricts the motion to within a specific range while static braces prevent motion entirely. Studies of the effectiveness of current brace designs on controlling wrist motion are needed to optimize these devices to allow for both rehabilitation and injury prevention. These aforementioned clinical scenarios often employ laboratory-based testing to determine the motion, stability and loading at the wrist with special interest in improving subsequent treatment techniques.

1.8 Biomechanical Testing & Simulation of Motion Pathways

Understanding wrist kinematics is crucial for advancing surgical methods as it allows for quantitative analysis to determine the overall quality of the technique. Alterations of wrist motion as a result of arthritic disorders or traumatic injuries such as ligament tears, or a fractured bone result in a decreased quality of life for the effected individual. Methods such as arthroplasty, soft tissue repairs, and fracture fixation techniques intended to alleviate these wrist complications must be deemed safe for clinical use before are adopted as a viable option.

New repair techniques may be validated through the use of virtual *in-silico* computer simulations or physical *in-vitro* cadaver models to simulate *in-vivo* conditions. Both methods have their associated strengths and weaknesses that will ultimately affect the likelihood of them being adopted as the primary method of pre-clinical testing.

Although testing devices and simulations exist to examine the kinematics of the wrist, none of the published platforms have been able to evaluate wrist motion with the arm in all the common orientations which occur in normal activities. The conventional approach has been to place the wrist in a vertical position relative to gravity so that motion mimics an inverted pendulum in neutral forearm rotation which does not encompass the full versatility of the wrist. To fully validate the functionality of an experimental procedure it should be tested at a range of pronation/supination positions to test its compatibility with the DRUJ as well as multiple gravity loaded orientations.

1.8.1 *In-Silico* Simulations

The use of *in silico* wrist models have the advantage of being relatively inexpensive when compared to *in vitro* studies and provide a high-speed computational platform eliminating the cumbersome task of monitoring and maintaining an experiment such as wear testing (Strickland, 2009). With virtual simulations anatomic specimens are not required, hence they not deteriorate with prolonged use. Wrist modeling allows for unlimited uses from which one specimen can encompass an entire array of variations for a single experiment thus strengthening the comparative results which is not available for *in vitro* experiments.

The drawbacks with this method are that soft tissues are *viscoelastic* in nature and therefore are difficult to accurately model in CAD software. This results in the creation of simplified models to mimic *in vivo* motions to achieve comparable results [26]. To validate a virtual model the results must lie within two standard deviations of the identical physical model to ensure the accuracy of the results for future studies. Since many assumptions are made during the creation of a virtual model, there are many variables that may influence the quality of the results. Therefore, these models must undergo sensitivity testing to ensure that small changes will not drastically alter the end result of the study.

The wrist joint is combination of complex articulations amongst the carpal bones of which their exact kinematics during wrist motion is not yet fully documented. The non-linear deformation and strain rate dependent properties of the tendons and ligaments associated with the wrist result in many assumptions required for modeling that set constants for variables such as bone density, ligament stiffness, and cartilage properties [55].

With improvements in technology, virtual simulations are rapidly becoming more reliable and wide spread within the research community but due to their limitations from assumptions and general unknowns they continue to be less reliable than what is currently achievable using *in vitro* experiments.

1.8.2 *In-Vitro* Simulators

1.8.2.1 Passive Motion Simulators

Wrist joint kinematics can be reproduced through passive motion simulators that use external forces from either the researcher or a mechanical apparatus to manipulate the position of the hand relative to the forearm. Human manipulation of a specimen may result in unrepeatable movements thus diminishing the quality of the results. A 6 DOF Stewart platform (Figure 1.23) simulator has been used to analyze the kinematics of the carpal bones during repeated hammering motions [56]. This simulator excises all subcutaneous tissue, disarticulates the phalanges, and transects the radius and ulna at the distal third, restricting to only intercarpal movement.



Figure 1.23: A Stewart platform for simulating 6DOF passive wrist motion uses six actuators to achieve 3 degrees of freedom of translation and rotation each with the wrist mounted on the top surface of the platform [57]

Nishiwaki *et al.* used a simulator (Figure 1.24) that fixed cadaveric upper limbs amputated at the mid humerus to a base, using an array of pneumatic actuators to maintain a minimum tone load on the *extensor carpi ulnaris*, *extensor carpi radialis longus & brevis*, *flexor carpi radialis*, *flexor carpi ulnaris*, and *abductor pollicis longus* [58]. Trackers were attached to the *radius*, *ulna*, *third metacarpal*, *scaphoid*, *lunate*, and *capitate*. All motions were passively generated by the investigator from a rod protruding distally from the third metacarpal.

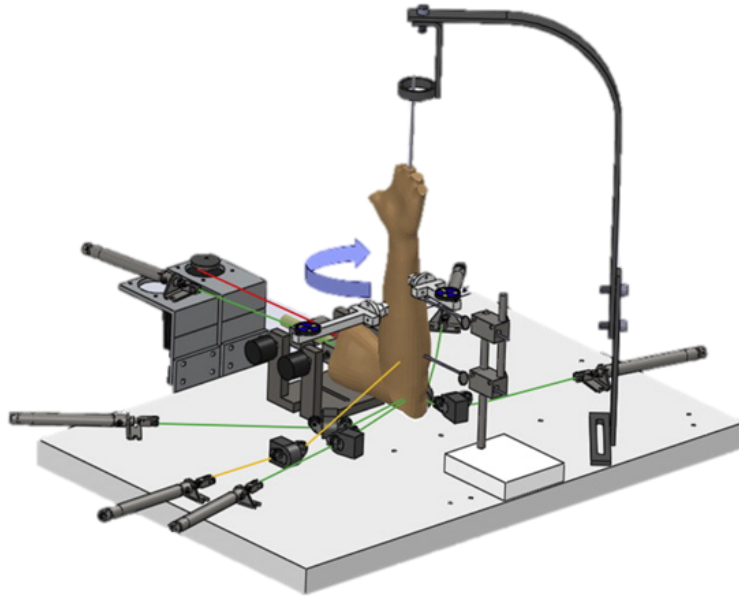


Figure 1.24: A platform that uses an array of pneumatic actuators sutured to the tendons of interest to maintain a tone across the wrist [59]

Passive motion relates to any force applied to an appendage that does not originate from a muscle anatomically responsible for the motion of that joint. For instance, an actuator attached at the distal insertion of the biceps intended to simulate elbow flexion would be considered passive motion. The importance to differentiate simulators as *active* and *passive* arises from the difference in potential kinematic outcomes as an external force may incorrectly simulate the motion of the joint if the true line of action of the muscle is not recreated. *In vivo* conditions have muscle tone that compresses a joint into its natural congruency which if not present in a passive simulator may increase joint laxity and provide 'sloppy' motions. Passive motion simulators that incorporate these muscle tones ultimately will provide more reliable results but are still subject to errors in the force vectors applied.

1.8.2.2 Active Motion Simulators

Active simulators are a more reliable method for joint simulation as the forces are applied directly to the muscle tendons of interest to manipulate joint position. Algorithms designed using antagonistic relationships between opposing muscles such as the flexors and extensors allow for conditions to more accurately model an *in vivo* scenario.

Motion of the wrist is generally controlled through force-position algorithms that work to move the wrist in a controlled manor from one position to the next using the antagonistic muscle pairs. The primary mover muscle in the direction of the motion is position controlled to maintain a continuous angular velocity while the opposing muscles hold the constant muscle tone load set for the simulator. To reverse the direction of motion the position-force algorithm switches so that the muscles previously under position control is maintaining a tone load while the antagonist acts to change position of the joint.

Linear actuators or servomotors may be used to apply forces to the tendons of interest. Linear actuators are relatively inexpensive and provide force feedback to the system but have no measure of position and are subject to compressibility if pneumatic. Servomotors are the more expensive option and require programming to sync the native software with the simulator but provide positional feedback and are not subject to position error. Force transducers are required to record the force output adding an additional level of complexity to the system.

Dunning *et al.* [51] developed a platform for simulating active motion on cadaveric upper limbs using a manifold of pneumatic actors to deliver computer controlled forces to nine muscles of interest (Figure 1.25). Specimens were mounted with the forearm horizontal, cables were sutured to the musculotendinous junctions of the tendon insertion, and electromagnetic receivers (Flock of Birds, Ascension Technologies, Burlington, VT) were used to track relative motion of unstable distal radial fractures. This method of actuation is more accurate at modeling *in-vivo* motion but is inherently unrepeatable as it is an open loop control system with no positional feedback of the wrist from the trackers. The system requires extensive heuristic

tuning for the magnitude of tendon forces prior to testing for each new specimen to achieve the desired motion which are visually assessed by the investigator for approval. This method is superior to passive motion but there is no guarantee that successive intra-specimen trials will be under identical conditions with regards to rate of angular rotation and loading.

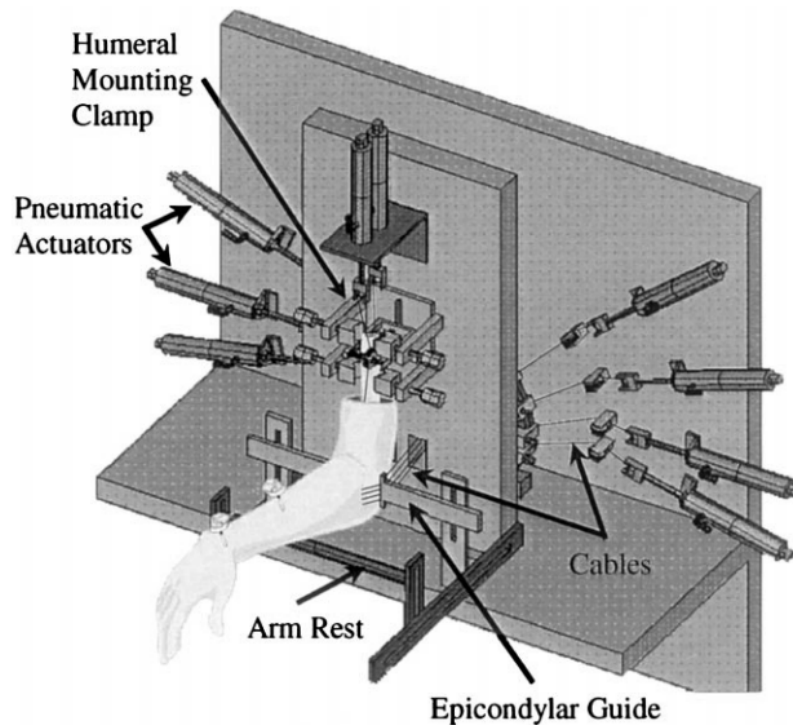


Figure 1.25: Active motion simulator using a manifold of pneumatic actuators acting on 9 muscles of interest to induce motion [51]

Werner *et al.* reported the first functional active wrist simulator (Figure 1.26) that produced repeatable wrist motion [16]. Using an electromagnetic spatial tracker the position of the third metacarpal, lunate, and ulna were recorded to provide real time feedback of the cadaver specimen to follow a determined path for the wrist to follow. The specimens were transected midway along the forearm and cemented into the base of the simulator with all soft tissue excised with exception to the tendons and ligaments of interest. Optical tracking is a more modern method for recording spatial position and was not a viable option during the development of this simulator ultimately introducing material limitations that prevent analysis of any procedures involving ferromagnetic metals commonly used in fracture fixation methods and joint

arthroplasty/arthrodesis.

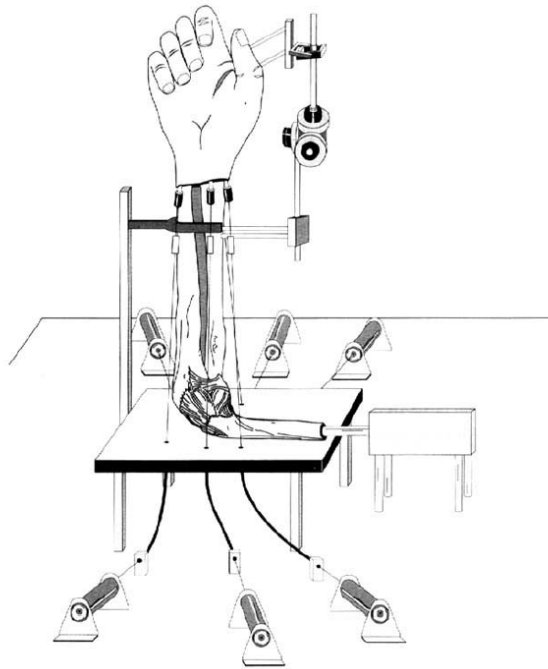


Figure 1.26: Palmar view of Werner's wrist joint simulator [16]

Erhart *et al.* recently published the most advanced active motion simulator to date that tracks the wrist motions using active optical markers [60]. Linear pneumatic actuators are used to induce motion following an antagonistic pair algorithm with the arm fixated vertically at 90 degrees flexion and a static forearm rotation. For this simulator the lines of action of the muscles are more accurately represented as they pass through their respective origins before diverting to the actuators.

Ideally, an active motion simulator will encompass the full range of motion with no limitations towards material compatibility or achievable forearm positions. All lines of action are recreated to resemble their anatomically correct position and the simulator is able to maintain tone loads during position-force controlled algorithms.

1.9 Thesis Rationale

Research into the development of a reliable *in vitro* wrist simulator to accurately recreate *in-vivo* conditions will provide a means to accelerate the development of improved methods of injury prevention, rehabilitation and joint reconstruction of the wrist. As outlined previously, while significant advances in wrist simulation have occurred in recent years, current simulators continue to be challenged to recreate relevant clinical motions.

The rationale for this thesis is to design a more versatile method for testing wrist motion that allows for active forearm rotation, more accurately model the natural anatomical line of action of the muscle-tendon units present *in-vivo*, and introduce the ability for testing in multiple gravity loaded positions. Moreover, a simulator designed with modern technology and not limited by material compatibilities is a secondary goal.

1.10 Objectives & Hypotheses

The objective of this research was to develop a reliable method for testing wrist specimens for common surgical techniques and prosthetics that include, but are not limited, to fracture fixation, ligament repair, and arthroplasty.

Specific Objectives:

1. To design & develop a platform to accurately maintain tone loads of various muscles in the forearm for passive motion trials in all planes of wrist motion.
2. To create reliable motion within an accuracy of 1 degree of the desired pathway in flexion/extension and radioulnar deviation.
3. Successfully produce active motion trials in multiple gravity loaded positions such as gravity flexion, gravity extension, and gravity neutral (inverted pendulum).

Hypotheses:

1. The system will be able to maintain the desired muscle tone to within 1.0 N with minimal influence from fluctuations of the other supporting muscles.
2. The system will be able to produce motion trials with inter-specimen variance less than 1.0° and minimal out of plane motion.
3. The effects of gravity on the wrist joint will produce significant increases in the muscles groups opposing the motion of gravity of the wrist while producing unrelated force curves (flat lines) for gravity assisted motion.

1.11 Thesis Overview

Chapter 2 describes the iterative design process undertaken to develop an active wrist simulator and validates the methods implemented to produce repeatable motion profiles with respect to passive trials.

Chapter 3 is an investigation into the effects of gravity on the kinematics of the wrist by examining percentage of muscles force increase as well as fluctuations in the center of rotation in the FEM plane.

Chapter 4 describes the study undertaken to improve muscle loading across the DRUJ by adjusting the ratio of forces applied within each muscle group based on EMG and PCSA data gathered from existing studies.

Chapter 5 is a summary of the work to date and provides closing thoughts on the relevance of developing an active motion wrist simulator and how it will affect orthopaedic research moving forward.

References

- [1] H. Gray, *Anatomy of the human body*. Philadelphia: Lea & Febiger, 1918.
- [2] T. Einhorn, R. O’Keefe, and J. Buckwalter, “Form and function of bone,” in *Orthopaedic Basic Science: Foundations of Clinical Practice*, pp. 129–174, Philadelphia: Lea & Febiger, 3rd ed., 2007.
- [3] J. Silverstein, J. Moeller, and M. Hutchinson, “Common issues in orthopedics,” in *Textbook of Family Medicine*, ch. 30, Philadelphia: Saunders Elsevier, 8th ed., 2011.
- [4] J. Leiberman, “Bone and joint biology,” in *AAOS Comprehensive Review*, pp. 41–52, Rosemont, IL: American Academy of Orthopaedic Surgeons, 2009.
- [5] T. D. White, M. T. Black, and P. A. Folkens, *Human osteology*. Academic press, 2011.
- [6] W. P. Cooney, *The wrist: diagnosis and operative treatment*. Lippincott Williams & Wilkins, 2011.
- [7] R. L. Technology, “Anatomy of the human hand.” <http://radiologicstechnology.org/content/82/2/161/F2.large.jpg>. [Online; accessed 2015-08-02].
- [8] B. Z. Phillips, S. T. Schmidt, and T. R. Gest, “Wrist joint anatomy.” <http://emedicine.medscape.com/article/1899456-overview>. [Online; accessed 2015-07-05].
- [9] C. R. Wheelless, *Wheelless’ textbook of orthopaedics*. DataTrace Internet Pub., 1996.
- [10] L. D. Ward, C. G. Ambrose, M. V. Masson, and F. Levaro, “The role of the distal radioulnar ligaments, interosseous membrane, and joint capsule in distal radioulnar joint stability,” *The Journal of hand surgery*, vol. 25, no. 2, pp. 341–351, 2000.
- [11] B. Z. Phillips, S. T. Schmidt, and T. R. Gest, “Wrist pain anyone?.” <http://www.40fit.com/wrist-pain-anyone/>. [Online; accessed 2015-06-01].
- [12] O. Jones, “The radioulnar joints.” <http://teachmeanatomy.info/upper-limb/joints/radioulnar-joints/>. [Online; accessed 2015-05-05].
- [13] L. Richards and J. Loudon, “Bone and joint structure.” <http://classes.kumc.edu/sah/resources/handkines/bone/radioartic.html>. [Online; accessed 2015-01-17].

- [14] S. S. Mader, *Understanding human anatomy & physiology*. Burr Ridge, IL: The McGraw-Hills Company Inc, 4th ed., 2001.
- [15] K. S. Saladin and L. Miller, *Anatomy & physiology - The Unity of Form and Function*. McGraw-Hill Company Inc, 2nd ed., 2008.
- [16] F. W. Werner, A. K. Palmer, J. H. Somerset, J. J. Tong, D. B. Gillison, M. D. Fortino, and W. H. Short, "Wrist joint motion simulator," *Journal of orthopaedic research*, vol. 14, no. 4, pp. 639–646, 1996.
- [17] S. Griffith, "The muscular system." <http://beauproductions.com/golfswingsws/healthpages/golf> [Online; accessed 2015-03-02].
- [18] G. Wu, F. C. Van Der Helm, H. D. Veeger, M. Makhsous, P. Van Roy, C. Anglin, J. Nagels, A. R. Karduna, K. McQuade, X. Wang, *et al.*, "Isb recommendation on definitions of joint coordinate systems of various joints for the reporting of human joint motionpart ii: shoulder, elbow, wrist and hand," *Journal of biomechanics*, vol. 38, no. 5, pp. 981–992, 2005.
- [19] S. L. Delp, A. E. Grierson, and T. S. Buchanan, "Maximumisometric moments generated by the wrist muscles in flexion-extension and radial-ulnar deviation," *Journal of biomechanics*, vol. 29, no. 10, pp. 1371–1375, 1996.
- [20] L. S. Lippert, *Clinical kinesiology and anatomy*. Philadelphia: F.A. Davis Company, 5th ed., 2011.
- [21] Morphopedics, "Physical therapy management of colles fracture." <http://morphopedics.wikidot.com/physical-therapy-management-of-colles-fracture>. [Online; accessed 2014-07-02].
- [22] N. Özkaya, M. Nordin, D. Goldsheyder, and D. Leger, *Fundamentals of biomechanics: equilibrium, motion, and deformation*. Springer Science & Business Media, 2012.
- [23] Wikipedia, "Synovial joint," 2015.
- [24] F. W. Werner, J. K. Green, W. H. Short, and S. Masaoka, "Scaphoid and lunate motion during a wrist dart throw motion 1, 2," *The Journal of hand surgery*, vol. 29, no. 3, pp. 418–422, 2004.
- [25] I. Pearson Education, "Antagonist muscle definition." <http://ushcgshots.com/articles/antagonist-muscles>, 2013. [Online; accessed 2014-12-05].
- [26] R. V. Gonzalez, T. S. Buchanan, and S. L. Delp, "How muscle architecture and moment arms affect wrist flexion-extension moments," *Journal of biomechanics*, vol. 30, no. 7, pp. 705–712, 1997.
- [27] W. R. Brough, "Body basics." <http://waergo.com/JES/BodyBasics.htm>. [Online; accessed 2015-08-02].

- [28] K. An, "Kinematic analysis of human movement," *Annals of biomedical engineering*, vol. 12, no. 6, pp. 585–597, 1984.
- [29] "Euler angles," 2015.
- [30] N. Ho, "Decomposing and composing a 33 rotation matrix," 2015.
- [31] S. Widnall, "Vectors, matrices and coordinate transformations." <http://ocw.mit.edu>. [Online; accessed 2014-04-13].
- [32] B. R. Burroughs, B. Hallstrom, G. J. Golladay, D. Hoeffel, and W. H. Harris, "Range of motion and stability in total hip arthroplasty with 28-, 32-, 38-, and 44-mm femoral head sizes: an in vitro study," *The Journal of arthroplasty*, vol. 20, no. 1, pp. 11–19, 2005.
- [33] J. E. L. Grohmann, "Comparison of two methods of goniometry," *Physical therapy*, vol. 63, no. 6, pp. 922–925, 1983.
- [34] R. Wood, "Top end sports: Flexibility testing using a goniometer." <http://www.topendsports.com/testing/tests/goniometer-flex.htm>. [Online; accessed 2015-03-30].
- [35] T. Connection, 2015.
- [36] M. El-Gohary and J. McNames, "Shoulder and elbow joint angle tracking with inertial sensors," *Biomedical Engineering, IEEE Transactions on*, vol. 59, no. 9, pp. 2635–2641, 2012.
- [37] P.-G. Jung, S. Oh, G. Lim, and K. Kong, "A mobile motion capture system based on inertial sensors and smart shoes," *Journal of Dynamic Systems, Measurement, and Control*, vol. 136, no. 1, p. 011002, 2014.
- [38] H. Long, *An advanced human motion image tracking algorithm of Gaussian model*. Taylor & Francis Group, 2015.
- [39] J. M. Wang, D. J. Fleet, and A. Hertzmann, "Gaussian process dynamical models for human motion," *Pattern Analysis and Machine Intelligence, IEEE Transactions on*, vol. 30, no. 2, pp. 283–298, 2008.
- [40] D. J. Fleet, *Motion Models for People Tracking*. Springer, 2011.
- [41] E. Machida, M. Cao, T. Murao, and H. Hashi, "Human motion tracking of mobile robot with kinect 3d sensor," in *SICE Annual Conference (SICE), 2012 Proceedings of*, pp. 2207–2211, IEEE, 2012.
- [42] L. Gurry, "The eyes, ears and brain of the all new kinect," 2013.
- [43] D. D. Frantz, A. Wiles, S. Leis, and S. Kirsch, "Accuracy assessment protocols for electromagnetic tracking systems," *Physics in medicine and biology*, vol. 48, no. 14, p. 2241, 2003.

- [44] Z. Yaniv, E. Wilson, D. Lindisch, and K. Cleary, "Electromagnetic tracking in the clinical environment," *Medical physics*, vol. 36, no. 3, pp. 876–892, 2009.
- [45] G. Welch and E. Foxlin, "Motion tracking survey," *IEEE Computer graphics and Applications*, pp. 24–38, 2002.
- [46] ioTracker, "Basic principles of optical tracking," 2013.
- [47] R. Khadem, C. C. Yeh, M. Sadeghi-Tehrani, M. R. Bax, J. A. Johnson, J. N. Welch, E. P. Wilkinson, and R. Shahidi, "Comparative tracking error analysis of five different optical tracking systems," *Computer Aided Surgery*, vol. 5, no. 2, pp. 98–107, 2000.
- [48] T. A. Forman, S. K. Forman, and N. E. Rose, "A clinical approach to diagnosing wrist pain," *Am Fam Physician*, vol. 72, no. 9, pp. 1753–1758, 2005.
- [49] R. Rønning, I. Rønning, T. Gerner, and L. Engebretsen, "The efficacy of wrist protectors in preventing snowboarding injuries," *The American Journal of Sports Medicine*, vol. 29, no. 5, pp. 581–585, 2001.
- [50] J. A. Stevens, "Falls among older adults risk factors and prevention strategies," *Journal of safety research*, vol. 36, no. 4, pp. 409–411, 2005.
- [51] C. E. Dunning, C. S. Lindsay, R. T. Bicknell, S. D. Patterson, J. A. Johnson, and G. J. King, "Supplemental pinning improves the stability of external fixation in distal radius fractures during simulated finger and forearm motion," *The Journal of hand surgery*, vol. 24, no. 5, pp. 992–1000, 1999.
- [52] D. Osada, S. F. Viegas, M. A. Shah, R. P. Morris, and R. M. Patterson, "Comparison of different distal radius dorsal and volar fracture fixation plates: a biomechanical study," *The Journal of hand surgery*, vol. 28, no. 1, pp. 94–104, 2003.
- [53] S.-J. Kim and C.-H. Cho, "2.4 mm volar locking compression plate for treatment of unstable distal radius fractures," *Journal of the Korean Fracture Society*, vol. 24, no. 2, pp. 151–155, 2011.
- [54] eOrthopod, "Artificial joint replacement of the wrist: A patient's guide to artificial joint replacement of the wrist." <http://www.eorthopod.com/artificial-joint-replacement-of-the-wrist/topic/4>, 2013. [Online; accessed 2015-08-30].
- [55] S. Fischli, *Simulation of wrist kinematics on the basis of a rigid body spring model*. Canadian theses, 2007.
- [56] F. Fraysse, J. J. Costi, R. M. Stanley, B. Ding, D. McGuire, K. Eng, G. I. Bain, and D. Thewlis, "A novel method to replicate the kinematics of the carpus using a six degree-of-freedom robot," *Journal of biomechanics*, vol. 47, no. 5, pp. 1091–1098, 2014.
- [57] K. Group, "A 6 dof stewart platform," 2013.

- [58] M. Nishiwaki, M. Welsh, B. Gammon, L. M. Ferreira, J. A. Johnson, and G. J. King, "Volar subluxation of the ulnar head in dorsal translation deformities of distal radius fractures: An in vitro biomechanical study," *Journal of orthopaedic trauma*, vol. 29, no. 6, pp. 295–300, 2015.
- [59] M. Nishiwaki, M. Welsh, B. Gammon, L. M. Ferreira, J. A. Johnson, and G. J. King, "Distal radioulnar joint kinematics in simulated dorsally angulated distal radius fractures," *The Journal of hand surgery*, vol. 39, no. 4, pp. 656–663, 2014.
- [60] S. Erhart, W. Schmoelz, and M. Lutz, "Clinical and biomechanical investigation of an increased articular cavity depth after distal radius fractures: effect on range of motion, osteoarthritis and loading patterns," *Archives of orthopaedic and trauma surgery*, vol. 133, no. 9, pp. 1249–1255, 2013.

Chapter 2

Development & Validation of an Active Motion Wrist Simulator

OVERVIEW: This chapter covers the methods employed to develop a wrist motion simulator platform capable of passive and active motion simulation. It includes hardware selection, controller design, and methods used to recreate motion profiles. Using five human cadaver upper limbs, a comparative analysis of active versus passive manipulation techniques was performed to test the repeatability of motion between inter-trial and inter-specimen motions.

(A portion of this work has been presented at the 2015 Vancouver Canadian Orthopaedic Research Society (CORS) conference.)

2.1 Introduction

In-vitro wrist kinematic research enables investigators to achieve a greater insight into the behaviours of individual bones and muscles during motion that would otherwise be unattainable from living patients. The most common method of reproducing *in-vitro* wrist motion is through *passive manipulation* of cadaver specimens, most commonly obtained by direct manipulation from an investigator or an actuator. This method is desirable due to the simplicity of apparatus design required and does not require complicated control algorithms to achieve results. The alternative method is *active manipulation* which differs from *passive* in the mechanisms of generating motion; actuators are attached directly to the tendon insertions at the wrist to achieve the desired motion. This method is significantly more complicated to implement successfully but has the potential to produce much more repeatable and relevant results when modeling *in-vivo* conditions than passive simulators.

As outlined in Chapter 1 (Section 1.8.2.1), *passive manipulation* provides the simplest means for reanimating cadaver limbs for the investigation of wrist kinematics as the muscles may be toned simply by attaching pneumatic actuators or hanging weights from the major muscles of interest (discussed later). The drawbacks to *passive manipulation* are to produce undesirable motions as a result of the application of external forces and the general inability of human investigators to outperform machine repeatability. First, there is no guarantee that natural motion is being achieved as minor translations of one bone relative to another, due to external forces, may render all data collected irrelevant. Using a human investigator will undoubtedly introduce irregularities between subsequent trials decreasing overall system repeatability with respect to variables as rate-of-motion and pathway variance. These subtle differences in the rate of motion or inconsistent translations of bones between trials become an issue when considering the viscoelastic tendencies of the tissues present in the wrist and may result in inconsistent kinematics due to hysteresis. Nishiwaki *et al.* [1, 2] developed a method of passive manipulation that used a manifold of computer controlled pneumatic actuators driving cables guided through a series of pulleys to maintain specific tones on the tendons of interest. All motion trials were induced by the investigator through a rigid pin protruding distally from the third metacarpal.

A 6 DOF Stewart platform was developed and shown to produce repeatable passive manipulation which eliminates human error from the trials but this approach is still at risk of producing unnatural wrist motions [3].

Active manipulation of a specimen will ultimately approximate *in-vivo* conditions more accurately as many of the inconsistencies that arise from external forces and fluctuations in trial repeatability are eliminated or significantly reduced. All forces applied to the wrist should be true to their anatomical lines of action present *in-vivo* from their insertion at the wrist to their origins at the epicondyles of the elbow. Dunning *et al.* [4] developed an open loop active motion platform that used a manifold of the pneumatic actuators attached to the distal musculotendinous junction of the nine muscles of interest to induce motion. The cadaver specimen was mounted in a horizontal position and the computer controlled tendon loading parameters were activated to produce motion of the wrist against gravity. The system was able to produce motion but there was no guarantee that successive trials would follow the same motion profile or angular rate of rotation. As demonstrated by Werner *et al.* [5], a simulator that reproduces motion by directly manipulating the major muscles of the wrist can provide a more reliable quantification into the subtle behaviour of the carpal bones within the dynamic wrist. However, some drawbacks to Werner's most recent version of the simulator [6] are the inability to investigate the effects of gravity on wrist kinematics and electromagnetic tracking limits the list of compatible materials that can be used in proximity to the simulator.

In order to accurately model conditions of an *in-vivo* wrist for the full investigation of kinematics, a simulator must be designed to limit the known errors associated with passive manipulation while building on the existing simulators that have pioneered the field of active wrist motion over the past two decades. Hence, the objective of this study was to develop a reliable method for testing wrist specimens for common surgical techniques and prosthetics that include, but are not limited, to fracture fixation, ligament repair, and arthroplasty.

2.2 Methods

2.2.1 Simulator Development

2.2.1.1 Platform Design

A single degree of freedom (1 DOF) platform was constructed from Derlin[®] (DuPont, Eleutherian Mills, DE) to allow for three attainable positions of a cadaver specimen including *neutral gravity* (forearm vertical), *gravity flexion* (forearm horizontal, flexion against gravity), and *gravity extension* (forearm horizontal, extension against gravity). The base of the platform attaches to the rotating frame via two cylindrical support blocks as illustrated in Figure 2.1 and are locked in position using a dowel pin. The simulator was balanced using CAD software (SolidWorks, MA) so that it would balance in place to reduce possible injury or pinch hazards due to a tendency to swing upon removing the dowel pin. This platform provides the underlying structure required to successfully achieve active manipulation of cadaver specimens as seen in Figure 2.1. The material is non-porous and abides by all health and safety requirements for equipment within a laboratory that handles biohazardous material.

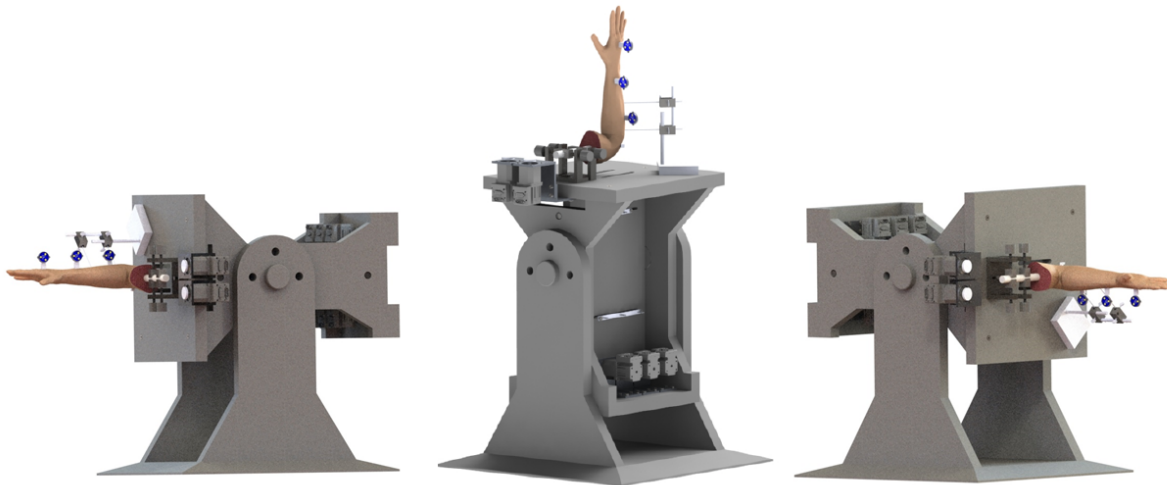


Figure 2.1: The DuPont™ Derlin[®] platform allows for three attainable position positions: *gravity neutral* (right), *gravity extension* (top left), and *gravity flexion* (bottom left).

2.2.1.2 Motor Manifold

To manipulate the position of the wrist and forearm seven muscles were required for full control as were reviewed in Chapter 1 (Section 1.1.4 and Figure 1.7): *extensor carpi radialis brevis (ECRB)*, *extensor carpi radialis longus (ECRL)*, *extensor carpi ulnaris (ECU)*, *flexor carpi radialis (FCR)*, *flexor carpi ulnaris (FCU)*, *pronator teres (PT)*, and *biceps brachii (BI)*. To provide forces to these muscles a manifold of seven SmartMotors (SM2316D-PLS2, SMI Animatics Corp., CA) were attached to the platform and daisy chained through the RS232 serial port on the data acquisition chassis (NI PXI 1050, National Instruments, Austin, TX). Motors were controlled through a LabVIEW (National Instruments, Austin, TX) interface and spooled to control the magnitude of forces applied to muscle-tendon units via suture. Factory tuning for the motors were left unaltered as they provided satisfactory response time between motor positions.

2.2.1.3 Force Transducers

Force transducers (Figure 2.2) were implemented onto each of the aluminum motor mounts to gain force feedback from each motor. Each motor mount was fitted with two 90 degree strain gage rosettes to create a full bridge (Full Bridge III) style force transducer that converts the bending moment of the motor mount into change in resistance. All force transducers were calibrated using an in-line 1DOF load cell (Vishay Precision Group, Raleigh, NC) (Appendix B). The force transducers were connected to the NI SCXI module on the data acquisition board and read into a custom LabVIEW program for the simulator.

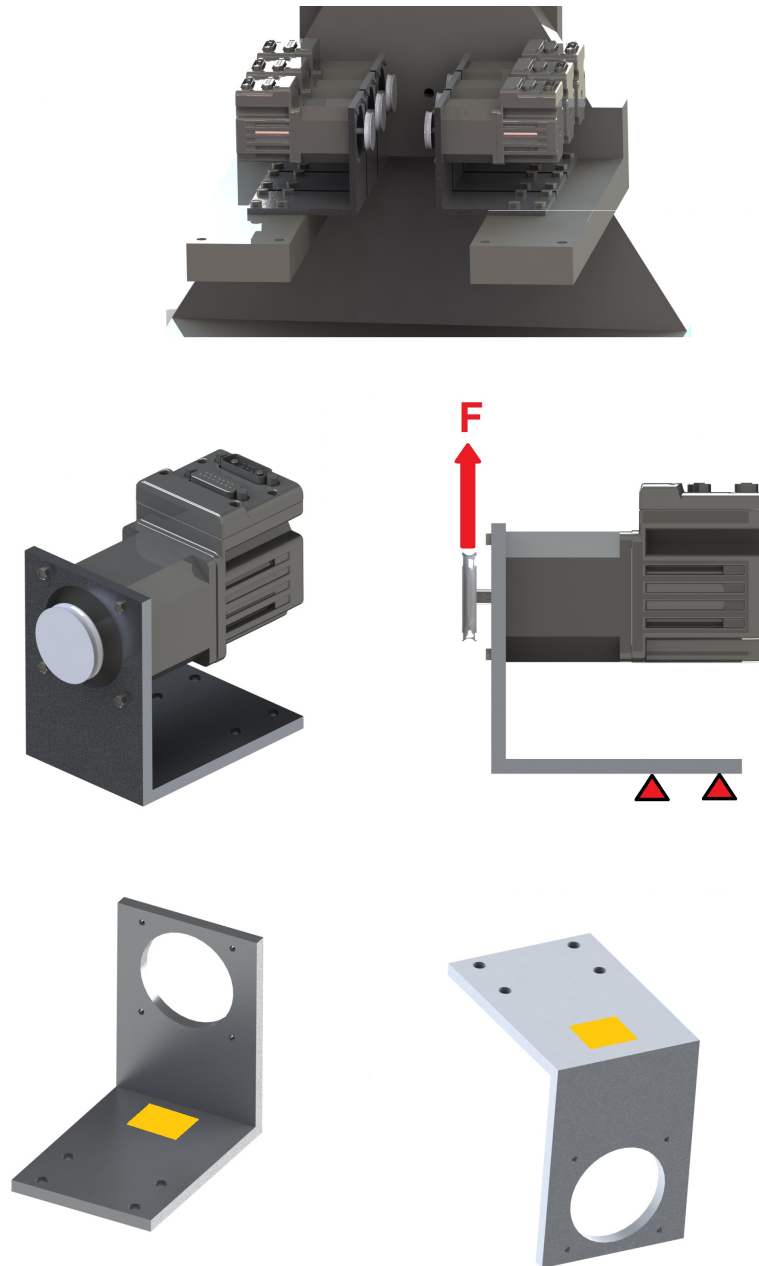


Figure 2.2: Motor manifold showing the arrangement of the 6 servomotors [top] (biceps brachii motor not shown) below the top surface of the simulator platform. A free body diagram [middle] represents the mount as a cantilever beam with rigid attachments [red triangle] and tendon force producing a bending moment through the beam,. The placement of the two tee rosette strain gages [orange squares] is shown on the top and bottom surfaces of the aluminum bracket [bottom].

2.2.1.4 Cable Guide Rail

Guide blocks with ceramic guide pins in conjunction with epicondyle guides were used to converge the suture lines from the motor manifold as they approached the specimen and closely mimic the anatomically correct line of actions present *in-vivo* (Figure 2.3). The guide blocks ensured that the suture lines maintained a perpendicular vector to the motors so as to not deviate from the calibrated state, and directed the cables to a narrower channel applying as little resistance at each junction as possible. The epicondyle guides are Delrin® blocks that fix to the lateral and medial epicondyles of the humerus (to mimic the origins of the FCR, FCU, ECRL, ECRB, and ECU) with three cable slots each to guide the sutures through their approximate anatomical origins.

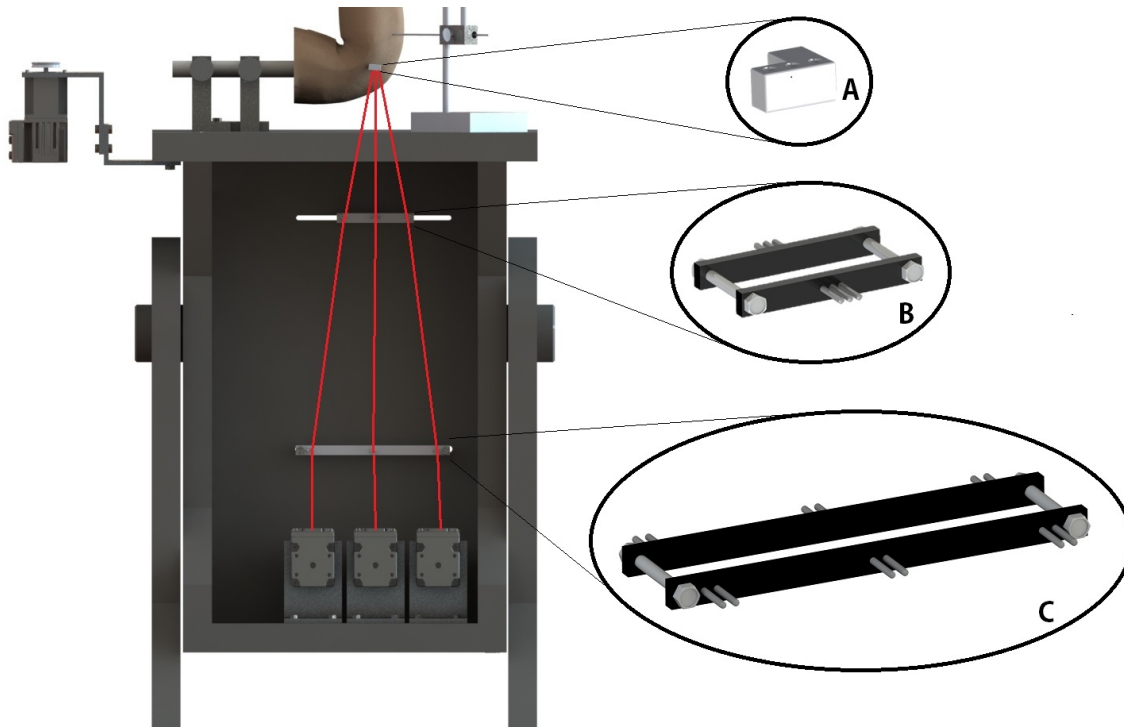


Figure 2.3: Three stage cable guide system acts to converge the sutures (red) from the motor manifold through the lower guide rail [C], upper guide rail [B], to the epicondyle guides [A] on the specimen

2.2.1.5 Humeral Clamp

A clamp was designed to rigidly fix the specimen to the simulator by gripping the exposed humerus in a vice like device (Figure 2.4). Four adjustable screws with semi-circular end blocks were used to applied force radially at two points on the humeral shaft to effectively create a cantilevered beam; two points of contact were required to prevent rotation from generated moments from the motor forces. Machined teeth on the inner radius of the end effectors act to prevent axial rotation of the specimen during the investigation (Appendix C).

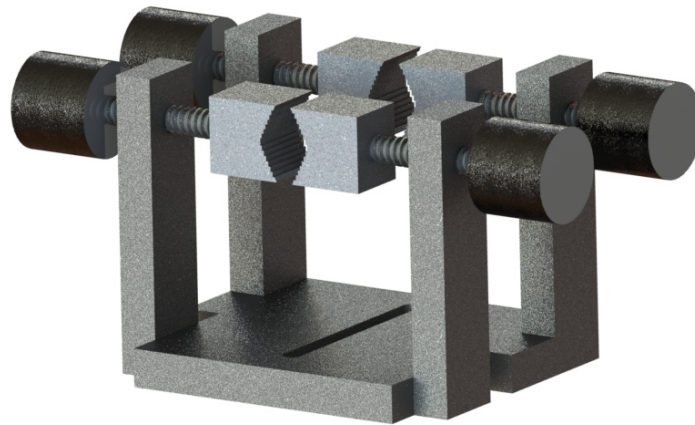


Figure 2.4: *A four screw cylindrical vice for rigidly attaching a cadaveric specimen to the surface of the simulator via the humerus*

2.2.1.6 Ulnar Support Tower

To maintain the cadaver specimen in 90 degrees of elbow flexion during the investigation, two pins were inserted in the ulna at proximal and distal thirds of the shaft extending perpendicular in the ulnar direction. Since the ulna has a stable articulation with the humerus and remains relatively stationary with negligible rotation during pronation and supination it can be assumed that rigidly fixating the ulna to the simulator will have no affect on DRUJ kinematics [7, 8]. A 4DOF *ulna support tower* , 1DOF rotation & 1DOF translation per block, attaches to the ulnar pins allowing for an adjustable base as shown in Figure 2.5 (Appendix C).



Figure 2.5: *Ulnar support tower with two pins to rigidly fix the ulna to the simulator base; refer to Figure 2.1 for the orientation of the ulnar support with respect to the arm*

2.2.1.7 Passive Guide Rail

An adjustable steel guide rail system with a slot to house the passive metacarpal guide pin was developed to further increase the repeatability of passive trials. At the beginning of each new position the guide rail was adjusted for height and neutral wrist position to ensure that planar motion was maintained. An array of light emitting diodes (LED), controlled from a microcontroller (Arduino, Italy), spaced evenly along the guide rail at 10° increments further aided the repeatability of passive manipulation motion trials and reduced errors from environmental stimulus. The LED array was illuminated sequentially to provide the investigator a constant rate of angular rotation between trials to improve overall performance during passive trials (Figure 2.6).

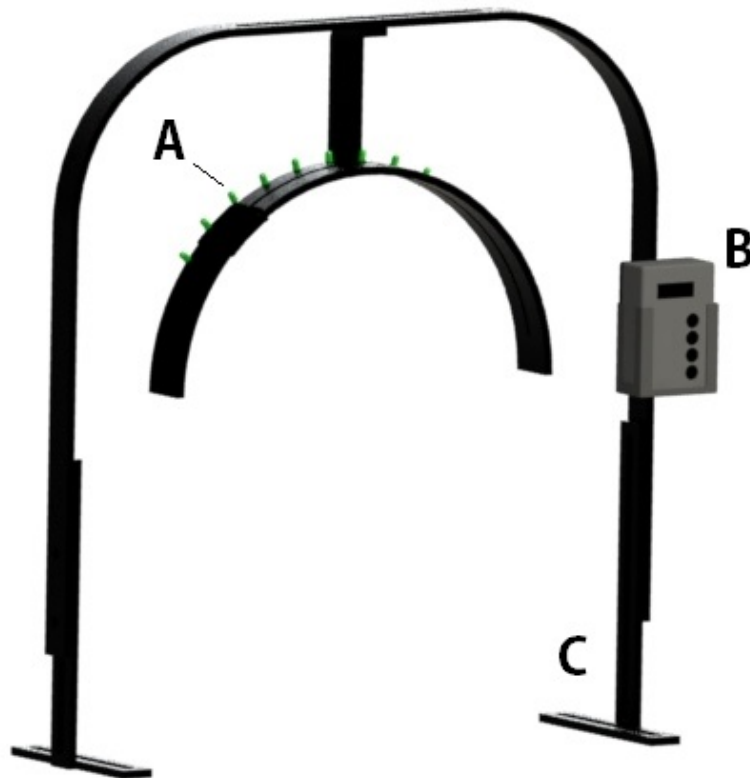


Figure 2.6: A guide rail system for passive motion trials that limits motion to a single plane. The track is equipped with an array of LEDs [A], connected to an Arduino microcontroller [B] mounted to the steel frame [C] that light up at a specified rate as a reference for the investigator

2.2.2 Control Algorithm Development

2.2.2.1 Force Controller Development

A method for reducing system error with respect to a set point is to use a proportional-integral-derivative controller (PID controller) that takes a series of input parameters consisting of a target value and current system values and output parameters which effect the behaviour of the system. Two types of PID controllers are open and closed loop. Open loop controllers operate without feedback from the system and tend to be unreliable or unrepeatable, while closed loop controllers continuously acquire system data. A closed loop PID force controller was developed to allow each motor to maintain a target load for a designated muscle. Input parameters were the current position of each motor and the calibrated force from the array of strain gages. The output parameter was a change in motor position, acting to spool in the cable to increase force and spool out to decrease the force. The system set point was an array of individual muscle forces for each motor to maintain.

Heuristic tuning was used to gain the appropriate responses from the motors that requires a series of steps that required tuning for a purely proportional (P controller), proportional-derivative (PD controller), and final the full controller. The proportional term, K_p , was scaled until the system oscillated continuously about the target point without growing or shrinking when under steady load. The derivative term, K_d was added to reduce system oscillation and achieve steady state, however not necessarily zero system error. Finally, the integral term, K_i was added to reduce steady state error and allow for the system to achieve the target force. The sum of these terms effect the system behaviour and are represented in a PID diagram in Figure 2.7.

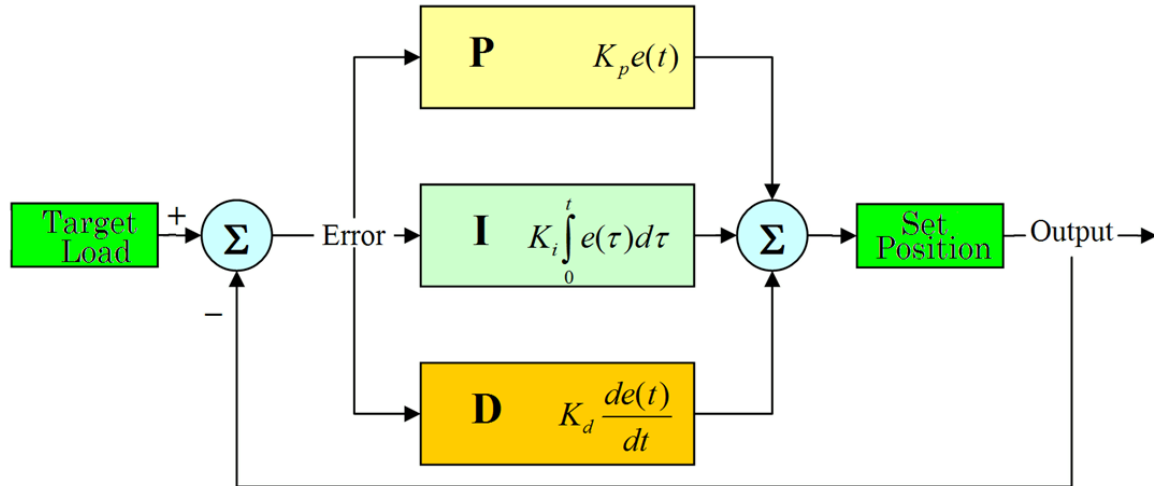


Figure 2.7: Closed loop PID controller to maintain target loads (set point) on each muscle based on input from the current motor position and strain gage force and effecting the motor position to increase/decrease force on the motor.

2.2.2.2 Position Controller Development

The conventional method of tracking wrist motion is to compare the position of the third metacarpal with respect to the radius to determine *flexion-extension motion* (FEM) and *radial-ulnar deviation* (RUD), and the radius with respect to the ulna to determine *pronation-supination motion* (PSM). Optical triad-cluster trackers (Certus Optotrak, Northern Digital Inc., VT) were attached to the third metacarpal, radius, and ulna to obtain their relative positions in real time during the investigation. Using digitized skin points from the specimen and a custom LabVIEW program, a local coordinate system per bone was constructed that adhered to the ISB standards (refer to Appendix A for the construction of ISB coordinate systems used for tracking).

Euler angles between the third metacarpal, radius, and ulna were decomposed in real time and paired with the target angles as the input parameters for the position PID controller as shown in Figure 2.8. The output was interpreted as a shift in force balance between antagonistic muscle groups that were categorized into quadrants of overlapping muscles: *flexors* (FCU/FCR),

extensors (ECRL/ECRB/ECU), *radial & ulnar deviators* (FCR/ECRL & FCU/ECU). By maintaining minimum loads of 8.9 N [5] in groups resisting motion and increasing the magnitude of groups aiding in motion the force imbalance result moved the wrist in the desired direction.

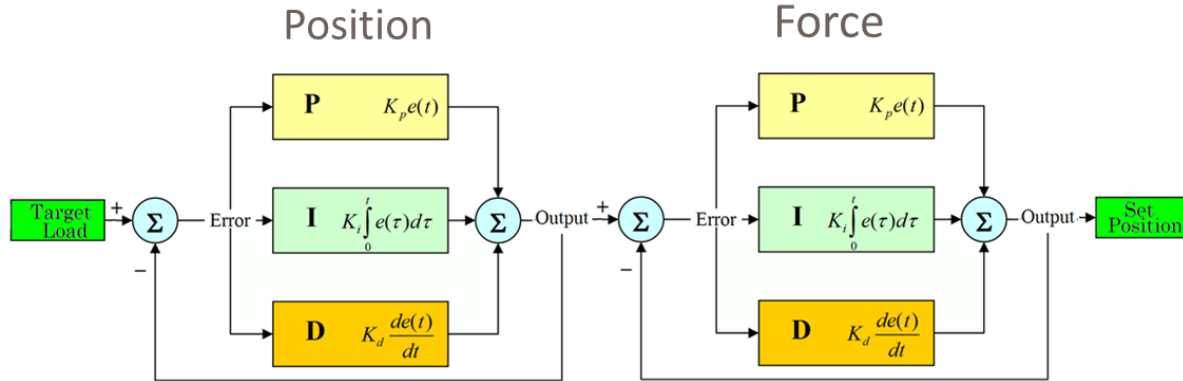


Figure 2.8: Cascading closed loop PID controller for the control of wrist position. An initial PID controller sets the force offsets required to induce motion and passes its output the force PID controller to coordinate the new force offsets.

The force feedback controller used for maintaining tone loads was a cascading loop responsible for adjusting the motor position to follow the fluctuating target tone loads of corresponding antagonistic quadrants to reduce positional error. For instance, a target angle of 10 degrees radial deviation and 20 degrees flexion with the wrist currently in neutral would result in an increase of the flexor and radial deviator groups' target forces while dropping the *extensor* and ulnar deviator groups' target to their minimum of 8.9 N. This shift in muscle force would result in an acceleration of the wrist in the desired direction to reduce the error between the target and actual wrist angle. Motion was achieved by running a script in the LabVIEW program to continually update the target angles at a desired rate.

2.2.3 Clinical Evaluation of the Active Motion Simulator

Five fresh frozen cadaver upper extremities, average age 70 ± 16 years (55 to 79 years, 3 male) were amputated at the mid-humeral level and attached to the simulator via the *humeral clamp* and the *ulna support tower* to maintain elbow position at 90 degrees flexion. To preserve the natural function of the arm and avoid tissue desiccation all soft tissue was left intact. Krackow sutures (#2 Ethibond) were placed on the distal musculotendinous junctions of each of the muscles involved in motion (Figure 2.9). Sutures of the flexors, extensors and *pronator teres* were passed under the skin, parallel to their muscle bellies, to their insertions at the lateral and medial epicondyles of the humerus and the biceps was oriented parallel to the humerus and attached to a satellite motor. The *biceps brachii* and *pronator teres* muscles were neglected for this investigation as they were each toned to 45.0 N and locked at neutral forearm rotation.

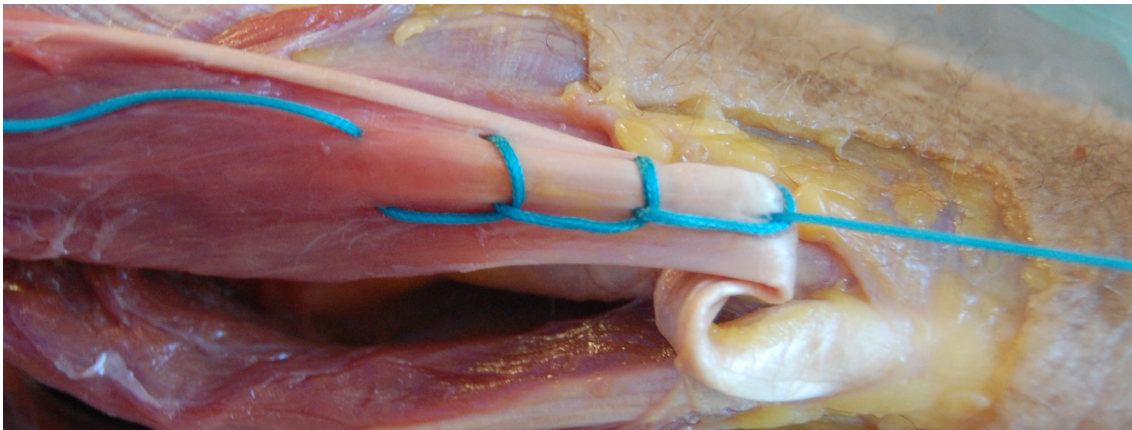


Figure 2.9: *Krackow suture made to the distal musculotendinous junction of each tendon to transfer forces from the servo motor manifold to the wrist*

Cable guides were anchored to the bone on both the lateral and medial epicondyles where the suture lines passed through to recreate and maintain the physiological lines of action throughout the study. The sutures were linked to their corresponding motors responsible for maintaining muscle tone loads. All skin incisions were sutured using techniques employed clinically, and remained closed through the duration of the study to preserve the specimen's natural fluids. Wrist positions were tracked in real time using active optical trackers attached to the ulna, radius and third metacarpal.

2.2.3.1 Motion Trials

The performance of the simulator was thoroughly assessed in the gravity neutral position as it is the most common among researchers [5, 9] (the kinematic effects between gravity loaded positions are thoroughly analyzed in Chapter 3). Five motion cycles were performed through the full range of flexion-extension and radioulnar deviation to ensure the wrist was performing under identical circumstances; an additional cycle at the beginning was discarded to eliminate undesirable behaviour associated with the onset of initial motion. Motion trials were performed at approximately $5^\circ/\text{s}$ for both passive and active manipulation methods and ranged from 50 degrees flexion to 50 degrees extension and 15 degrees radial deviation to 20 degrees ulnar deviation while restricting out-of-plane motion. All trials were performed in the gravity neutral position as stated above since it is the most challenging of the three gravity positions to achieve motion due to the inherent instabilities associated with the inverted pendulum configuration. The guide rail (Section 2.2.1.7) was mounted for on the simulator for passive trials and calibrated to the specimen to ensure pure planar motion with minimal out-of-plane deviation. To reduce investigator errors, the LED array was programmed to activate sequential for the investigator to follow to provide the desired rate of motion. Active trials were performed independently of the guide rail with no restrictions to motion from any external apparatus or guide mechanism; all motion was controlled through the loading of the tendons.

2.2.3.2 Static Position Trials

To test the simulator's ability to reproduce a static position five trials were collected by moving the wrist in increments of ten degrees between the extremes in flexion-extension and radioulnar deviation. Passive trials followed the LED array on the guide rail to maintain consistency between trials, and active motion was dependent on the positional feedback from the optical trackers. To account for subtle fluctuations in motion, a sample period of three seconds in each position was recorded and averaged to a single point for each trial.

2.2.3.3 Center of Rotation Algorithm

A three dimensional fitting algorithm for matching points to a circle of best fit was adapted from an online source in accordance to the Berkeley Software Distribution (BSD) license [10]. From three points in space two vectors are created and normalized to determine a set of orthonormal vectors that define a reference plane. A centroid is established using root means square to determine a point with the lowest summed distance to all three points and returns the set of orthonormal vectors and radius of the circle (Figure 2.10). This process is applied through the range of data to determine the overall centroid of the range motion (Appendix D).

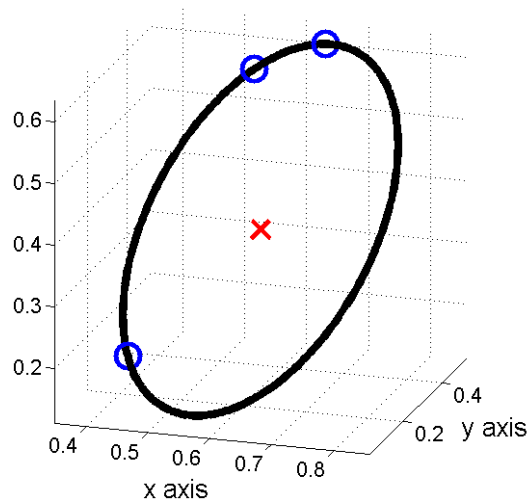


Figure 2.10: Circle fitting algorithm that matches three points [blue circles] in 3-dimensional space to a circle and returns the centroid [red x] and vectors defining the plane of best fit [10]

2.2.4 Outcome Variables & Statistical Analysis

The repeatability of motion passive and active trials was compared by reporting inter-trial average standard deviation (ASD) between specimens (N=5). A one-way (manipulation method) Repeated Measures ANOVA (RM-ANOVA) was performed to determine significant effects ($p < 0.05$) of actuation techniques on the profile trends of wrist motions collected from average motion profiles between trials.

2.3 Results

2.3.1 Repeatability of Motion Profiles

The accuracy of the simulator during active motion trials far outperformed the passive motion trials by approximately 12 times ($N=5$ specimens). The mean error for active motion trials did not exceed 0.23° while passive trials were high as 3.04° with an ASD of 0.25° and 1.54° respectively (Figure 3.2). Overall, the magnitude of mean errors during active motion were 9% of those present during passive motion and 16% the size for ASD. A one-way (manipulation method) RM-ANOVA test measuring mean error between trials showed significant difference between passive and active trials ($p<0.002$), however no difference was found between static trails ($p<0.05$).

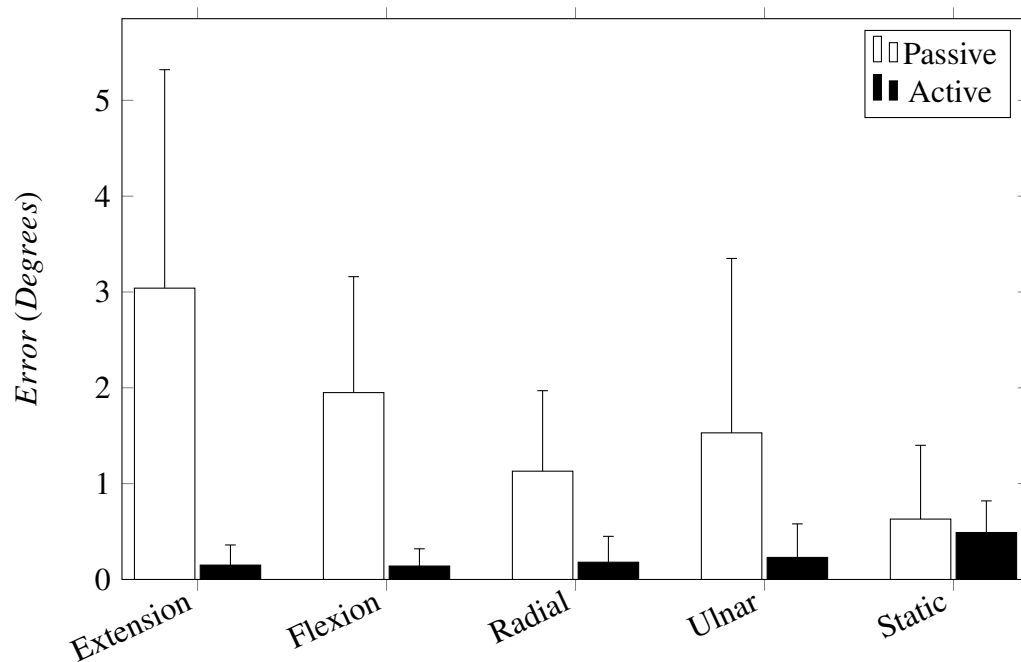


Figure 2.11: A comparison between the repeatability of static position and motion trials between passive [white] and active [black] manipulation methods. The data shows the overall mean error from trials and the standard deviation of mean errors between specimens ($N=5$).

2.3.1.1 FEM Motion Trials

The cycles were split into their individual motions and the leading 1 s of data was removed to eliminate disturbances present at the point of motion inversion. All five motion trials in flexion and extension were overlaid to present a visual representation of the consistency of performance for each method of actuation. Positive angles represent flexion and negative angles represent extension as presented in Figure 2.12. Passive motion trials were less repeatable than active as each individual trial is visible while the individual active trials are indistinguishable from one another.

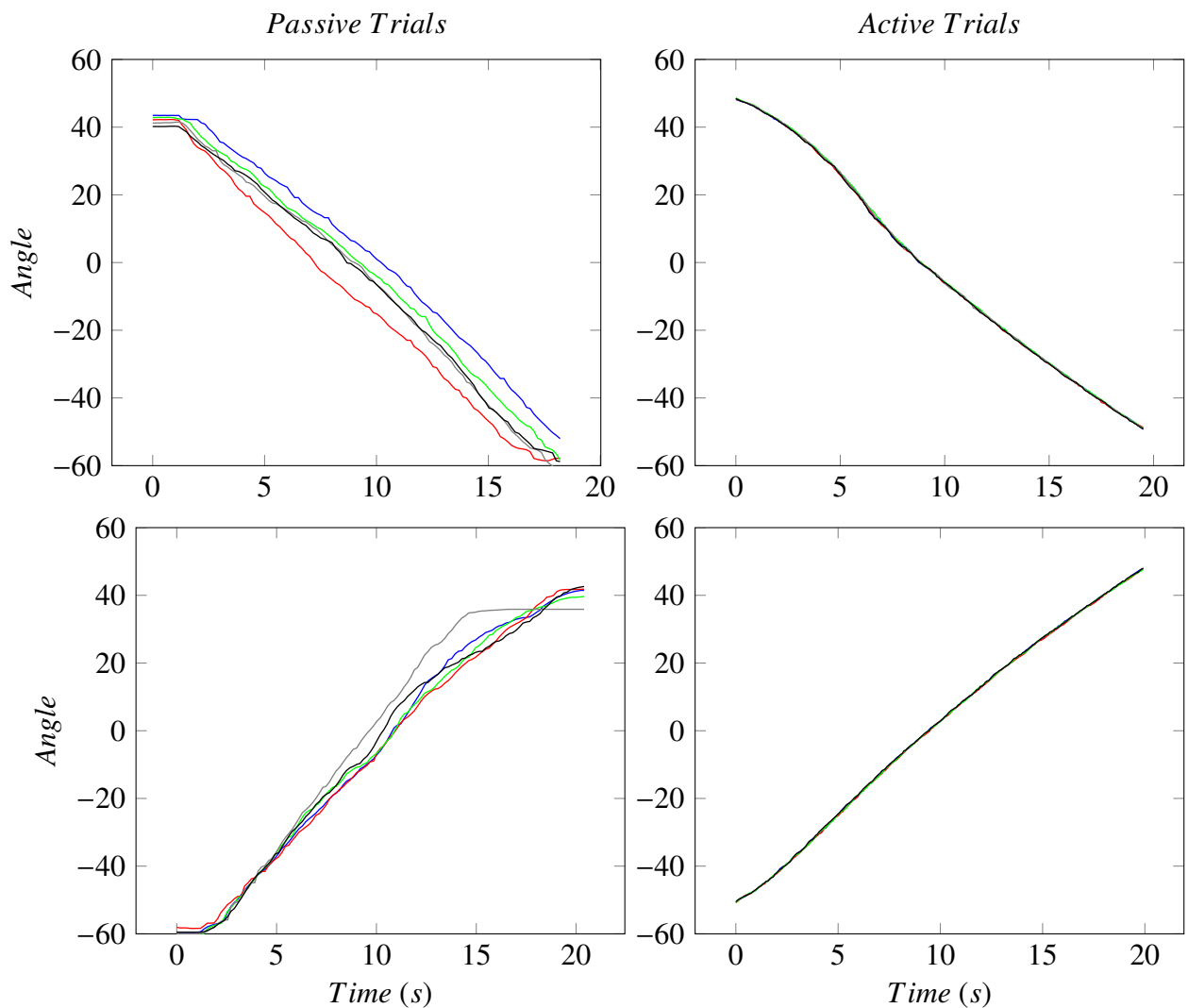


Figure 2.12: Repeatability of all passive [right] and active [left] motion trials for extension [top] and flexion [bottom] for a single specimen

2.3.1.2 RUD Motion Trials

The cycles were conditioned as previously mentioned for flexion-extension and overlaid on Figure 2.13 to present a visual representation of the consistency of performance for each method of actuation. Positive angles represent ulnar deviation and negative angles represent radial deviation with time along the horizontal axis. Again, passive motion trials were less repeatable than active motion trials as noticed by the correlation of data for both methods.

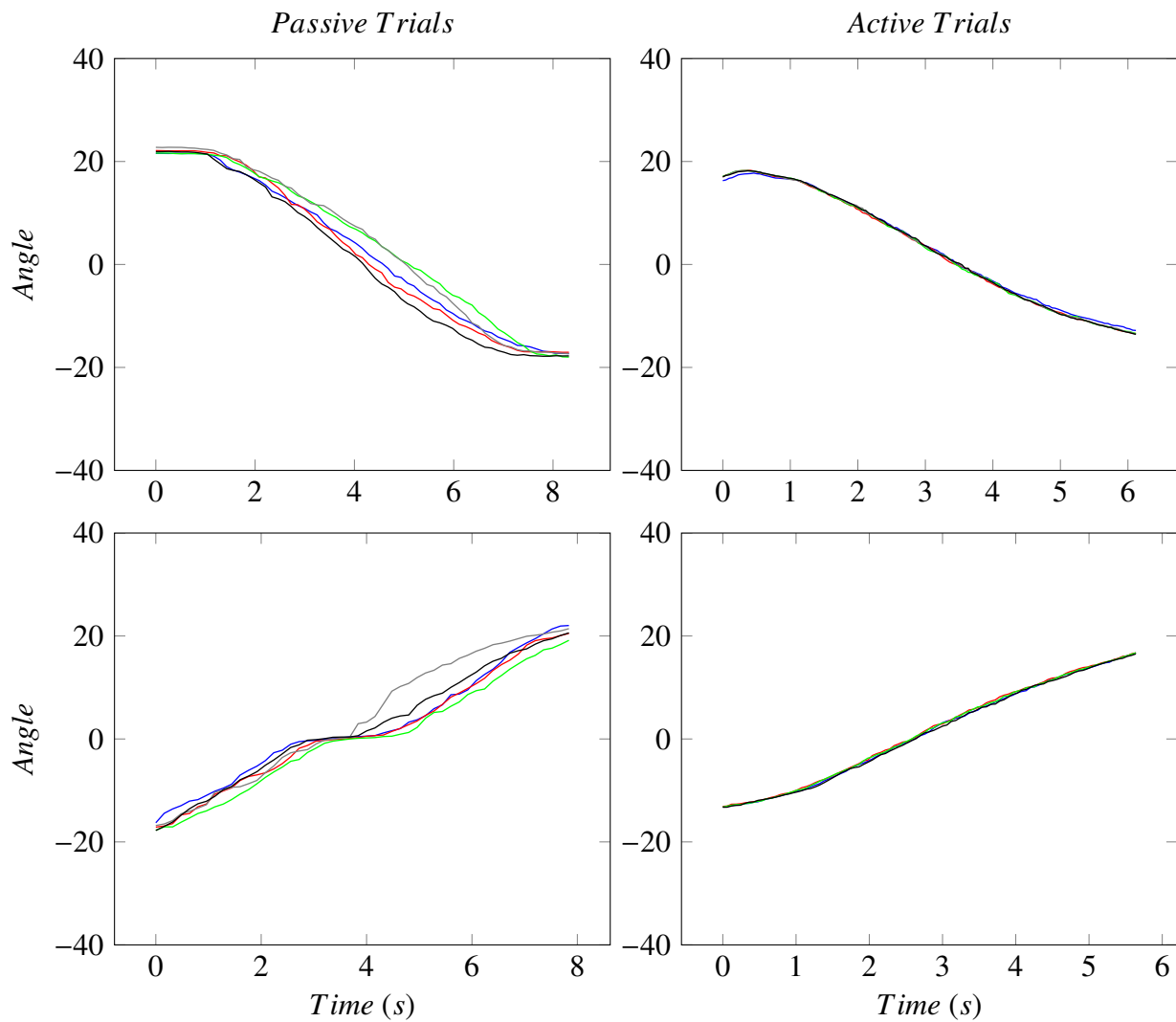


Figure 2.13: Repeatability of all active [left] and passive [right] motion trials for radial [top] and ulnar [bottom] deviation for a single specimen

2.3.1.3 Static Trials

Active trials were able to reproduce static positions marginally better than found in passive trials as shown in Figure 2.14 with exception to near neutral wrist positions in FEM. Note that three of the specimens were unable to achieve 20 degrees of radial rotation during active trials due to forces exceeding the safety limits of the simulator and therefore were excluded from the results. Overall, active trials were more effective at reproducing static positions than passive trials.

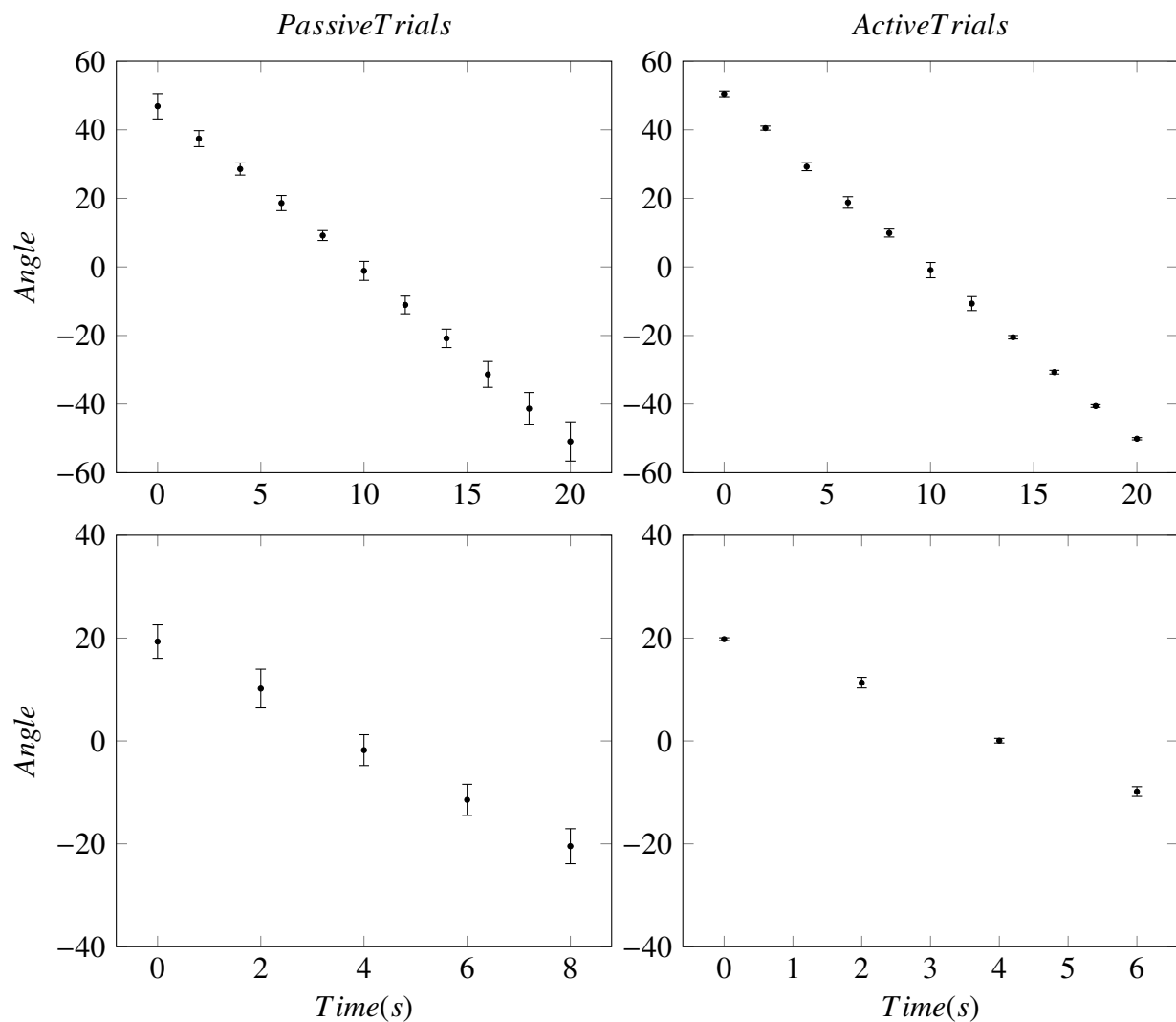


Figure 2.14: Repeatability of all active [left] and passive [right] trials in the FEM [top] and RUD [bottom] planes for a single specimen

2.3.2 Center of Rotation Repeatability

Using the 3D circle fitting algorithm to determine the *center of rotation* of each motion trial, with respect to the radial coordinate system, the mean error and standard deviation for each specimen was averaged to determine the overall average performance of the the simulator (Table 3.1). Active trials overall had a lower error and standard deviation than passive trials by 71.5% and 66.0% respectively in the FEM plane of motion with a mean error of 0.26 mm from the average COR (0.26 ± 0.18 mm & 0.90 ± 0.53 mm).

Table 2.1: Average center of rotation in all three gravity loaded positions (mm[SD])

	Passive	Active
Extension	0.55[0.31]	0.34[0.23]
Flexion	1.24[0.75]	0.17[0.13]

2.3.3 Repeatability of Tendon Forces

Any trends in the tones generated to produce the desired motion were a byproduct of the position-force controller during active manipulation trials. To maintain consistency with other investigators the reporting of tendon forces will cover peak forces during motion, and average forces required to maintain static positions [5]. Passive trials were neglected for this comparison as the tendons were maintaining minimum tone loads and therefore provided no insight on the behaviour of muscles during motion.

2.3.3.1 Static Trials

Trends in the tendon forces behaved as expected during static position trials for active motion with muscles responsible for motion in the related direction having larger magnitudes than their antagonist pair. Table 2.2 displays the average muscle forces required to maintain the extreme positions in each plane of motion in the gravity neutral position. Note that the differences in percent contribution between positions in FEM was relatively small since the wrist was stationary with gravity to assist in maintaining the position, while the differences between positions in RUD was much larger.

Table 2.2: Average of five specimens for muscle forces required to hold the wrist in a static position during active manipulation (percent of total muscle force [SD])

	FCR	FCU	ECRL	ECRB	ECU
<i>Gravity Neutral</i>					
50° of flexion	0.12[0.06]	0.18[0.01]	0.21[0.02]	0.21[0.01]	0.28[0.06]
50° of extension	0.22[0.12]	0.11[0.01]	0.32[0.07]	0.17[0.10]	0.18[0.10]
20° of radial deviation	0.21[0.04]	0.10[0.06]	0.31[0.07]	0.20[0.03]	0.20[0.03]
20° of ulnar deviation	0.06[0.03]	0.19[0.05]	0.20[0.03]	0.20[0.03]	0.34[0.02]

2.3.3.2 Motion Trials

The peak tendon forces from each motion were averaged amongst the five specimens and are shown in Table 3.3. The gravity neutral position is unique as it behaves as an inverted pendulum where the effects of gravity inverse as the wrist passes through neutral (vertical). This trend was observed most clearly for extension and flexion motions as the extensor and flexor tendon groups, respectively, displayed higher magnitudes of force while the opposing group maintained near minimum tones. During motions in the RUD plane subtle trends between the radial and ulnar deviator groups emerge with each group displaying greater magnitudes during its respective motion.

Table 2.3: Average peak tendon forces in the gravity neutral position during FEM and RUD planar motions of the wrist (N [SD])

	FCR	FCU	ECRL	ECRB	ECU
<i>Extension</i>	23.0[15.4]	20.7[8.8]	50.0[25.7]	39.9[15.2]	47.1[17.6]
<i>Flexion</i>	26.4[12.0]	21.3[4.5]	19.00[12.0]	13.1[3.6]	15.0[3.5]
<i>Radial</i>	40.6[15.9]	24.1[19.1]	57.34[20.8]	38.5[29.4]	53.8[47.7]
<i>Ulnar</i>	33.0[19.6]	32.0[15.5]	50.92[25.7]	38.5[29.5]	59.4[44.5]

The forces over two cycles of FEM and RUD motion trials are shown below in Figure 2.15 & 2.16. There are noticeable increases in the extensor and flexor muscle groups at the onset on motion during each of their respective motions, which subsides as the wrist passes neutral. The minor force increase in the flexor group at the onset of extension is the result of the transfer of force from the extensors through the wrist and to the flexors which is quickly compensated for by the force controller.

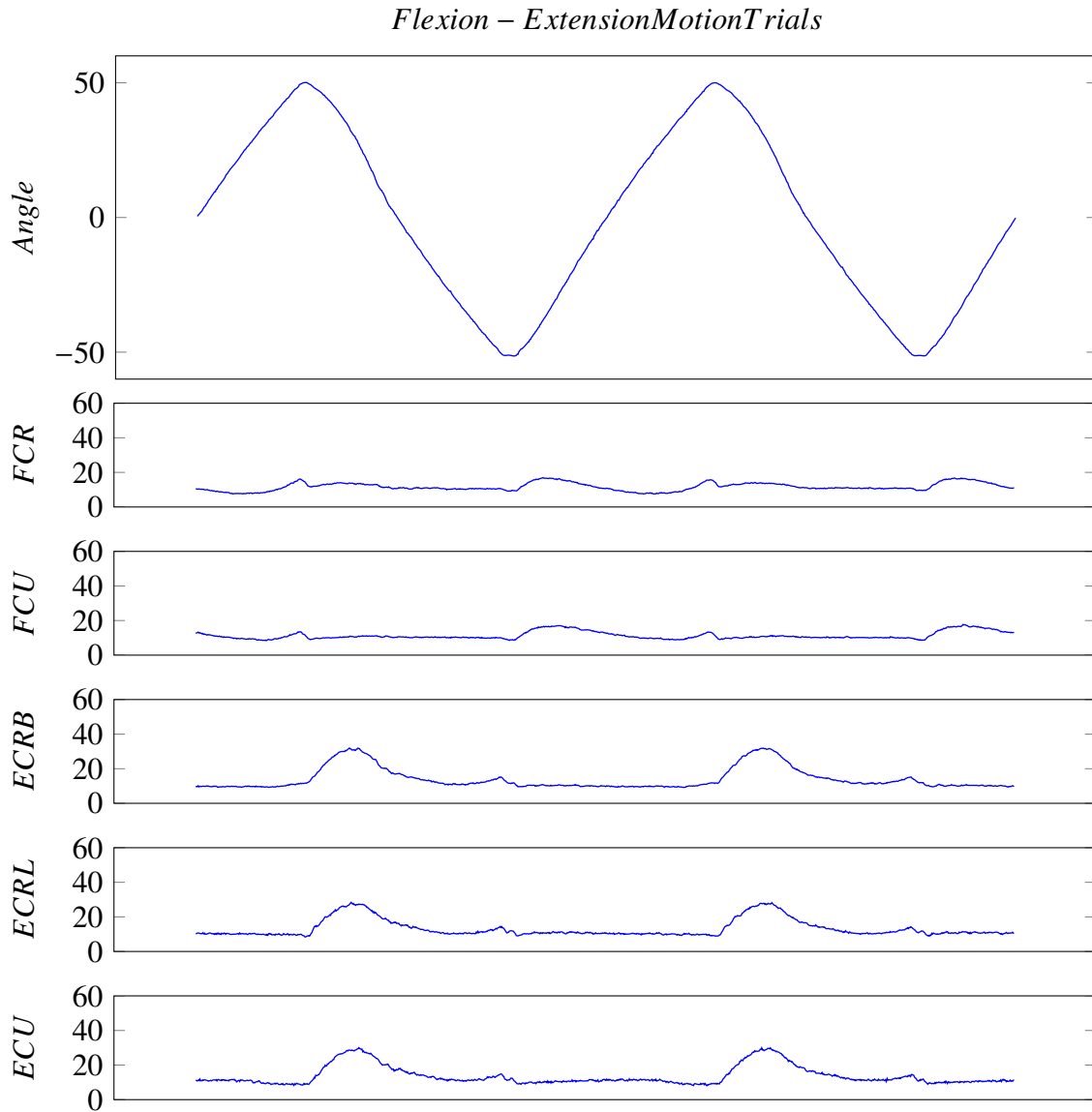


Figure 2.15: Tendon forces during active FEM motion (forces[N] in gravity neutral position). Two full cycles of motion are shown with positive angles representing flexion

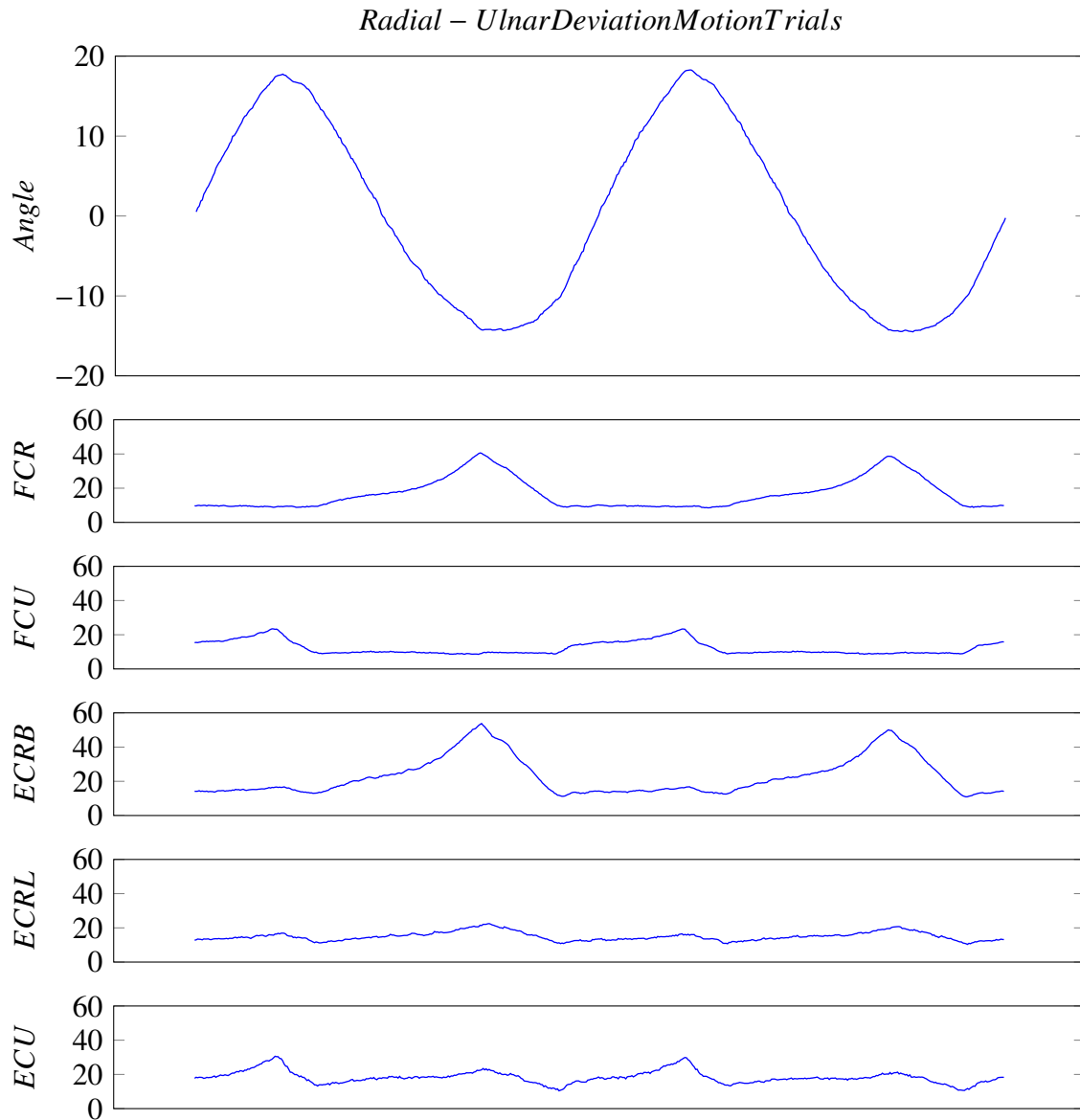


Figure 2.16: Tendon forces during active RUD motion (forces[N] in gravity neutral position). Two full cycles of motion are shown with position angles representing ulnar deviation

2.4 Discussion

The results from the wrist simulator were as expected with active motion trials greatly outperforming those from passive trials for both inter-specimen and center of rotation repeatability. It is important to note that the comparison of a computer-aided guidance system against a human investigator as the means of manipulating motion is an unfair match up, however it provides valuable reassurance to the use of an automated system for controlling the motion of the wrist to achieve low states of operational error.

The passive motion trials in this investigation were modeled after the simulator developed by Nikiwashi *et al.* with regards to method of manipulation and restraint to motion from a passive guide rail system. As there were no published results on the performance of this simulator, our passive motion data was assumed to be a suitable substitute. The significant increase in repeatability of active versus passive motion trials provides a clear indication of the benefits to using active manipulation methods to achieve motion. The major discrepancy between these simulators are the methods of actuation; pneumatic actuators are subject to positional errors due to the compressibility of air while servomotors are effectively rigid with negligible positional error.

Werner *et al.* reported forces necessary to hold the wrist in static positions through a range of circumduction using a clock position system for a right arm that related the 6 o'clock position to flexion and 3 o'clock to radial deviation [5]. The results between the two simulators are in strong agreement with percent contribution of the wrist extensors in these positions but larger magnitudes of error are present within the flexor group. These inconsistencies may be due to the absence of the APL in our simulator that would ultimately effect the contribution patterns of the flexors. This trend remained true for the maximum required tendon forces during cyclic FEM motion trials, with the flexor forces considerably lower than those reported by Werner. For cyclic RUD motion trials the results were larger than reported by Werner, with exception to the FCR and ECU, which again may be due to the absence of the APL or difference in controller logic. Discrepancies between the forces could result from apparatus interference

from redirecting suture cables through guide blocks and pulleys at large angles which would ultimately increase the system friction and required force unlike our current design.

Since there are no published reports on the effect of the method of wrist manipulation on the *center of rotation* during FEM motion trials there is no data to reference. However, the difference in COR error between methods validates the need for further investigation into translational errors associated with passive motion from the application of external forces to manipulate motion. The 'sloppy' behaviour exhibited during passive motion may be result of restricted tendon forces resulting in loads that are five times less than experienced during active motion. It should be noted that this difference in loading during passive motion is unrepresentative of *in-vitro* conditions and therefore kinematic investigations should use active motion when possible.

Due to the anatomy of the wrist the RUD motion profiles were incompatible with the center of rotation algorithm described in Section 2.2.3.3 which fits points along a curve in three dimensional space to a single centroid of motion. The nature of the wrist joint having two articulations, *radiolunate* and *radioscaphoid*, effectively generated two centroids which resulted in skewed and unrealistic data. The COR for RUD motions were neglected for this analysis.

Simulating motion with the wrist oriented in a vertical gravity loaded position models the behaviour of an inverse-pendulum which are inherently unstable due to the effects of gravity (as is discussed later in Chapter 3, Section 1). This instability was most apparent during static trials in the FEM plane with the wrist near neutral position because the standard deviations of mean error was noticeably larger than during larger angles of flexion or extension. This trend was not present during RUD mostly probably due to the dual points of contact of the wrist.

Limitations to this study worth noting arise from the use of elderly cadaver specimens for kinematic analysis, absence of an investigation into the effects of rate, and neglecting the APL from the study. *In-vitro* studies with cadaveric specimens raise potential issues with the relevance of data collected as reported by King *et al.* that showed a significant degradation of cyclic peak loads in dense connective tissues of $8.6 \pm 4.6 \%$ over an 18 hour period ($p <$

0.0001) at room temperature ($23 \pm 2^\circ\text{C}$) [11]. Although data collection for this thesis used cadavers at room temperature for periods up to 23 hours, any degradations such as creep to the tendons would be compensated by the motors; tendon creep would decrease the load resulting in motor spooling to adjust for the offset in load. However, degradation to ligaments would effectively 'loosen' the DRUJ and may effect normal carpal bone motion. An 18 hour post-day study determined no significant degradation ($p < 0.05$) in motion repeatability for a cadaveric specimen (Appendix E). Further investigations to understand the effects that the rate of motion has on the repeatability of the simulator would provide insight into the roll that hysteresis has post-mortem on wrist kinematics and the ability of the simulator to compensate for positional errors at higher speeds.

With the design of a new simulator comes the advantages from modern technology, and an ever increasing base of literature to learn from. Technologies present today such as optical tracking and smart motor interfacing abilities far exceed what was available to researchers two decades ago allowing simulator platforms to be made smaller, smarter, and more repeatable. The ability to use optical tracking rather than an electromagnetic tracking system eliminates the ferric material restrictions due to interference on the systems resolution opens the clinical investigations to arthroplasty, external fixation, and open reduction & internal fixation of the wrist. The ability to rotate the wrist into multiple states of gravity loading will allow investigations into the affects of gravity on wrist kinematics and muscle loading within the forearm. Smart motor interfacing increases the response time and reliability of actuation as well as allow for higher resolution of position accuracy with respect to hydraulic or pneumatic actuators.

With any method to simulate *in-vivo* conditions there are limitations in accuracy due to either a general lack of knowledge or the inability recreate the anatomically correct conditions. Although the simulator was successful in creating repeatable motion between specimens, the forces represented by each muscle may not truly represent those present in a living person. Forces for this study had a minimum set point of 8.9 N and even though each effectively acted independently from the other muscles in the group (FEM or RUD), they may not be representative of the ratios present *in-vivo*.

2.5 Conclusions

To properly study the biomechanics of the wrist it should be under simulated active conditions rather than passive motion where abnormal forces and moments are applied by the investigator. A simulator that uses actuators to simulate the shortening of tendons in fresh-frozen cadaver forearms successfully reanimated cadaver upper limbs more repeatedly than possible from human investigators [5]. Future work should explore the appropriate ratios of muscle contributions during wrist motion obtained from electromyography (EMG) collected from people to more accurately model *in-vivo* conditions. This may lead to more relevant scaling of the force outputs to ultimately model wrist motion more realistically.

References

- [1] M. Nishiwaki, M. Welsh, B. Gammon, L. M. Ferreira, J. A. Johnson, and G. J. King, “Volar subluxation of the ulnar head in dorsal translation deformities of distal radius fractures: An in vitro biomechanical study,” *Journal of orthopaedic trauma*, vol. 29, no. 6, pp. 295–300, 2015.
- [2] M. Nishiwaki, M. Welsh, B. Gammon, L. M. Ferreira, J. A. Johnson, and G. J. King, “Distal radioulnar joint kinematics in simulated dorsally angulated distal radius fractures,” *The Journal of hand surgery*, vol. 39, no. 4, pp. 656–663, 2014.
- [3] F. Fraysse, J. J. Costi, R. M. Stanley, B. Ding, D. McGuire, K. Eng, G. I. Bain, and D. Thewlis, “A novel method to replicate the kinematics of the carpus using a six degree-of-freedom robot,” *Journal of biomechanics*, vol. 47, no. 5, pp. 1091–1098, 2014.
- [4] C. E. Dunning, C. S. Lindsay, R. T. Bicknell, S. D. Patterson, J. A. Johnson, and G. J. King, “Supplemental pinning improves the stability of external fixation in distal radius fractures during simulated finger and forearm motion,” *The Journal of hand surgery*, vol. 24, no. 5, pp. 992–1000, 1999.
- [5] F. W. Werner, A. K. Palmer, J. H. Somerset, J. J. Tong, D. B. Gillison, M. D. Fortino, and W. H. Short, “Wrist joint motion simulator,” *Journal of orthopaedic research*, vol. 14, no. 4, pp. 639–646, 1996.
- [6] B. J. Harley, M. L. Pereria, F. W. Werner, D. A. Kinney, and L. G. Sutton, “Force variations in the distal radius and ulna: Effect of ulnar variance and forearm motion,” *The Journal of hand surgery*, vol. 40, no. 2, pp. 211–216, 2015.
- [7] M. C. Tynan, S. Fornalski, P. J. McMahon, A. Utkan, S. A. Gree, and T. Q. Lee, “The effects of ulnar axial malalignment on supination and pronation*,” *The Journal of Bone & Joint Surgery*, vol. 82, no. 12, pp. 1726–1726, 2000.
- [8] W. B. Kleinman and T. J. Graham, “The distal radioulnar joint capsule: clinical anatomy and role in posttraumatic limitation of forearm rotation,” *The Journal of hand surgery*, vol. 23, no. 4, pp. 588–599, 1998.
- [9] S. Erhart, W. Schmoelz, and M. Lutz, “Clinical and biomechanical investigation of an increased articular cavity depth after distal radius fractures: effect on range of motion, osteoarthritis and loading patterns,” *Archives of orthopaedic and trauma surgery*, vol. 133, no. 9, pp. 1249–1255, 2013.

- [10] J. Korsawe, "Circlefit3d - fit circle to three point in 3d space." <http://www.mathworks.com/matlabcentral/fileexchange/34792-circlefit3d-fit-circle-to-three-points-in-3d-space>, 2012. [Online; accessed 2015-08-30].
- [11] G. J. King, C. L. Pilon, and J. A. Johnson, "Effect of in vitro testing over extended periods on the low-load mechanical behaviour of dense connective tissues," *Journal of Orthopaedic Research*, vol. 18, no. 4, pp. 678–681, 2000.

Chapter 3

The Effects of Gravity on Wrist Kinematics in Multiple Loaded Positions

OVERVIEW: This chapter compares the effects of gravity on wrist kinematics during active motion trials in three positions; gravity neutral (vertical, as conducted in Chapter 2), gravity flexion, and gravity extension. Measured outcomes looked at differences in repeatability during FEM and RUD motion trials, out-of-plane deviation, discrepancies between the center of rotation between positions, and changes in tendon forces. A comparative analysis discussing the outcomes and their relevance to validating the need for developing a reliable method of simulating wrist motion is also included.

(A portion of this work was been presented at the 2015 Vancouver Canadian Orthopaedic Research Society (CORS) conference.)

3.1 Introduction

In-vitro kinematic research of wrist biomechanics on cadavers has allowed for the investigation into the complex articulations between bones and soft tissues at the distal forearm and wrist joints. Mechanical apparatuses have been developed to apply loads directly to the tendons of interest (as discussed in Chapter 2, Section 2.2.3) to more accurately simulate *in-vivo* conditions during motion trials and track relative motion using appropriate spatial tracking methods (Chapter 1.3) for kinematic analysis. Given that the majority of the day is spent with our wrists by our sides during walking or in a horizontal gravity loaded extension position while sitting and typing at a keyboard or driving a vehicle, no investigation to date has reported on the effects of gravity on the wrist during simulated active motion trials for either trends in motion pathways or force between positions.

The difference between gravity loaded positions stem from the balance of the antagonistic nature of the wrist joint with the influence of gravity on the center of mass of the wrist. Gravity effectively acts at the center of mass of an object, which for the wrist in a non-vertical position should never cross the joint center of rotation on the horizontal plane, unless exceeding 90 degrees of wrist flexion-extension, and therefore will always resist motion in a single direction. For instance, in a horizontal gravity loaded extension position, the weight of the hand will naturally result in wrist flexion no matter the position in the FEM plane. This is not the case for a vertical gravity loaded position which requires the balance of forces between the flexor and extensor, where one group is active and the other is maintaining minimum tone, to inverse at approximately neutral to effectively resist the tendency of the wrist to accelerate during motion. 'Approximately' is used as there is a period of transition through neutral where gravitational effects momentarily subside as the center of mass passed the center of rotation on the horizontal plane (Figure 3.1). Simulators, such as those used by Dunning et al. [1, 2] and Gordon et al. [3, 4], used the approach where cadaveric upper limbs were tested with the humerus in a vertical orientation with the wrist pointing down, and then immobilize the elbow at 90 degrees flexion with the forearm parallel to the floor. Although these were passive motion simulators, they reported the tendon forces necessary to maintain a neutral wrist position through a range of

forearm rotation, hence providing insight into force differences between the flexors and extensors in gravity loaded flexion and extension positions. Issues with these methods arise from the shift in muscle force required to hold neutral wrist positions between pronation and supination as reported by Mogk *et al.* [5] who stated that extensor forces increased in pronation and flexor forces increased in supination. Fully functional active motion simulators, like those reported by Werner *et al.* [6] and Erhart *et al.* [7], were capable of recreating motion using computer control algorithms to adjust tendon forces from a manifold of actuators to ultimately achieve a static position or follow a motion profile. Specimens were rigidly fixed at 90 degrees of elbow flexion with the forearm in a vertical position pointing upwards, hence restricting all motion to the vertical gravity position.

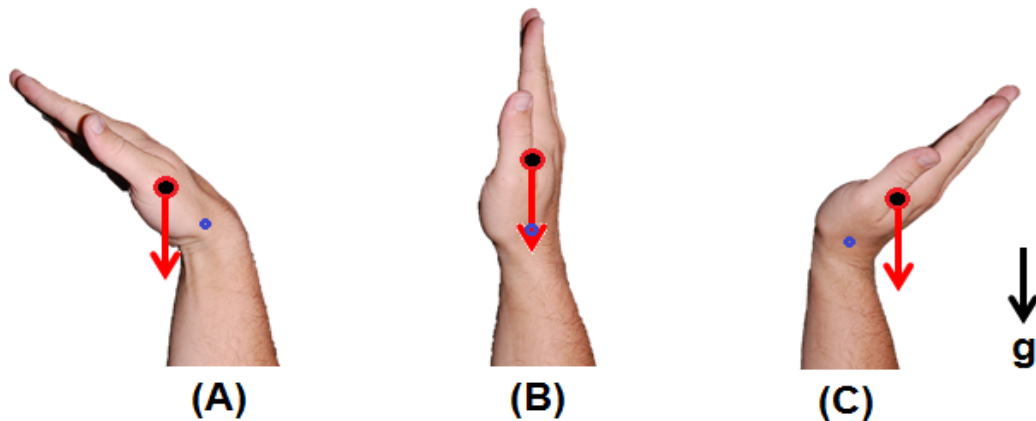


Figure 3.1: *The wrist in a vertical gravity loaded position showing the affect of gravity [red dot] acting at the center of mass [black dot] with respect to the center of rotation [blue dot] about the wrist. In flexion [left] gravity acts to further flex the wrist. In extension [right] gravity acts to further extend the wrist. In neutral [center] the center of mass is vertically in line with the center of rotation and generates a negligible about of torque about the wrist.*

A simulator capable of producing repeatable active motion trials between multiple gravity loaded positions would enable researchers to perform more comprehensive investigations into differences between pre and post-operative as well as healthy wrist kinematics. Hence, the purpose of this study was to validate the ability of an active motion simulator to reproduce repeatable motion trials under a variety of gravity loaded conditions.

3.2 Methods

3.2.1 Specimen Preparation

Five fresh frozen cadaver upper extremities, average age 70 ± 16 years (55 to 79 years, 3 male) were amputated at the mid-humeral level and attached to the active motion wrist simulator outlined in Chapter 2 at 90 degrees elbow flexion. Sutures (#2 Ethibond) were made, using the Krackow method, into the distal musculotendinous junction of the *biceps brachii* (BI), *pronator teres* (PT), *flexor carpi ulnaris* (FCU), *flexor carpi radialis* (FCR), *extensor carpi ulnaris* (ECU), *extensor carpi radialis longus* (ECRL), and *extensor carpi radialis brevis* (ECRB). All incisions were closed using suture techniques employed clinically during the investigation to preserve the natural fluids and the sutures were routed through guide blocks to mimic anatomical lines of action. Electric servomotors (SMI 2316D-PLS, Animatics, CA), force transducers (Vishay Precision Group, Raleigh, NC), and optical trackers (Certus Optotrack, Northern Digital Inc., Waterloo, Canada) were used to control the tendon force and wrist position during the investigation. A custom LabVIEW (National Instruments, Austin, TX) program set all motions to $5^\circ/\text{s}$ with a sampling rate of 15.0 Hz. The *biceps brachii* and *pronator teres* tendons were toned to 45.0 N and locked at neutral forearm rotation. Wrist position is presented as the metacarpal with respect to the radius as outlined by the ISB standards in Chapter 1 (Section 1.5).

3.2.2 Data Collection

Five active trials, each consisting of five cycles through a full range *flexion-extension* (FEM) and *radioulnar deviation* (RUD), were performed in each of the three gravity loaded positions. The initial trial from each cycle as well as the peaks of motion were neglected from the analysis to prevent non-steady motion and force spikes from effecting the results. All five specimens were able to perform a range of motion of 50 degrees flexion to 5 degrees *extension* while only four could achieve 10 degrees radial deviation to 20 degrees ulnar deviation; motions that did not satisfy the range of motion were neglected. Trials were performed at $5^\circ/\text{s}$ lasting approximately 20 s during FEM and 7 s during RUD.

To test the simulator's ability to reproduce a static position five trials were collected by moving the wrist in increments of 10 degrees between the extremes in FEM and RUD. A sample period of 3 s was collected for each static position in case of optical marker dropout and to smooth subtle fluctuations in the position controller. Each trial recorded the time stamp, motor forces, wrist angles, and raw tracker transformations used in post processing to determine the kinematic characteristics of each motion and the repeatability between trials. All data was collected in the same day and tested under identical conditions. Note: there was no significant difference in repeatability of motion trials ($p < 0.05$) with respect to time in the first 18 hours of testing (Appendix E).

3.2.3 Outcome Variables & Statistical Analysis

The repeatability of motion for the simulator was reported using an inter-trial average standard deviation (ASD) between specimens ($N=5$). A one-way (gravitational position) Repeated Measures ANOVA (RM-ANOVA) was performed to determine significant effects ($p < 0.05$) of gravity on the profile trends of wrist motions collected from average trial error from the target motion pathway.

3.3 Results

3.3.1 Repeatability of Motion Profiles

The mean errors and average standard deviations was computed between consecutive trials for all motions in each position (N=5 specimens). The accuracy of the simulator was quite high with average error between trials never exceeding 0.23° for extension, 0.7° for flexion, 0.21° for radial deviation, and 2.8° for ulnar deviation with ASD of 0.24° , 0.31° , 0.24° , and 0.45° respectively (Figure 3.2). A significant increase in error for flexion in the gravity flexion position was present ($p < 0.05$). Overall, the simulator achieved the best performance in the gravity neutral position with a mean error of $0.18 \pm 0.25^\circ$ between all motion trials. The simulator performed similarly in the gravity loaded extension and flexion positions with mean error of $0.22 \pm 0.32^\circ$ and $0.33 \pm 0.51^\circ$ respectively.

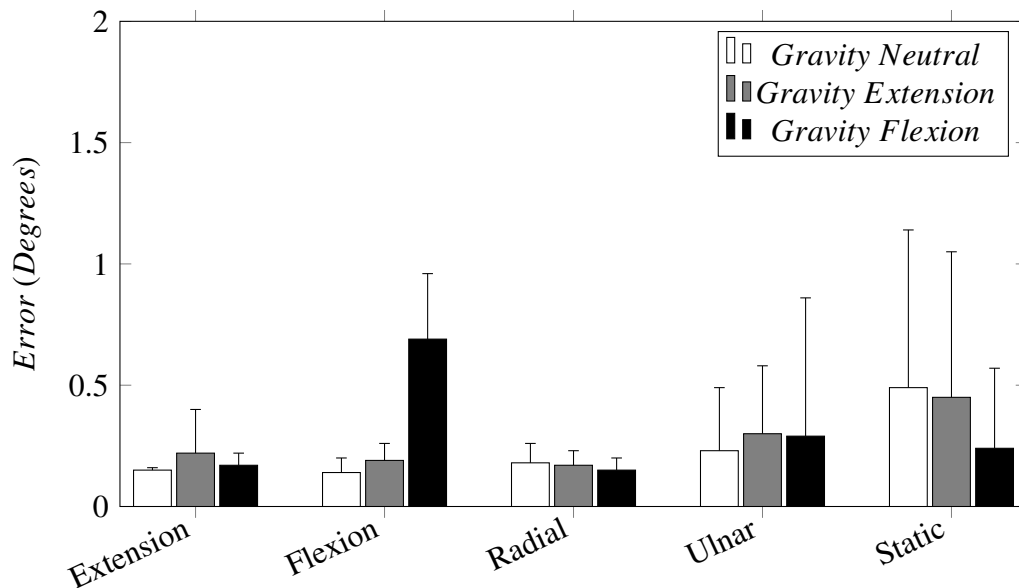


Figure 3.2: A comparison between the repeatability of static position and motion trials between gravity neutral [white], gravity extension [gray], and gravity flexion [black] positions showing standard error within each specimen and the standard deviation between error in specimens [$+1$ SD]

3.3.1.1 In-Plane Motions

For each specimen (N=5) the mean trial error with respect to the target angle was computed in all three positions and were sampled at intervals of 10 degrees for FEM trials (Figure 3.3) and at 5 degrees for RUD trials (Figure 3.4). A one-way RM-ANOVA test indicated that there were no significant differences of average error from target between the three positions ($p < 0.05$) during flexion-extension or radioulnar deviation motions. A latency of 5 degrees behind the target angle was present at the onset of each trial during FEM motions that was not present in RUD motions resulting in larger magnitudes of error early in the trial, however the error converged on zero approximately halfway through each trial when the wrist passed neutral position. Unlike the FEM trials that converged at zero error with the wrist in neutral position, the motions in the RUD plane maintained the initial error of 5 degrees and only converged on zero error at the final stage of the trials (the termination point). Note that minor changes to the PID controller were made regarding tuning the proportional constant to achieve a desirable response; rule of thumb being that limbs from larger specimens require a large proportional constant to handle the increased forces required to induce motion.

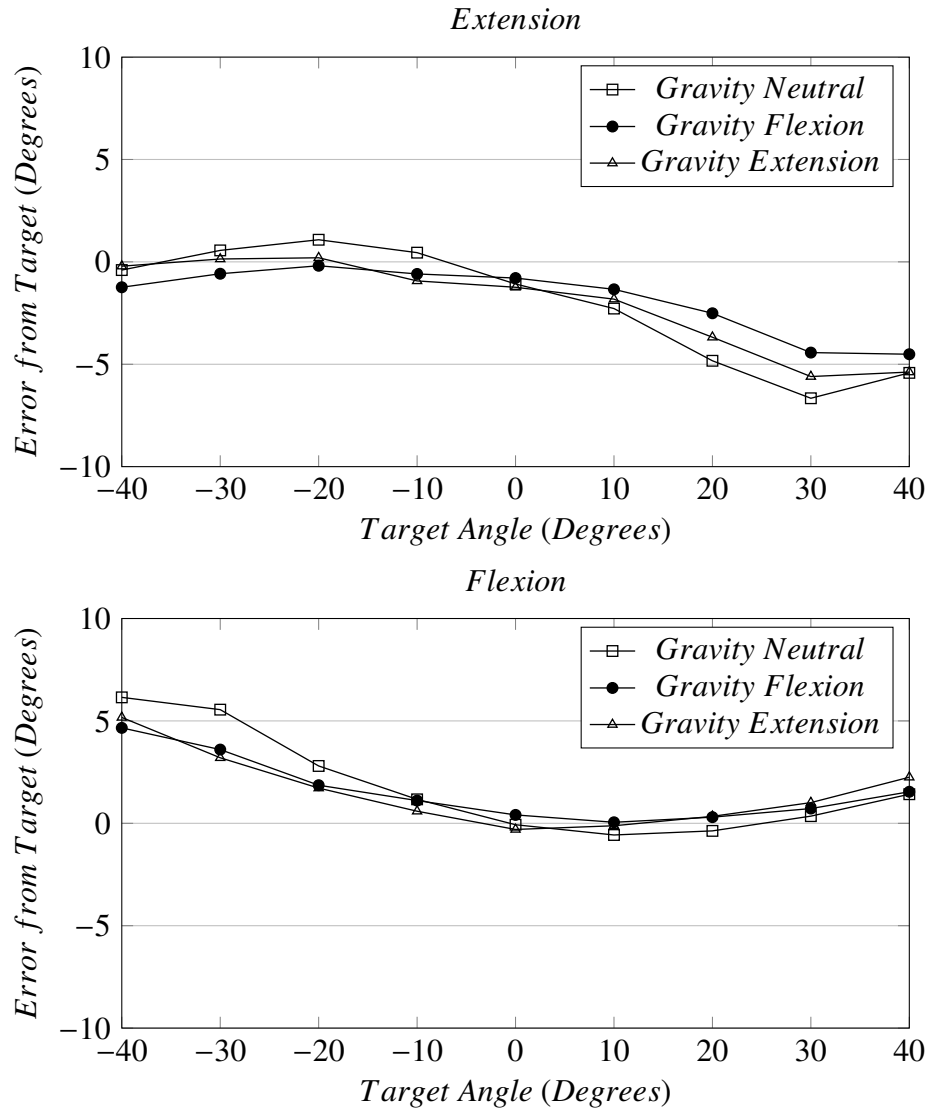


Figure 3.3: Repeatability of extension [top] and flexion [bottom] motions in all three positions are displayed showing the overall mean error of all motion trials with respect to the desired angle of all specimens ($N=5$)

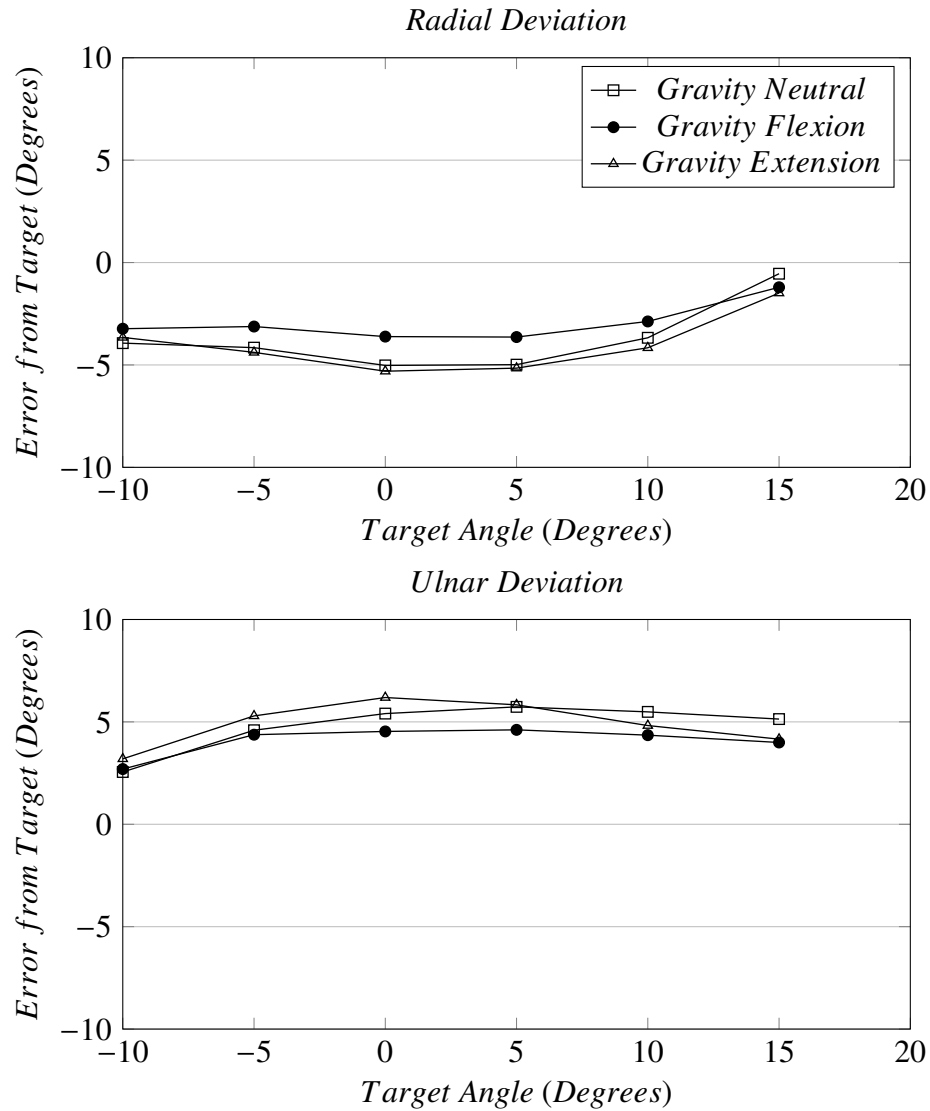


Figure 3.4: Repeatability of extension [top] and flexion [bottom] motions in all three positions are displayed showing the overall mean error of all motion trials with respect to the desired angle of all specimens ($N=5$)

3.3.1.2 Out-of-Plane Motions

Out-of-plane motion for this study was undesirable as all the trials were restricted to unidirectional motion within a single plane. As discussed in Chapter 2 (Section 2.2.2), the position controller acts to reduce error between the actual and desired angle of the wrist by adjusting the magnitude of tendon forces as groups; extensors, flexors, radial deviators, and ulnar deviators, however a change to one group may have undesired effect to motion in other planes. Figures 3.3 & 3.4 illustrate tendency of the wrist to deviation from planar motion during FEM and RUD. A one-way RM-ANOVA revealed no significant differences between gravity loaded positions for flexion, extension, and ulnar deviation trials at a significance level of $p=0.05$. However, a significant difference in trial error for radial deviation was determined resulting in the rejection of the null hypothesis that all trials were equal. Motion in the FEM plane performed better than in the RUD plane as the out-of-plane motion was minimal with the mean out-of-plane error between trials less than 1 degree from neutral while those in the RUD plane had FEM errors that exceeded 1 degree from neutral, with the worst out-of-plane error at approximately 4 degrees. The simulator FEM performance operated within 1 degree of error satisfying the objectives of this thesis as outlined in Chapter 1, Section 1.10.

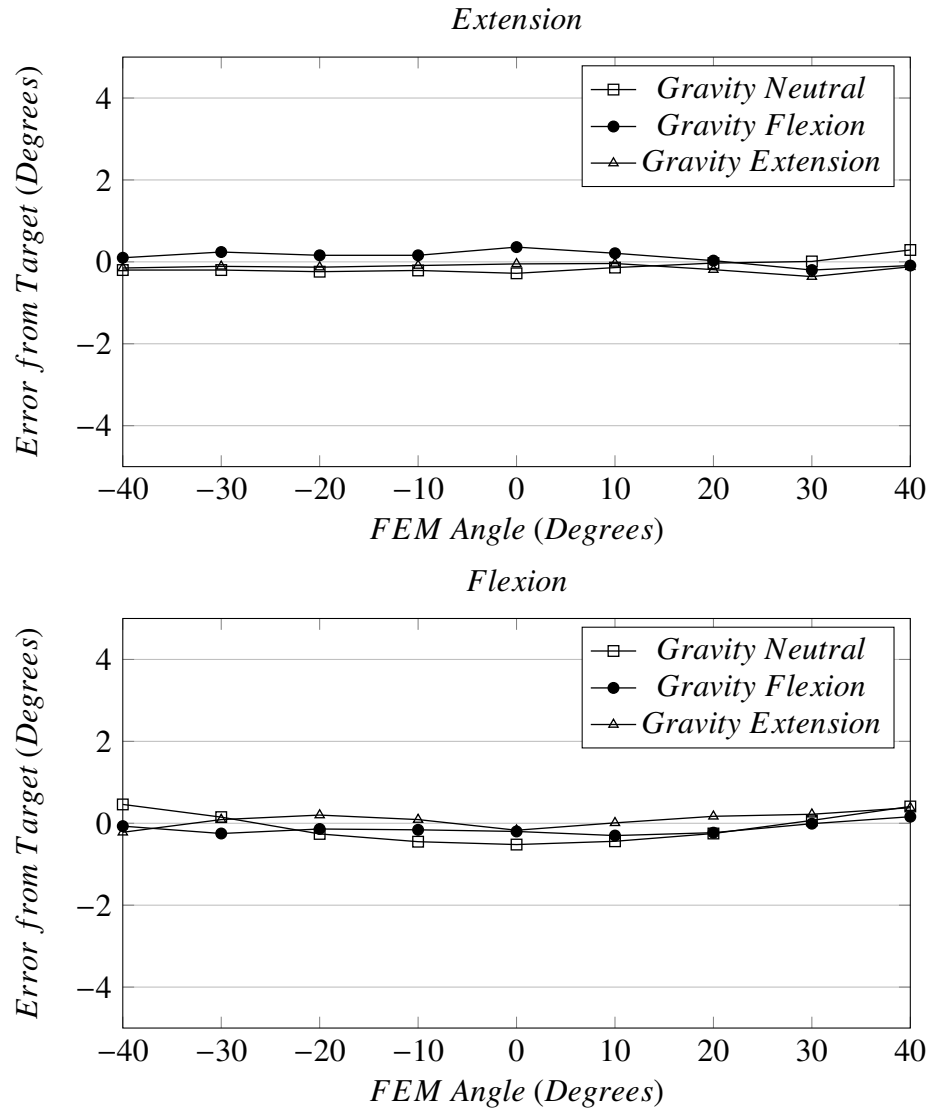


Figure 3.5: The mean out-of-plane deviation with respect to the wrist angle during extension [top] and flexion [bottom] motions in all three positions illustrates the ability of the simulator to produce planar motion ($N = 5$ specimens)

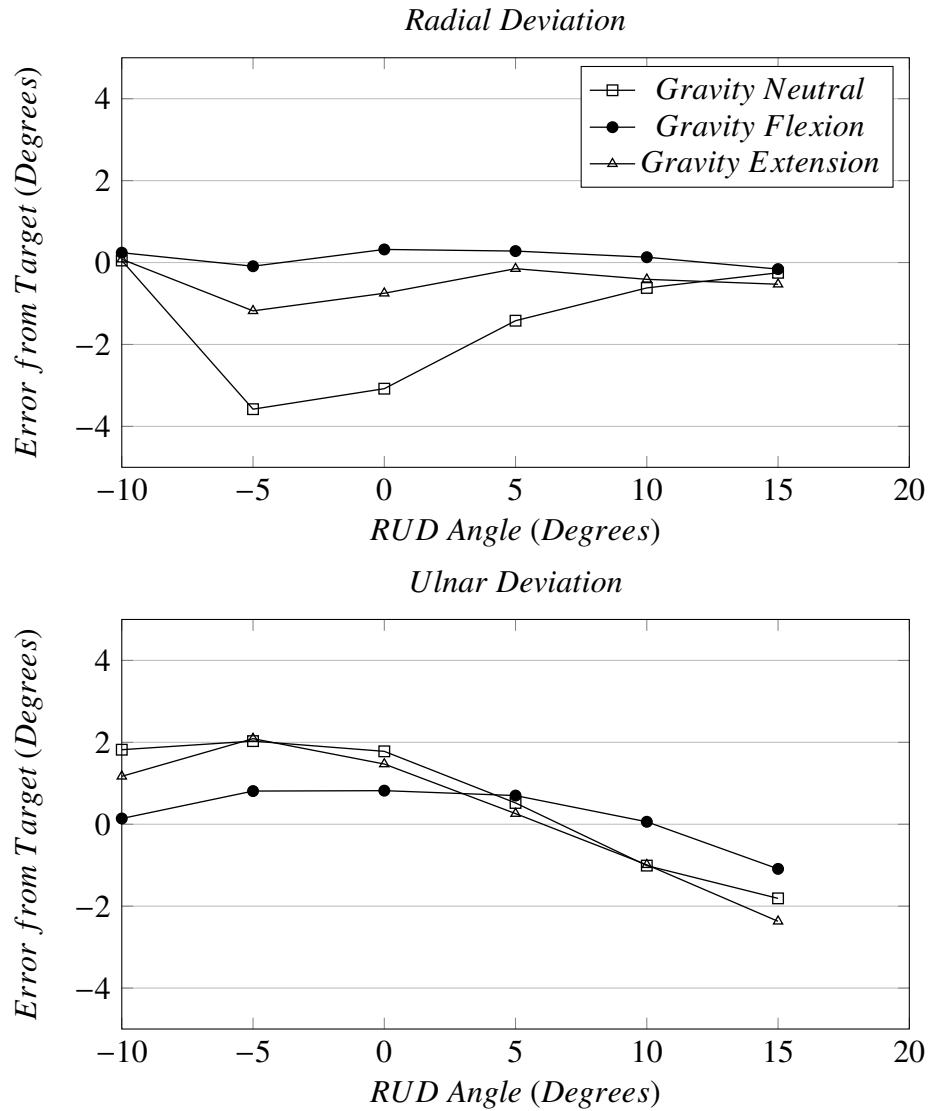


Figure 3.6: The mean out-of-plane deviation with respect to the wrist angle during radial [top] and ulnar [bottom] deviations in all three positions illustrates the ability of the simulator to produce planar motion ($N = 5$ specimens)

3.3.2 Center of Rotation Repeatability

Using a circle fitting algorithm to match points along the motion pathway to a centroid of best fit, as discussed in Chapter 2 (Section 2.2.3.3), the mean centroid of motion and standard deviation for each arm in the series was determined. There were no apparent differences between the variability of the *center of rotation* between either positions or motions, however it is important to note that the optical tracking method used has a resolution of 0.01 mm with an positional accuracy of 0.1 mm [8] and therefore no statistical analysis was performed. The overall repeatability of the center of rotation (COR) in the FEM plane for active motion was $0.28 \pm 0.14^\circ$. The motion profiles for the COR in the RUD plane produced non-circular profiles that were incompatible with the circle fitting algorithm and therefore were neglected for this investigation.

Table 3.1: Average center of rotation in all three gravity loaded positions (mm[SD])

	Active
<i>Gravity Neutral</i>	
Extension	0.34[0.23]
Flexion	0.17[0.13]
<i>Gravity Flexion</i>	
Extension	0.35[0.07]
Flexion	0.24[0.14]
<i>Gravity Extension</i>	
Extension	0.28[0.10]
Flexion	0.32[0.10]

3.3.3 Repeatability of Tendon Forces

Tendon forces acted independently during motion trials with the control algorithm acting to maintain a wrist position through the fluctuation of force. Consequently, any trends in the force profiles were not an intentional result yet strong trends emerged between motions for each specimen. To maintain consistency with other investigators [6] the reporting of tendon forces covers peak forces during motion, and average forces required to maintain static positions.

3.3.3.1 Static Trials

The mean force and standard deviation for each tendon required to hold the wrist in a position for each of the three gravity loaded positions was sampled over a 3 second period and averaged between all 5 specimens (Table 3.2). The tendon forces behaved as expected, with respect to gravity, where positions that resisted gravitation force on the hand had larger force magnitudes and those that were assisted by gravity had lower force magnitudes. With the gravity neutral position as the normal, trends in the gravity loaded flexion and extension positions displayed increased forces in the flexor and extensor groups, respectively, as the weight of the hand had to be overcome. The *biceps brachii* and *pronator teres* muscles were neglected for this investigation as they were each toned to 45.0 N and locked at neutral forearm rotation.

Table 3.2: Average of five arms for muscle forces required to hold the wrist in a static position during active manipulation (percent of total muscle force [SD])

	FCR	FCU	ECRL	ECRB	ECU
<i>Gravity Neutral</i>					
50° of flexion	0.12[0.06]	0.18[0.01]	0.21[0.02]	0.21[0.01]	0.28[0.06]
50° of extension	0.22[0.12]	0.11[0.01]	0.32[0.07]	0.17[0.10]	0.18[0.10]
10° of radial deviation	0.21[0.04]	0.10[0.06]	0.31[0.07]	0.20[0.03]	0.20[0.03]
20° of ulnar deviation	0.06[0.03]	0.19[0.05]	0.20[0.03]	0.20[0.03]	0.34[0.02]
<i>Gravity Flexion</i>					
50° of flexion	0.23[0.06]	0.19[0.04]	0.22[0.06]	0.17[0.03]	0.19[0.05]
50° of extension	0.34[0.04]	0.28[0.06]	0.16[0.06]	0.12[0.03]	0.11[0.03]
10° of radial deviation	0.33[0.06]	0.17[0.05]	0.27[0.07]	0.11[0.04]	0.11[0.04]
20° of ulnar deviation	0.15[0.01]	0.31[0.01]	0.13[0.01]	0.13[0.01]	0.29[0.02]
<i>Gravity Extension</i>					
50° of flexion	0.15[0.05]	0.14[0.06]	0.25[0.06]	0.22[0.03]	0.24[0.04]
50° of extension	0.25[0.09]	0.20[0.08]	0.22[0.05]	0.16[0.07]	0.17[0.06]
10° of radial deviation	0.23[0.06]	0.09[0.04]	0.32[0.05]	0.18[0.04]	0.18[0.04]
20° of ulnar deviation	0.08[0.02]	0.20[0.05]	0.20[0.04]	0.19[0.03]	0.32[0.01]

3.3.3.2 Motion Trials

The peak tendon forces from each motion were averaged amongst the five specimens in each of the three gravity loaded positions (Table 3.3). The gravity neutral position is unique from the other two as it behaves as an inverted pendulum where the effects of gravity inverse as the wrist passes through neutral (vertical). This trend was observed most clearly for extension and flexion motions as the extensor and flexor tendon groups, respectively, displayed higher magnitudes of force while the opposing group maintained near minimum tones. The trends between the gravity flexion and extension positions were similar in the sense that the forces in tendon groups required to move the wrist against gravity were observed to be active during both motions in the FEM plane while the antagonist group maintained neutral force with little contribution to motion. RUD motion trials in gravity neutral exhibited trends between the radial and ulnar deviation groups with each group displaying greater magnitudes during its respective motion. This trend holds true for the remaining gravity loaded positions but with a shift in balance within each group in favour of the muscle opposing gravity. For instance, during ulnar deviation in gravity extension the tendons, ECU & FCU, are activated to induce motion but the ECU displays higher magnitudes to overcome the effect of gravity on the wrist.

Table 3.3: Average peak tendon forces for each plane of motion of the wrist (N [SD]).

	FCR	FCU	ECRL	ECRB	ECU
<i>Gravity Neutral</i>					
Extension	23.0[15.4]	20.7[8.8]	50.0[25.7]	39.9[15.2]	47.1[17.6]
Flexion	26.4[12.0]	21.3[4.5]	19.00[12.0]	13.1[3.6]	15.0[3.5]
Radial	40.6[15.9]	24.1[19.1]	57.34[20.8]	38.5[29.4]	53.8[47.7]
Ulnar	33.0[19.6]	32.0[15.5]	50.92[25.7]	38.5[29.5]	59.4[44.5]
<i>Gravity Flexion</i>					
Flexion	14.2[4.0]	17.0[7.7]	21.6[4.5]	19.0[2.3]	24.8[8.8]
Extension	28.2[10.4]	30.6[12.3]	13.0[3.1]	12.2[1.3]	15.5[7.0]
Radial	38.3[13.5]	14.4[2.7]	35.9[11.2]	9.4[0.7]	12.7[1.3]
Ulnar	28.6[13.7]	22.8[1.0]	24.3[12.6]	11.2[0.4]	19.6[2.7]
<i>Gravity Extension</i>					
Extension	13.9[3.1]	18.0[7.3]	38.5[8.9]	36.4[10.3]	43.2[16.9]
Flexion	17.1[8.9]	17.5[8.2]	14.3[2.5]	14.5[2.6]	17.5[5.5]
Radial	37.4[16.2]	12.9[3.1]	46.5[15.6]	21.5[7.5]	26.1[10.5]
Ulnar	27.5[16.7]	25.9[4.8]	37.5[11.0]	22.7[7.4]	36.7[13.7]

3.4 Discussion

The results of this simulator were quite accurate and indicated a high level of repeatability between all trials with respect to motion profile, *center of rotation*, and force trends produced which could have the potential for further improvement with system revisions and tuning of the PID parameters.

The mean error and standard deviation between consecutive motion trials, with exception of flexion in the gravity loaded flexion position, were less than 0.5° and 1.0° respectively, suggesting that the simulator was able to achieve steady state motion for each trial. The trends in trial error with respect to the target angle, as shown in Figures 3.3 & 3.4, are the result of the tuning parameters of the system. The latency is inherited from force-position algorithm explained in Chapter 2 (Section 2.2.2.2) that reads a motion profile from a text script to adjust the target angle, which will ultimately result in the motion response to lag behind the desired position but may be reduced through further tuning of the proportional, derivative, and integral constants of the PID controller. Note that the point of convergence with zero error on each plot was at approximately neutral wrist position which is not by coincidence; rather the trend was influence by the joint anatomy and the fluctuations of tendon moment arms as discussed in chapter Chapter 1 (Section 1.2.5).

The moment arms for the *extensor carpi radialis longus & brevis* tendons are greatest at 40 degrees extension and decrease linearly to 40 degrees flexion by approximately 50% while the *extensor carpi ulnaris* tendon remains relatively constant [9]. The same is true for the *flexor carpi radialis* that has its greatest moment arm at 40 degrees flexion and decreases linearly to 40 degrees extension decreasing by approximately 50% while the *flexor carpi ulnaris* remains relatively constant. These changes in moment arms may account for the latent behaviour in the FEM profiles as the influence of the tendon forces begin at their lowest state and gradually increase through out the trials causing the wrist to converge on zero error at neutral. This trend was not present during RUD trials and at no time were these motions influence directly by gravity.

Out-of-plane motion trials behaved as expected during FEM trials where there were minor RUD errors that followed no particular trend between the three gravity loaded conditions, most likely due to the absence of gravitational effects in that plane. In the RUD plane, radial deviation trials had near zero out-of-plane error in both gravity flexion and extension positions while the neutral position experienced error in extension approximately 4 times larger than the others. The behaviour was most likely due to the differences in loading across the wrist between the gravity neutral position and the rest since the FEM muscle groups responsible for correcting error were constantly trading responsibility when the wrist moved out of plane. This behaviour was not present in the gravity loaded flexion and extension positions since there was always one FEM muscle group responsible for opposing gravity. The trend during ulnar deviation was an extension error at extreme radial deviation and a flexion error at extreme ulnar deviation. This suggests that the *extensor carpi ulnaris* overpowers the *flexor carpi ulnaris* and that the *flexor carpi radialis* overpowers the *extensor carpi radialis longus* at extreme ranges of motion.

The differences in the variances of the *center of rotation* between positions were negligible since they were at the scale of the lowest resolution of the optical tracking system. The fluctuations in the centroid of motion may have been the result of resolution error rather than from actual translations of the bones during motion.

The active motion simulator used by Dunning *et al.*, as reviewed in Chapter 1 (Section 1.8.2.1), was most comparable to the gravity loaded positions with exception to the minimum tone load of 11.3 N and the orientation of the humerus requiring the forearm to be in pronation for extension trials and supination for flexion trials. Regardless of these discrepancies there was no notable differences in performance between the two simulators, as both exhibited similar magnitudes of force required to maintain neutral wrist position. Note that in order to compare our results to those published by Dunning, the forces of the ECRL and ECRB from our studies were summed to compare against the ECRL forces of Dunning's. Table 3.4 illustrates the similar performances of both simulators. A noticeable difference between the ECU loads in pronation/gravity extension was most likely due to the change in the line of action of the ECU

as it had to span across the dorsal forearm in pronation thus decreasing its effectiveness as it diverges from the perpendicular tangent line of action.

Table 3.4: *The average forces for balancing the wrist in neutral for gravity loaded positions between the simulator developed for this investigation and Dunning's (N[SD])*

	<i>Dunning</i>	<i>Current</i>
<i>Gravity Extension</i>		
<i>Pronation</i>		
FCU	11.3[0.9]	14.0[5.7]
FCR	11.1[0.9]	10.7[1.7]
ECRL	67.5[10.8]	29.6[18.6]
ECRB	—	24.9[18.6]
ECU	50.9[11.0]	26.3[13.5]
<i>Gravity Flexion</i>		
<i>Supination</i>		
FCU	19.0[4.0]	17.2[6.3]
FCR	16.1[4.8]	15.7[3.4]
ECRL	17.3[5.5]	10.9[3.4]
ECRB	—	8.9[3.3]
ECU	12.5[1.1]	9.3[0.5]

Limitations to this study worth noting, as discussed in Chapter 2 (Section 2.4), arise from several areas including: the use of elderly cadaver specimens for kinematic analysis, a lack of understanding of the effect of the rate of motion on the repeatability of motion cycles, and the effect of generating motion with the absence of the *abductor pollicis longus* as used by other investigators [6, 10]. King *et al.* reported significant degradation of cyclic peak loads in dense connective tissues of $8.6 \pm 4.6\%$ over an 18 hour period ($p < 0.0001$) at room temperature ($23 \pm 2^\circ\text{C}$) [11] for *in-vitro* testing. This may influence the overall laxity of the joint over time and some minor effect on repeatability, but any elongations to the tendons would ultimately be compensated for by an adjustment to the servo motor. As mentioned in Chapter 2 (Section 2.4), an 18 hour post-day study determined no significant degradation ($p < 0.05$) in motion repeatability for a cadaveric specimen (Appendix E).

3.5 Conclusions

The overall effects of gravity on the simulator's ability to produce repeatable motion were negligible as there were no major differences in error between each of the three gravity loaded positions with exception to radial deviation trials in a gravity neutral position. Due to the inherited behaviours from the PID controller for minimizing the positional error, there exists a latency at the onset which may be reduced through further tuning of the PID parameters. The forces recorded for static and motion trials in all three gravity loaded positions agreed with those published by other researchers on their simulator platforms with minor differences arising from methods used for actuation. Regardless of these limitations, the overall trial repeatability met with the objective outlined in Chapter 1 (Section 1.4).

References

- [1] J. A. Johnson, D. A. Rath, C. E. Dunning, S. E. Roth, and G. J. King, "Simulation of elbow and forearm motion in vitro using a load controlled testing apparatus," *Journal of biomechanics*, vol. 33, no. 5, pp. 635–639, 2000.
- [2] C. E. Dunning, C. S. Lindsay, R. T. Bicknell, S. D. Patterson, J. A. Johnson, and G. J. King, "Supplemental pinning improves the stability of external fixation in distal radius fractures during simulated finger and forearm motion," *The Journal of hand surgery*, vol. 24, no. 5, pp. 992–1000, 1999.
- [3] K. D. Gordon, C. E. Dunning, J. A. Johnson, and G. J. King, "Influence of the pronator quadratus and supinator muscle load on druj stability," *The Journal of hand surgery*, vol. 28, no. 6, pp. 943–950, 2003.
- [4] K. Gordon, C. Dunning, J. Johnson, and G. King, "Kinematics of ulnar head arthroplasty," *Journal of Hand Surgery (British and European Volume)*, vol. 28, no. 6, pp. 551–558, 2003.
- [5] J. Mogk and P. Keir, "The effects of posture on forearm muscle loading during gripping," *Ergonomics*, vol. 46, no. 9, pp. 956–975, 2003.
- [6] F. W. Werner, A. K. Palmer, J. H. Somerset, J. J. Tong, D. B. Gillison, M. D. Fortino, and W. H. Short, "Wrist joint motion simulator," *Journal of orthopaedic research*, vol. 14, no. 4, pp. 639–646, 1996.
- [7] S. Erhart, M. Lutz, R. Arora, and W. Schmoelz, "Measurement of intraarticular wrist joint biomechanics with a force controlled system," *Medical engineering & physics*, vol. 34, no. 7, pp. 900–905, 2012.
- [8] NDI, "Optotrak certus ndi." <http://www.ndigital.com/msci/products/optotrak-certus/>, 2015. [Online; accessed 2015-08-02].
- [9] R. V. Gonzalez, T. S. Buchanan, and S. L. Delp, "How muscle architecture and moment arms affect wrist flexion-extension moments," *Journal of biomechanics*, vol. 30, no. 7, pp. 705–712, 1997.
- [10] S. Erhart, W. Schmoelz, and M. Lutz, "Clinical and biomechanical investigation of an increased articular cavity depth after distal radius fractures: effect on range of motion, osteoarthritis and loading patterns," *Archives of orthopaedic and trauma surgery*, vol. 133, no. 9, pp. 1249–1255, 2013.

- [11] G. J. King, C. L. Pilon, and J. A. Johnson, "Effect of in vitro testing over extended periods on the low-load mechanical behaviour of dense connective tissues," *Journal of Orthopaedic Research*, vol. 18, no. 4, pp. 678–681, 2000.

Chapter 4

The Effects of Muscle Portioning on the Loading Conditions & Kinematics of the Wrist in a Vertically Oriented Gravity Loaded Position

OVERVIEW: This chapter investigates the effects of applying tendon portioning to the active motion simulator developed in Chapter 2 and performs a comparative analysis for the overall repeatability of motion profiles and loading across the wrist. Tendon loading ratios were established from published data on the physiological cross sectional area (PCSA) of muscles and compared to passive and active motion trials using equal tendon loading portions in the flexion-extension plane. Outcomes examined was the influence of portioning on the repeatability of motion profiles for both in-plane and out-of-plane motion, and the influence on overall loading of the wrist during motion.

4.1 Introduction

The development of active motion simulators to reanimate cadaver specimens has improved researchers' abilities to produce more reliable data for the investigation of joint kinematics. Accurately modeling the *in-vivo* behaviour and portions of individual muscles for an *in-vitro* experiment poses a challenging task as there is limited literature on this subject, however theoretical ratios may be derived from existing data on the cross sectional areas of the muscles of the wrist. As discussed in Chapter 1 (Section 1.2.4), the *physiological & anatomical cross sectional areas* of the muscles in the forearm primarily responsible for wrist motion are coincident as the muscle fibers all run parallel to the longitudinal axis [1].

Skeletal muscles are the method of actuation for human joints such as the wrist, elbow or shoulder and are contracted voluntarily when innervated by an action potential from the central nervous system [2]. The force which a muscle can produce is determined by the combination of the intensity of an action potential and the *physiological cross sectional area* PCSA of the muscle at its thickest section. The magnitude of the cross sectional area is directly proportional to the quantity of motor units within the muscle belly where more motor units will generate a larger overall contractile force [3]. Other factors such as tendon moment arms and *electromyography* (EMG) [4, 5, 6, 7] have been used for investigation of muscle portioning but there is not enough published data on literature and therefore will not be discussed in this thesis.

Existing simulators have recreated loading scenarios during *in-vitro* studies by either assigning equal magnitudes to all muscles [8], heuristically tuning the loading ratios until achieving the desired result [9], or by applying a scaling method based from anatomically relevant data drawn from cross sectional area of muscles [10, 11, 12, 13]. Gordon *et al.* made efforts to scale forces of the supinator and pronator muscles in the forearm drawing from previously established relationships between PCSA and EMG data [14] to scale agonist tendons in a group with respect to the primary mover. Kedgley *et al.* investigated the effect of tendon loading ratios of a glenohumeral joint on the repeatability of active motion trials using a shoulder simulator. Four sets of ratios based on: (1) equal tendon loading, (2) average PCSA of the muscles, (3) product

of constant EMG and PCSA, and (4) variable ratios of EMG and PCSA data. Overall, all ratios were reported effective in producing repeatable motion within 2 degrees [15, 16]. Similar methods were implemented with an active motion shoulder simulator developed by Giles *et al.* [17] which drew from previously reported PCSA and EMG ratios to provide a more realistic loading scenario of the shoulder throughout the range of motion. However, the most relevant simulators developed by Werner *et al.* [18] or by Erhart *et al.* [19] make no mention of scaling of forces in the algorithm used to produce motion of the wrist, rather, each muscle acts independently to increase force offsets about the wrist to gain the desired position.

In view of the foregoing, the purpose of this study was to investigate the effects of tendon loading ratios on the repeatability of active wrist motion using passive motion trials as common point for comparison. Two sets of ratios were drawn from: (1) equal tendon loading, and (2) averaged PCSA of the muscles of the forearm.

4.2 Methods

A simulator developed to animate cadaver upper limb specimens along motion profiles was developed in Chapter 2.0 for the investigation of wrist kinematics. To summarize, seven electric servo motors SmartMotors (SM2316D-PLS2, SMI Animatics Corp., CA) were attached to the *flexor carpi radialis*, *flexor carpi ulnaris*, *extensor carpi radialis longus*, *flexor carpi radialis brevis*, *extensor carpi ulnaris*, *pronator teres* and *biceps brachii* to achieve the full motion of the wrist in *flexion-extension*, *radial-ulnar deviation*, and *pronation-supination*. Force transducers were mounted to each motor for force feedback with a resolution within 1.0 N and 6 DOF optical trackers (Optotrak Certus, NDI, Waterloo, ON) on the third metacarpal, radius, and ulna provided force and position feedback for a custom LabVIEW (National Instruments, Austin, TX) control algorithm.

One fresh frozen cadaver upper limb (78 years, male) was tested on a custom active motion wrist simulator. Incisions were made to suture to the *flexor carpi ulnaris* (FCU), *flexor carpi radialis* (FCR), *extensor carpi radialis longus* (ECRL), *extensor carpi radialis brevis* (ECRB), *extensor carpi ulnaris* (ECU), *pronator teres* (PT), and *biceps brachii* achieve the full range of motion of the wrist. Sutures (#2 Ethibond) were passed under the skin adjacent to the respective muscle to a guide block rigidly fixed on each the medial and lateral epicondyles (depending on origin of tendon) to maintain an appropriate anatomical line of action. All incisions were closed to preserve the natural fluids of the specimen. The sutures were attached to electric servo-motors (SMI 2316D-PLS, Animatics) to provide means of motion. Each motor mount was fitted with a force transducer (half-bridge strain gage) to provide force feedback in real time allow a motor to maintain a tone load. Optical trackers (Certus, NDI) were mounted to the third metacarpal, radius, and ulna to provide real time position of the wrist in *flexion/extension motion* (FEM), *radial/ulnar deviation* (RUD), and *pronation/supination motion* (PSM). Trials were performed at 5°/s and collected at a sampling rate of 15 Hz using a custom LabVIEW algorithm. A PID controller was responsible for balancing the loads of the muscles to maintain the desired wrist orientation.

It was expected that scaling forces with respect to anatomical ratios drawn from PCSA data will ultimately reduce the overall force across the wrist and result in less dramatic fluctuations during motion from sudden adjustments to the tone loads. Passive and active motion trials were performed in a gravity neutral (vertical) position through 50 degrees flexion to 50 degrees extension while maintaining non-planar motion to zero. Passive trials used equal tendon loading and maintained a minimum tone of 8.9 N for each muscle through the full range of motion. To determine the effect of portioning the repeatability of motion and change in loading, scaling trials were compared to the default condition with all tendon having equal magnitudes. To summarize, three simulation approaches were employed: (1) passive manipulation, (2) equal tendon loading, and (3) PCSA ratio loading.

For PCSA ratios the tendon with the largest contribution was set to the upper limit at 100.0% scaling of the original portion while the percent contribution of the remaining tendons were calculated with respect to this value. Table 4.1 illustrates the relative values for each muscle in each of the methods and their calculated percentages within the *flexor* and *extensor* groups [3]. The portions were implemented on the simulator in the *flexion-extension* plane of motion by restricting the target loads of each tendon accordingly while maintaining an absolute lowest value of 8.9 N as reported by Werner [18]. No portioning was applied to the *radial* or *ulnar deviator* groups for this investigation as this was a preliminary study to prove the concept of muscle portioning in active motion.

Table 4.1: Relative sizes of PCSA [cm^2] for the flexor and extensor muscle groups with the percent of total calculated from the sum of each group [3]

	PCSA	%
<i>Flexors</i>		
FCU	3.4	100.0
FCR	2.0	58.8
<i>Extensors</i>		
ECRB	2.7	100.0
ECU	2.6	96.3
ECRL	1.5	55.6

4.3 Results

4.3.1 Repeatability of Motion Trials

4.3.1.1 In-Plane Motion Profiles

Both active motion trials were more repeatable than those produced using passive motion as illustrated by Figure 4.1 & 4.2. Passive motion trials were more variable in both *flexion* and *extension* as indicated by the magnitude of standard deviation with respect to the active trials as they were clearly distinguishable while the active motion plots for the equal tendon loading and PSCA ratio portions were not. In extension, all three experiments performed with similar error with respect to the target position with exception to the beginning of motion for active trials. An initial latency was present for both active loading techniques that was not present during passive motion trials resulting in an overcompensation of position at 4 s eventually settling down near zero error after 12 s of motion. Note that this trend was repeated very consistently between active trials and cannot be considered random error rather a behaviour inherited from the PID controller logic. The magnitudes of standard deviation between trial in *flexion* were similar to those in *extension*, however the latency in position was not present and active motion trials performed repeatably at near zero error as of 4 s in to the trial.

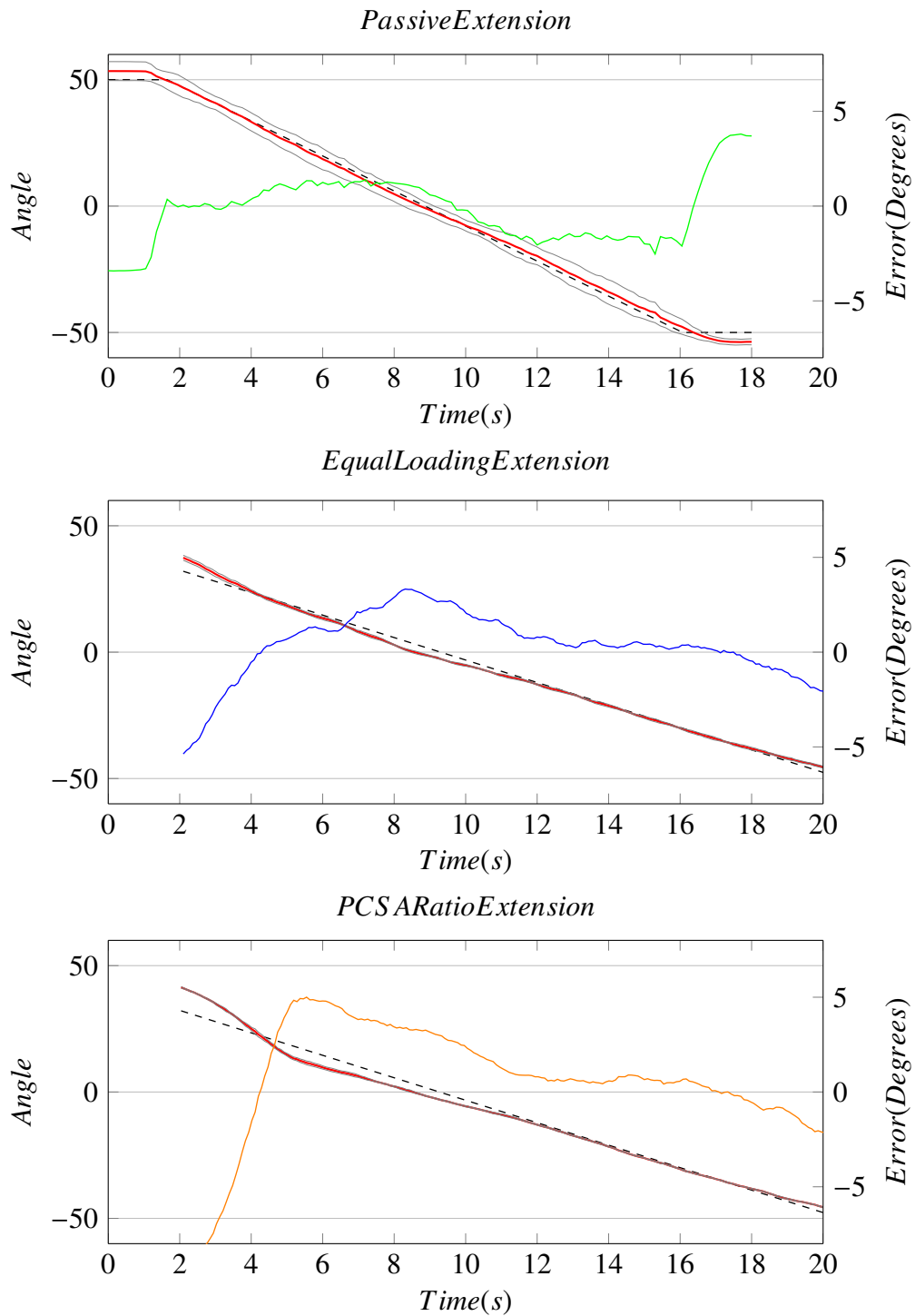


Figure 4.1: Repeatability of extension motion showing average motion trial [red], target angle [dashed black line], and standard deviation [gray lines]. The average trial error from the target is represented as green [passive], blue [equal loading], or orange [PCSA ratio]

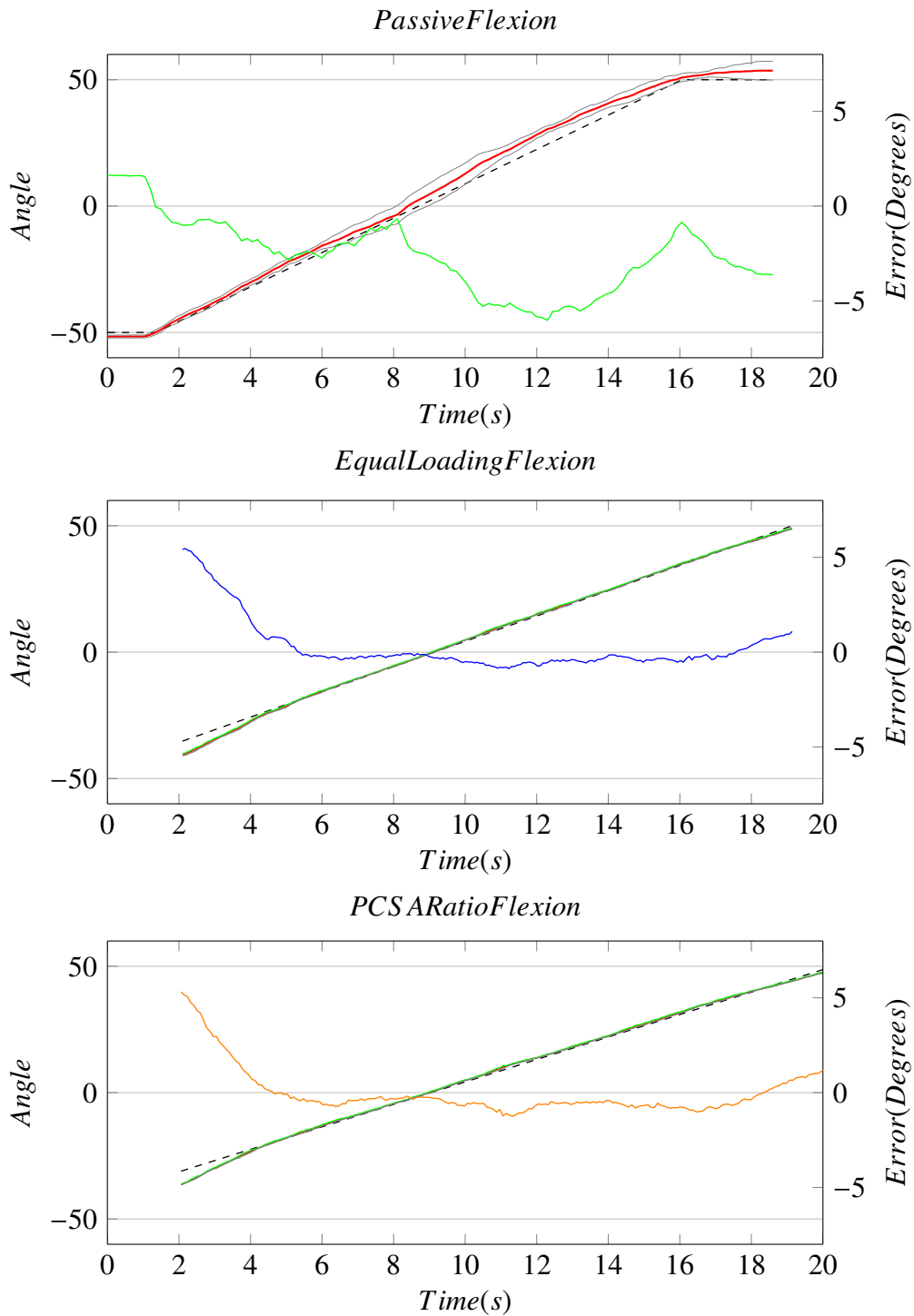


Figure 4.2: Repeatability of flexion motion showing average motion trial [red], target angle [dashed black line], and standard deviation [gray lines]. The average trial error from the target is represented as green [passive], blue [equal loading], or orange [PCSA ratio]

4.3.1.2 Non-Planar Deviations

There were no notable differences in out-of-plane active motion, that being tendency to abductor or adduct during FEM motion, between the two portioning techniques in either flexion or extension (Figure 4.3). The similar performance was most likely occurred because there was no tendon portioning was applied to the *radial* or *ulnar deviator* muscle groups and were identical between trials. However, the trials with the PCSA loading ratio were more consistent with respect to the equal tendon loading trials with standard deviation between all trials approximately 15.7% lower during extension and 32.8% lower during flexion.

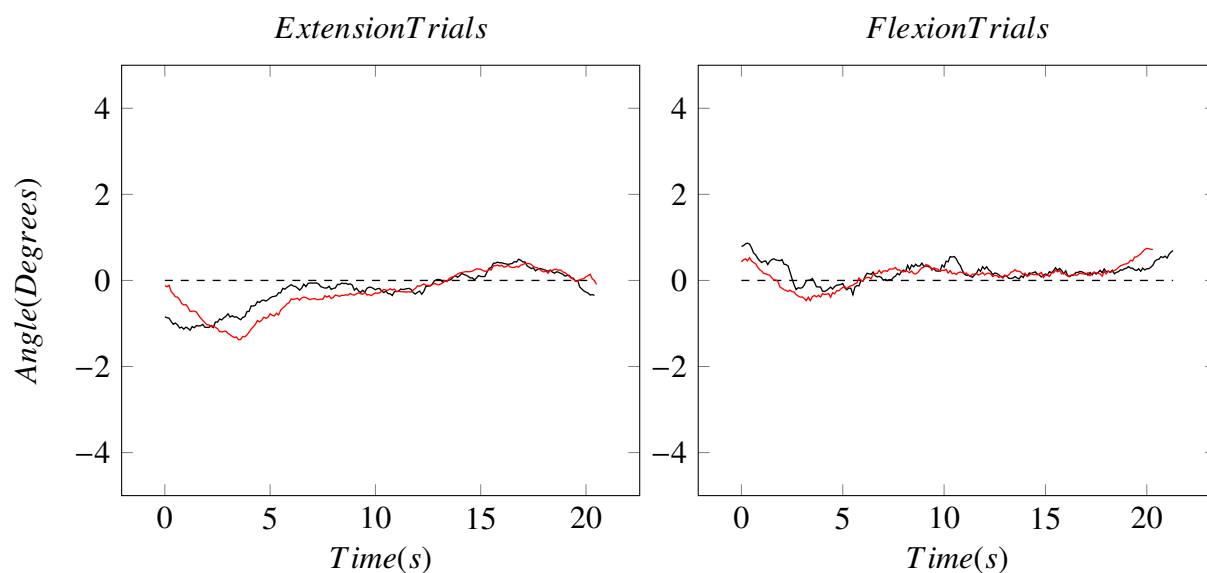


Figure 4.3: Repeatability of experimental motion [solid lines] with respect to desired [dashed line] for out plane motion (RUD plane) during PCSA portioned [red] and equal loading [black] loaded scenarios in extension [left] and flexion [right]

4.3.2 Repeatability of Tendon Forces

An effect of portioning the tendon forces was found to reduce overall force during extension but not in flexion as seen in Figure 4.4. The latency observed from the motion trials carries through to the force data as an inherent characteristic of the PID controller; since there exists a larger magnitude of error between the actual and desired angles the proportional constant will ultimately increase the forces to reduce error. Once the PCSA portioned trials 'catch up' during extension, there is a noticeable difference of 5-10 N between the trials with PCSA falling below that of the default state. The same trend is present during flexion trials, however the effect is too subtle to state any differences.

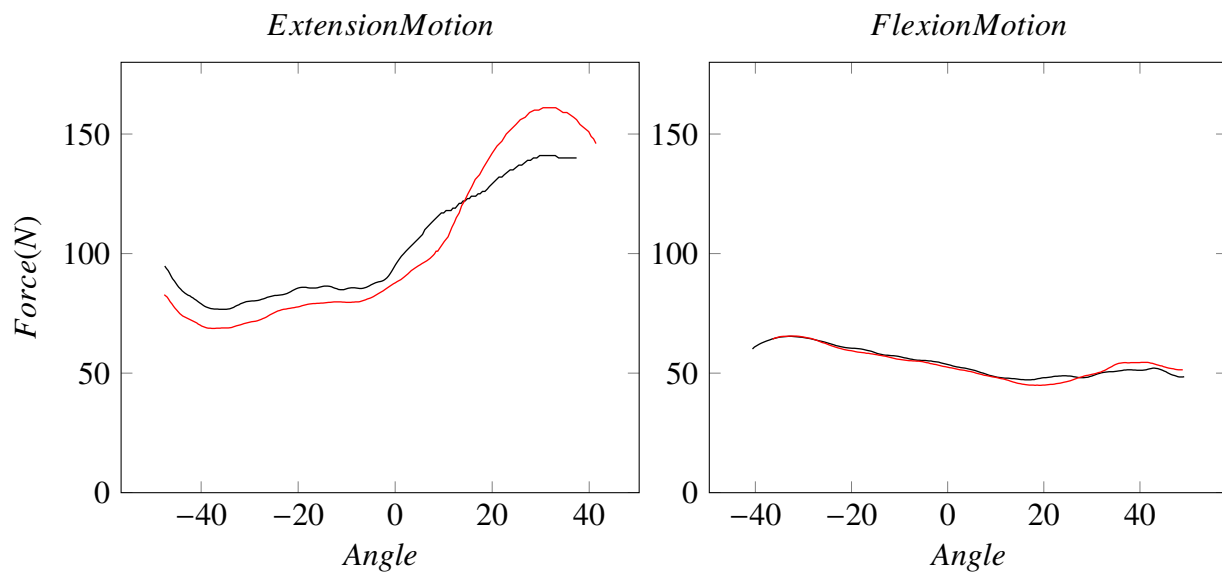


Figure 4.4: The sum of all tendon forces averaged between trials for extension [left] and flexion [right] motions comparing equal loading [black] to the PCSA portioning [red]

4.4 Discussion

There were no apparent difference in the performance of planar FEM motion trials between equal loading and PCSA portioned methods, however evidence of subtle improvements to performance in the later regions of motion and decreased overall forces supports the need for further investigation.

4.4.1 Effects of Portioning on the Motion Profile

The latency for achieving steady state extension motion in portioned trials was most likely attributed to the combination of the behaviour of the force controllers and the portioning method itself that establishes a primary mover. The onset of the latency occurred at the inception of *extension* motion where there had been a reduction of total extensor force available by 16.0% requiring the majority of load to be provided by the ECRB and ECU muscles. Naturally, the larger load required by these two muscles to compensate for the restricted ECRL would take a longer time to reach, under identical PID parameters for the position-force controllers, as well as overshoot the target upon reaching the desired angle. These behaviours may be reduced with further tuning of the position-force controller parameters used to move the wrist along the desired path. Flexion motion on the other hand did not behave any differently between either of the portioning methods regardless of a 41.2% reduction to the FCR (20.2% overall reduction to flexor group). This was most probably the result of larger moment arms present for the FCR and FCU with respect to the extensor muscles (with exception of the ECRB) therefore increasing the influence of motion over the extensors.

There was no apparent difference between out-of-plane deviations during motion with regards to error from desired path, but there was a considerable decrease in variance of motion between the portioned and default loading conditions. Understanding that the FCR and ECRL were restricted by 41.2% and 44.4% respectively the unintentional tendency to induce radial deviation during sudden fluctuations in the extensor or flexor forces seemed to subside and result in a smoother motion profile as seen in Figure 4.3.

4.4.2 Effects of Portioning on Magnitude of Forces

Portioning the tendon forces only influenced the performance of the arm during extension trials where a noticeable decrease in overall force was present in the second half of the trial. This provides evidence that the ECRL may be more influential as a wrist abduction, due to its insertion on the second metacarpal, and less as an extensor with respect to the ECRB with its insertion onto the third metacarpal. By portioning the ECRL the wrist had less tendency to abduct during extension and required less corrective forces from the adductors to eliminate non-planar motion resulting in overall lower magnitudes of force across the wrist.

4.4.3 Developing Tendon Portioning Ratios

Where there is an abundance of published literature on loading ratios derived from PCSA, moment arms, and EMG data for the *pronator quadratus* and *biceps brachii* muscles in forearm rotation as used by Gordon *et al.* or for the *deltoid* and *rotator cuff* muscles during shoulder motion as used by Giles *et al.*, there remains a shortage of data necessary for developing accurate loading conditions of the wrist during motion. Published data on the PCSA and moment arm of forearm muscles as well as the EMG contributions of flexor and extensor muscles as groups are readily available in literature but there remains a lack of availability of individual EMG data on the *extensor carpi radialis longus*, *extensor carpi radialis brevis*, *extensor carpi ulnaris*, *flexor carpi radialis*, and *flexor carpi ulnaris* during motions of the wrist. Without this insight from the EMG data it remains largely speculative as to what the individual force contributions actually are and must be drawn from PCSA and MA data until available.

This study has limitations. First, attempts to implement portioning ratios established from the combination of moment arm and PCSA data were unsuccessful in providing a suitable means of actuation as the reduction for the extensors was too great to overcome the flexors past the point of inflection (neutral wrist position). Deficiencies were present in the process from which these ratios were established and their failure cannot be attested to a lack a relevance. Second, only one specimen was tested due to time constraints present. More specimens are required for a complete quantitative analysis on the effects of the PCSA portioning on wrist kinematics.

4.5 Conclusions

Portioning is a well established method for modeling *in-vivo* conditions during active motion cadaveric studies as demonstrated by several investigators already for the shoulder, elbow, and forearm. Loading ratios drawn from PCSA data demonstrated the potential to reduce inter-trial variance as well as lower overall force across the wrist by 5-10 N when tuned accordingly. Further tuning may reduce the latency present in the first half of the portioned trials to sustain steady state motion which would make this the desirable method over the current default loading conditions for further investigations. Future work will investigate deeper into loading ratios drawn from EMG signals as published data becomes more readily available.

References

- [1] S. L. Delp, A. E. Grierson, and T. S. Buchanan, "Maximum isometric moments generated by the wrist muscles in flexion-extension and radial-ulnar deviation," *Journal of biomechanics*, vol. 29, no. 10, pp. 1371–1375, 1996.
- [2] K. S. Saladin and L. Miller, *Anatomy & physiology - The Unity of Form and Function*. McGraw-Hill Company Inc, 2nd ed., 2008.
- [3] R. V. Gonzalez, T. S. Buchanan, and S. L. Delp, "How muscle architecture and moment arms affect wrist flexion-extension moments," *Journal of biomechanics*, vol. 30, no. 7, pp. 705–712, 1997.
- [4] O. Fukuda, T. Tsuji, M. Kaneko, and A. Otsuka, "A human-assisting manipulator teleoperated by emg signals and arm motions," *Robotics and Automation, IEEE Transactions on*, vol. 19, no. 2, pp. 210–222, 2003.
- [5] R. A. R. C. Gopura and K. Kiguchi, "Emg-based control of an exoskeleton robot for human forearm and wrist motion assist," in *Robotics and Automation, 2008. ICRA 2008. IEEE International Conference on*, pp. 731–736, IEEE, 2008.
- [6] O. Fukuda, T. Tsuji, A. Ohtsuka, and M. Kaneko, "Emg-based human-robot interface for rehabilitation aid," in *Robotics and Automation, 1998. Proceedings. 1998 IEEE International Conference on*, vol. 4, pp. 3492–3497, IEEE, 1998.
- [7] K. Farry, I. D. Walker, R. G. Baraniuk, *et al.*, "Myoelectric teleoperation of a complex robotic hand," *Robotics and Automation, IEEE Transactions on*, vol. 12, no. 5, pp. 775–788, 1996.
- [8] M. Nishiwaki, M. Welsh, B. Gammon, L. M. Ferreira, J. A. Johnson, and G. J. King, "Distal radioulnar joint kinematics in simulated dorsally angulated distal radius fractures," *The Journal of hand surgery*, vol. 39, no. 4, pp. 656–663, 2014.
- [9] C. E. Dunning, C. S. Lindsay, R. T. Bicknell, S. D. Patterson, J. A. Johnson, and G. J. King, "Supplemental pinning improves the stability of external fixation in distal radius fractures during simulated finger and forearm motion," *The Journal of hand surgery*, vol. 24, no. 5, pp. 992–1000, 1999.
- [10] K. Gordon, C. Dunning, J. Johnson, and G. King, "Kinematics of ulnar head arthroplasty," *Journal of Hand Surgery (British and European Volume)*, vol. 28, no. 6, pp. 551–558, 2003.

- [11] K. D. Gordon, R. D. Pardo, J. A. Johnson, G. J. King, and T. A. Miller, "Electromyographic activity and strength during maximum isometric pronation and supination efforts in healthy adults," *Journal of orthopaedic research*, vol. 22, no. 1, pp. 208–213, 2004.
- [12] C. E. Dunning, Z. D. Zarzour, S. D. Patterson, J. A. Johnson, and G. J. King, "Ligamentous stabilizers against posterolateral rotatory instability of the elbow," *The Journal of Bone & Joint Surgery*, vol. 83, no. 12, pp. 1823–1828, 2001.
- [13] K. D. Gordon, C. E. Dunning, J. A. Johnson, and G. J. King, "Influence of the pronator quadratus and supinator muscle load on druj stability," *The Journal of hand surgery*, vol. 28, no. 6, pp. 943–950, 2003.
- [14] A. Amis, D. Dowson, and V. Wright, "Muscle strengths and musculoskeletal geometry of the upper limb," *Engineering in Medicine*, vol. 8, no. 1, pp. 41–48, 1979.
- [15] A. Kedgley, G. Mackenzie, L. Ferreira, D. Drosdowech, G. King, K. Faber, and J. Johnson, "The effect of variable muscle loading ratios on the kinematics of glenohumeral abduction," *Trans Orthop Res Soc*, vol. 606, 2005.
- [16] A. E. Kedgley, G. A. Mackenzie, L. M. Ferreira, D. S. Drosdowech, G. J. King, K. J. Faber, and J. A. Johnson, "The effect of muscle loading on the kinematics of in vitro glenohumeral abduction," *Journal of biomechanics*, vol. 40, no. 13, pp. 2953–2960, 2007.
- [17] J. W. Giles, L. M. Ferreira, G. S. Athwal, and J. A. Johnson, "Development and performance evaluation of a multi-pid muscle loading driven in vitro active-motion shoulder simulator and application to assessing reverse total shoulder arthroplasty," *Journal of biomechanical engineering*, vol. 136, no. 12, p. 121007, 2014.
- [18] F. W. Werner, A. K. Palmer, J. H. Somerset, J. J. Tong, D. B. Gillison, M. D. Fortino, and W. H. Short, "Wrist joint motion simulator," *Journal of orthopaedic research*, vol. 14, no. 4, pp. 639–646, 1996.
- [19] S. Erhart, W. Schmoelz, and M. Lutz, "Clinical and biomechanical investigation of an increased articular cavity depth after distal radius fractures: effect on range of motion, osteoarthritis and loading patterns," *Archives of orthopaedic and trauma surgery*, vol. 133, no. 9, pp. 1249–1255, 2013.

Chapter 5

General Discussion & Conclusions

***OVERVIEW:** This chapter reviews the objectives and hypotheses outlined in Chapter 1 (Section 1.4). The steps taken during the development of the simulator and decisions for the method of approach are highlighted. The strengths and weaknesses are reviewed, as are the testing methods used to validate the performance of the wrist simulator and compare it to other existing simulators. Finally, an outline for future work to further improve simulator performance and the clinical research is proposed.*

5.1 Summary

The understanding of wrist kinematics *in-vivo* is crucial when quantitatively analyzing reparative methods such as fracture fixation, arthroplasty, and ligament repair with respect to the healthy state. In Chapter 2 the process behind the design and development of an active motion simulator was outlined with emphasis on the rationale for the methods of actuation and tracking. The seven tendons of interest for controlling wrist motion and forearm rotation were sutured and attached to a manifold of seven electric servomotors (SM2316D-PLS2, SMI Animatics Corp., CA) responsible for applying forces. Each motor was instrumented with a full bridge style strain gage (Vishay Precision Group, Raleigh, NC) and calibrated (Appendix B) to provide force feedback. The simulator was able to maintain target tendon loads and effectively simulate passive motion trials comparable to the simulator used by Nishiwaki *et al.* [1, 2]. Using optical tracking methods (Certus Optotrak, Northern Digital Inc., VT), the relative positions of the third metacarpal, radius, and ulna were obtained to provide real time positional feedback to the system without restricting the material compatibilities present with electromagnetic tracking. The tendons were divided into four quadrants; flexors, extensors, radial deviators, and ulnar deviators to influence motion of the wrist in flexion-extension and radioulnar deviation. Using a minimum tone load of 8.9 N the muscle groups were activated to produce motion in the desired direction. A cascade PID controller was developed to limit positional error between the actual and desired wrist position by adjusting the balance of forces between the muscle quadrants.

Objectives 1 & 2 outlined the generic performance requirements of the simulator based off existing simulator platforms. These were satisfied in Chapter 2 as the simulator was successful in reproducing motions in all planes of the wrist. Five cadaver specimens were tested for planar motion for flexion-extension and radioulnar deviation in a gravity neutral position which ultimately was the least stable position to generate motion due to the shifting gravitational effects at neutral wrist position. Motion trials were collected in each of the planes from 50 degrees flexion to 50 degrees extension for FEM and 20 degrees ulnar deviation to 10 degrees radial deviation. Static trials were then performed through each range of motion at intervals of 10

degrees for FEM and 5 degrees for RUD to gain an understanding of the stability of the wrist at each stage of motion. Overall, the simulator was able to produce motion along a pathway to within $0.3 \pm 0.4^\circ$ between trials which exceeded the objective of 1 degree.

Chapter 3 outlined the steps taken to satisfy *Objective 3* by investigating the effects of gravity on the ability for the simulator to produce repeatable motion as well as comment on the kinematic differences between planar motion, non-planar motion, and force trends. As hypothesized, the force trends between the gravity loaded positions showed noticeable increases in the muscles groups responsible for opposing gravitational forces; the flexor group was greater in gravity loaded flexion and the extensor group was larger in gravity loaded extension. However, the position of the arm had no significant effect on either the repeatability or motion profile in the FEM plane as discussed in Chapter 3 (Section 3.4). The tendon force distribution to hold a static neutral position in gravity flexion and extension positions compared closely to those reported by Dunning *et al.* [3] with minor discrepancies that arose from differences in forearm position between studies; Dunning reported forces in supination and pronation while ours reported in neutral forearm rotation.

Chapter 4 focused on an early investigation into the effects of portioning the tendon loads to more closely match those present *in-vivo* used ratios drawn from published literature on the *physiological cross sectional area* (PCSA) [4, 5, 6, 7, 8, 9, 10]. These ratios interfered with the tuning parameters of the PID controller introducing a latency at the onset of motion during each trial due to the restricted tendon forces. Overall, the PCSA reduced the trial variation and produced smoother motion as a result of a restriction to the *flexor carpi radialis* and *extensor carpi radialis longus* tendons that ultimately reduced the tendency of the wrist to rotate radially during flexion or extension motion trials.

5.2 Strengths & Limitations

To our knowledge, the simulator developed in this thesis was the first ever with capabilities of performing both passive and action *in-vitro* motion trials as well as having the freedom to test flexion-extension and radioulnar deviation between three gravity loaded positions. Using optical cameras to track the relative positions of the bones removes the limitations of using ferric materials in the proximity of the study as is present with electromagnetic tracking systems used by other investigators. This freedom allows for the use of conventional fasteners and apparatus for collecting data such as load cells, eliminating the need for custom designed plastic components. Using electric servo motors provided a more desirable resolution and more precise increments in position than attainable by hydraulic or pneumatic actuators used by others.

The simulator and investigations presented in this thesis have some limitations. Optical tracking requires a line of sight between the cameras and trackers to maintain a fix on the position, requiring the investigation design to adapt to these needs that could possibly hinder the process. For instance, during attempted pronation-supination trials the trackers rotated out of view of the camera after 40 degrees of rotation, hence multi-bodied trackers would be needed to incorporate forearm rotation into investigations. The investigations discussed in this thesis used elderly cadavers which are suboptimal due to the poor bone quality and degrading articular cartilage generally present in the joints of these specimens. However, elderly specimens were acceptable as the purpose of this thesis was to validate the performance of the active motion simulator and there were no clinical measures being performed. Finally, studies only considered static positions and motion trials along a single plane (FEM or RUD) and did not perform multi-planar motions such as the *dart throw* which would have provided an understanding of the simulator's ability to follow two continually changes target positions.

5.3 Current & Future Directions

The simulator satisfied the objectives outlined at the beginning of the study in Chapter 1 (Section 1.10), however there are a variety of avenues ahead to further improve the performance of motion trials. Future studies will look further into tendon loading ratios developed from published data on *moment arms*, *physiological cross sectional area*, and *electromyography* signals to more accurately model *in-vivo* conditions during motion trials as well as a specific PID tuning process to reduce the latency present at the onset of motion. With the simulator able to accurately reproduce motion trials in all three positions, there are several clinical studies on the horizon. One such study is the investigation into the contribution and behaviour of individual carpal bones (*scaphoid*, *lunate*, *capitate*) during wrist motion, requiring three additional trackers to be incorporated into the apparatus design. As there are already reports published by Nishiwaki *et al.* in a neutral gravity position it will act a benchmark to compare to before continuing to gravity loaded flexion and extension positions.

The list of clinically relevant studies that can be undertaken now is very robust. A series of studies of the kinematics and stability of the carpal bones, both intact and subsequent to injury and repair, is needed and can be achieved readily using this system. Implant development for wrist replacements is in its infancy, but is an exciting clinical option. However, a wide range of biomechanical studies will be required, and the simulator herein is well positioned to undertake this task. Also, a series of studies looking into the influence of forearm instabilities and repairs can also be easily conducted. A relatively new field that is emerging and lacks research is the kinematic effects of dynamic wrist bracing for post-operative support or preventative injury for sports. Braced versus unbraced motion trials while tracking the third metacarpal, radius, ulna, and the carpal bones of interest would provide valuable insight into how bracing actually effects the kinematics of the wrist. However, given that braces generally require rigid components on the dorsal and volar surfaces of the wrist to provide the necessary support, access to the carpal bones becomes a challenge and may require custom designed components and modifications to allow for tracking without tracker impingement. This will be well-suited using the technology developed in this treatise.

References

- [1] M. Nishiwaki, M. Welsh, B. Gammon, L. M. Ferreira, J. A. Johnson, and G. J. King, “Volar subluxation of the ulnar head in dorsal translation deformities of distal radius fractures: An in vitro biomechanical study,” *Journal of orthopaedic trauma*, vol. 29, no. 6, pp. 295–300, 2015.
- [2] M. Nishiwaki, M. Welsh, B. Gammon, L. M. Ferreira, J. A. Johnson, and G. J. King, “Distal radioulnar joint kinematics in simulated dorsally angulated distal radius fractures,” *The Journal of hand surgery*, vol. 39, no. 4, pp. 656–663, 2014.
- [3] C. E. Dunning, C. S. Lindsay, R. T. Bicknell, S. D. Patterson, J. A. Johnson, and G. J. King, “Supplemental pinning improves the stability of external fixation in distal radius fractures during simulated finger and forearm motion,” *The Journal of hand surgery*, vol. 24, no. 5, pp. 992–1000, 1999.
- [4] K. Gordon, C. Dunning, J. Johnson, and G. King, “Kinematics of ulnar head arthroplasty,” *Journal of Hand Surgery (British and European Volume)*, vol. 28, no. 6, pp. 551–558, 2003.
- [5] K. D. Gordon, R. D. Pardo, J. A. Johnson, G. J. King, and T. A. Miller, “Electromyographic activity and strength during maximum isometric pronation and supination efforts in healthy adults,” *Journal of orthopaedic research*, vol. 22, no. 1, pp. 208–213, 2004.
- [6] C. E. Dunning, Z. D. Zarzour, S. D. Patterson, J. A. Johnson, and G. J. King, “Ligamentous stabilizers against posterolateral rotatory instability of the elbow,” *The Journal of Bone & Joint Surgery*, vol. 83, no. 12, pp. 1823–1828, 2001.
- [7] K. D. Gordon, C. E. Dunning, J. A. Johnson, and G. J. King, “Influence of the pronator quadratus and supinator muscle load on druj stability,” *The Journal of hand surgery*, vol. 28, no. 6, pp. 943–950, 2003.
- [8] A. Kedgley, G. Mackenzie, L. Ferreira, D. Drosdowech, G. King, K. Faber, and J. Johnson, “The effect of variable muscle loading ratios on the kinematics of glenohumeral abduction,” *Trans Orthop Res Soc*, vol. 606, 2005.
- [9] A. E. Kedgley, G. A. Mackenzie, L. M. Ferreira, D. S. Drosdowech, G. J. King, K. J. Faber, and J. A. Johnson, “The effect of muscle loading on the kinematics of in vitro glenohumeral abduction,” *Journal of biomechanics*, vol. 40, no. 13, pp. 2953–2960, 2007.

- [10] J. W. Giles, L. M. Ferreira, G. S. Athwal, and J. A. Johnson, "Development and performance evaluation of a multi-pid muscle loading driven in vitro active-motion shoulder simulator and application to assessing reverse total shoulder arthroplasty," *Journal of biomechanical engineering*, vol. 136, no. 12, p. 121007, 2014.

Appendix A

Establishing Bone Coordinate Systems

Coordinate systems for the ulna, radius, and third metacarpal were established in accordance to ISB standards outlined in Chapter 1 (Section 1.5). Methods for establishing coordinate systems for the ulna and radius were adapted from previous research at our laboratory, however no convention previously existed for referencing a metacarpal bone. The following section outlines the bony landmarks digitized for each bone, after denuding, and the process used to create a left/right standard reference frame.

A.1 Local Reference Frame: Ulna

The *coronoid process* (CP), *ulnar styloid process* (US), and a *distal medial aspect* of distal head (UM) were digitized as points and a trace following the circumference of the trochlear notch was collected (Figure A.1). From these points, a vector was drawn between the CP and UM to establish a midpoint that would serve as the distal point for the longitudinal axis. The centroid from the trochlear notch trace was determined using the circle fitting algorithm from Appendix D and was set to the proximal point for the longitudinal axis of the ulna. The midpoint of the longitudinal axis was set as the origin (UO) of the ulnar coordinate system from which the remaining vectors were related to. For a left arm, a vector was established between UO and the distal point of the longitudinal axis, v_1 , to establish the y axis directed distally. A reference vector was created from UO and US, v_2 , to define a plane along the y-axis. The x axis was established by crossing v_2 with v_1 ($v_2 \times v_1$) so positive x was directed dorsally. For a right arm, a vector was established between UO and the proximal point of the longitudinal axis, v_1 , to establish the y axis directed proximally. A reference vector was created from UO and US, v_2 , to define a plane along the y-axis. The x axis was established by crossing v_2 with v_1 ($v_2 \times v_1$) so positive x was in the volar direction. Regardless of side, the x axis was crossed with the y axis ($x \times y$) to establish the z axis.

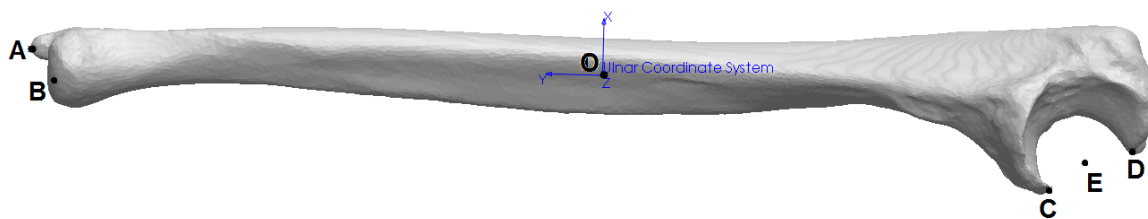


Figure A.1: An ulnar coordinate system is established from bony landmark digitizations of the ulnar styloid [A], distal medial head [B], coronoid process [C], and olecranon process [D] and the calculated locations of the trochlear notch centroid [E] and origin [O]

A.2 Local Reference Frame: Radius

The *radial styloid process* (RS), *dorsal sigmoid notch aspect* (DSiN), *proximal radial dish* (RD) and *volar sigmoid notch aspect* (VSiN) were digitized and the proximal radial dish was traced with the stylus (Figure A.2). Using an open source sphere fitting algorithm (Appendix D), the proximal radial dish trace was matched to a sphere to determine the approximate centroid, however if the articular surface was damaged or flat then the RD was substituted. Either of these points served as the proximal point for the longitudinal axis. A vector was drawn between *dorsal* and *volar sigmoid notch aspects* from which a midpoint was established. Another vector was then drawn from this midpoint to the RS; the midpoint of this vector established the distal point of the longitudinal axis of the radius. The midpoint of the longitudinal axis was set as the origin (RO) of the radial coordinate system from which the remaining vectors were related to. For a left arm, a vector was established between RO and the distal point of the longitudinal axis, v_1 , to establish the y axis directed distally. A reference vector was created from RO and RS, v_2 , to define a plane along the y-axis. The x axis was established by crossing v_2 with v_1 ($v_2 \times v_1$) so positive x was directed dorsally. For a right arm, a vector was established between RO and the proximal point of the longitudinal axis, v_1 , to establish the y axis directed proximally. A reference vector was created from RO and RS, v_2 , to define a plane along the y-axis. The x axis was established by crossing v_2 with v_1 ($v_2 \times v_1$) so positive x was in the volar direction. The x axis was crossed with the y axis ($x \times y$) to establish the z axis.

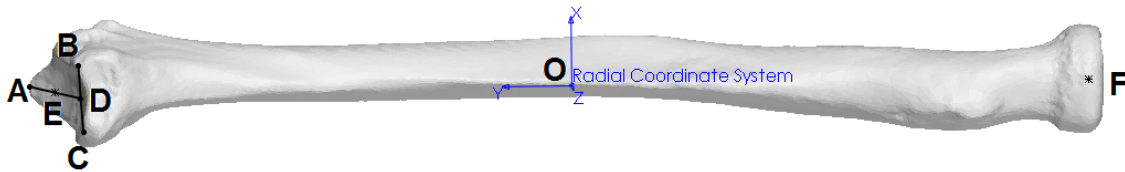


Figure A.2: A radial coordinate system is established from bony landmark digitizations of the radial styloid [A], dorsal sigmoid notch aspect [B], and volar sigmoid notch aspect [C] and the calculated locations of mid-sigmoid notch [D], distal longitudinal marker [E], proximal longitudinal marker [F], and the origin [O]

A.3 Local Reference Frame: Metacarpal

Note: This is a novel method designed for the purpose of this investigation to apply a reference frame to the third metacarpal that conforms to the ISB standards outlined in Chapter 1 (Section 1.5).

The proximal head centroid (PH), distal head centroid (DH), dorsal-radial aspect (DR), and dorsal-ulnar aspect (DU) were collected. A vector was drawn between proximal and distal centroids to serve as the longitudinal axis of the third metacarpal (Figure A.3). The midpoint of the longitudinal axis was set as the origin (MO) of the metacarpal coordinate system from which the remaining vectors were related to. A vector was drawn between the radial and ulnar dorsal aspects to establish a midpoint, P_{mid} , that served as a reference point for establishing the z axis. For a left arm, a vector was established between MO and the distal point of the longitudinal axis, v_1 , to establish the y axis directed distally. A reference vector was created from MO and P_{mid} , v_2 , to define a plane along the y-axis. The z axis was established by crossing v_2 with v_1 ($v_2 \times v_1$) so positive z was directed ulnarly. For a right arm, a vector was established between MO and the proximal point of the longitudinal axis, v_1 , to establish the y axis directed proximally. A reference vector was created from MO and P_{mid} , v_2 , to define a plane along the y-axis. The z axis was established by crossing v_2 with v_1 ($v_2 \times v_1$) so positive z was directed radially. Regardless of side, the y axis was crossed with the z axis ($y \times z$) to establish the x axis.

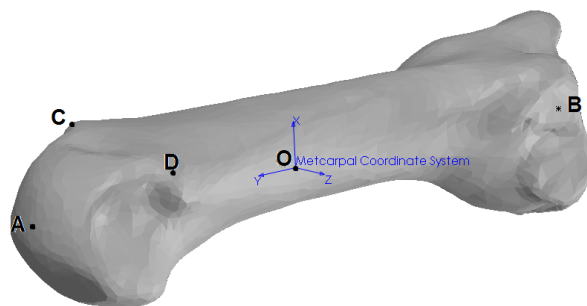


Figure A.3: A metacarpal coordinate system is established from bony landmark digitizations of the distal head [A], proximal head [B], dorsal radial aspect [C], and dorsal ulnar aspect [D] and the calculated location of the origin [O]

A.4 Applying Local Transforms

With the local coordinate systems established, the transformation matrices from each bone with respect to its tracker were used to relate the raw tracker data to each bone. Using transformation chains, as discussed in Chapter 1 (Section 1.4.2), raw tracker data in the global frame was manipulated to describe bone to bone motions by using a series of steps; bone to tracker, tracker to global, global to tracker, and tracker to bone. The two transformations for this thesis were the relation of the third metacarpal to the radius (Equation A.1), and the radius to the ulna (Equation A.2).

$${}^MCT = {}^{MC}T_{C1} {}^{C1}T_G {}^G T_{C2} {}^{C2}T_R \quad (A.1)$$

$${}^R T_U = {}^R T_{C2} {}^{C2}T_G {}^G T_{C3} {}^{C3}T_U \quad (A.2)$$

Where C1, C2, and C3 refer to the optical trackers (Certus Optotrak, Northern Digital Inc., VT) attached to the third metacarpal, radius, and ulna respectively.

Appendix B

Force Transducer Calibration

B.1 Validation of a Load Cell

To ensure that the load cell (Model 31 Low, Honeywell, NJ) was capable of providing reliable force data, a series of known masses were hung in small increments with the load cell in a vertical orientation; note that the load cell was zeroed before the first mass was applied. The default calibration for the load cell was in strong agreement with the masses with a coefficient of determination of $R^2 = 0.9952$ and an average error of 0.17 ± 0.03 g (Figure B.1).

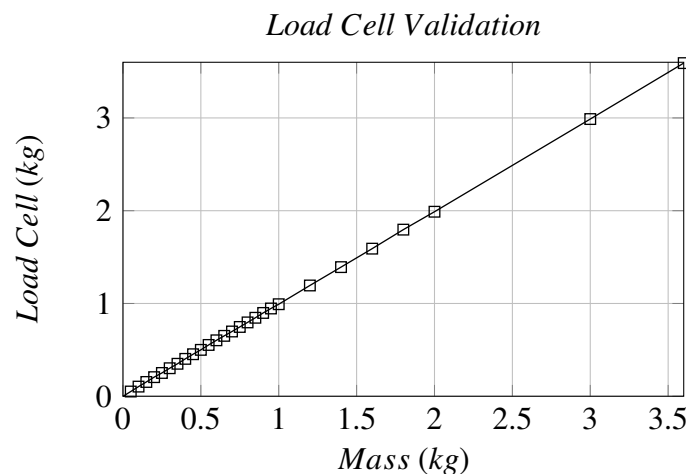


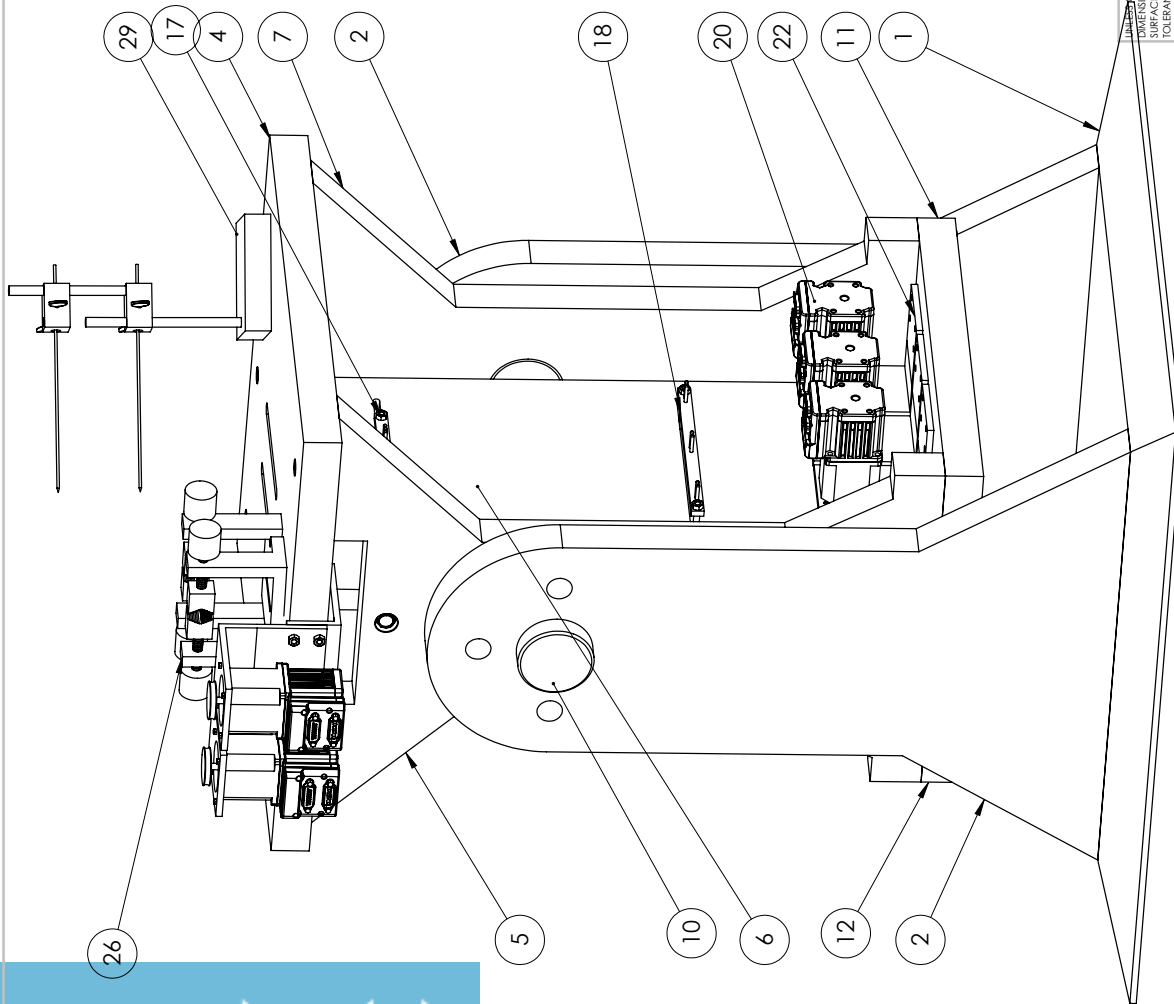
Figure B.1: The load cell was validated by hanging masses of known quantities in incremental and had an R^2 value of 0.9952

B.2 Force Transducer Calibration

Since each force transducer was made in house there using two 90 degree tee rosette strain gages each (Vishay Precision Group, Raleigh, NC), there was no guarantee of consistency between units. The calibration was a three stage process that gained an initial calibration for gain and bias, tested the calibration against the load cell, and then checked for error between gravity loaded positions. First, the load cell was attached in line between the motor and a rigid attachment to the simulator; note that the line of action was maintained perpendicular to the motor as would be relevant during testing. To reduce the magnitude of spikes in force, spring was added between the load cell and simulator to allow small fluctuations in motor position. The motor position was incremented by small steps of approximately 5 N and 5 samples were recorded at each position to compare to the load cell force and strain reading from the transducer to obtain the gain and bias for each unit. Unloaded measurements at rest states had a standard deviation of 0.09 N due to measurement noise. Next, the experiment was repeated for the same transducer but instead the strain value, the calibrated force value was collected with respect to the load cell force and then replotted to confirm agreement between methods. If correlation was poor ($R^2 < 0.95$) then the first two steps were repeated. Finally, the simulator was rotated into the gravity loaded positions and the experiment was repeated again for each with the same gain and bias values determined from the gravity neutral position. All correlations collected were larger than 0.99, suggesting a very strong agreement with the load cell. *Note: when rotating between gravity loaded positions there was a shift in bias for each load cell which was compensated by zeroing the data at the begin off each trial.*

Appendix C

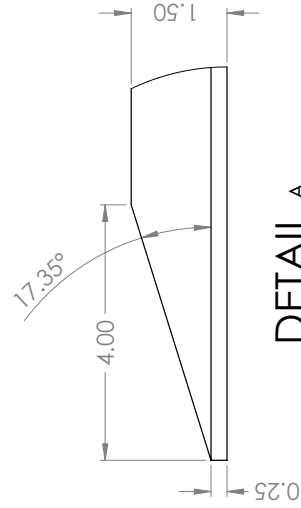
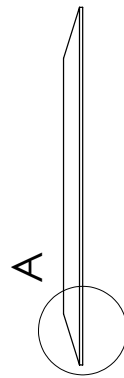
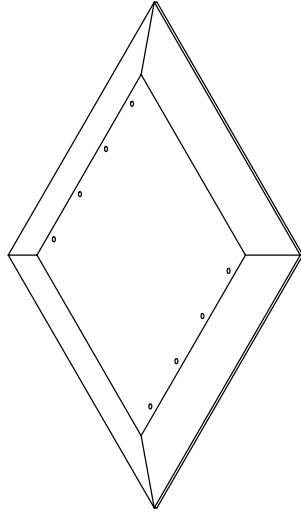
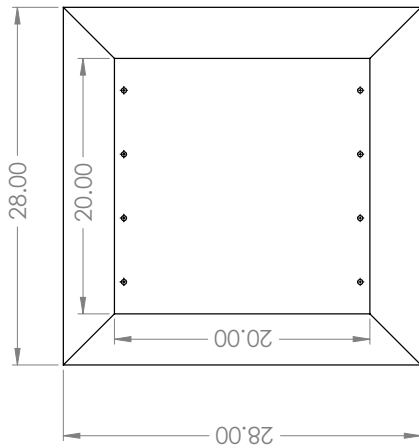
Simulator Mechanical Drawings



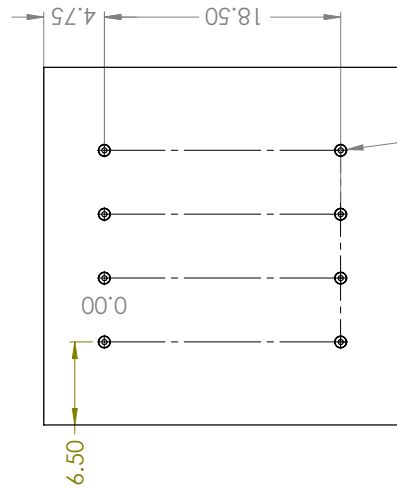
ITEM NO.	PART NUMBER	DESCRIPTION	QTY.
1	Platform_Base		1
2	Platform_Base_Support		2
4	Platform_Top		1
5	Platform_Center_Support_R		1
6	Platform_Center		1
7	Platform_Center_Support_L		1
10	Platform_Pivot_Block		2
11	Platform_Motor_Shelf_R		1
12	Platform_Motor_Shelf_L		1
14	Guide_Top		2
15	Guide_Pin		18
18	Guide_Rail_Lower		2
20	Motor_SM2316		8
22	Motor_Mount_Upper		8
24	Motor_Mount_Lower		2
26	humeral clamp base		1
29	Ulna fixation base		1

OTHERWISE SPECIFIED FINISH: DIMENSIONS ARE IN MILLIMETERS		DEBUR AND BREAK SHARP EDGES	DO NOT SCALE DRAWING	REVISION	V1.0
SURFACE FINISH: TOLERANCES: LINEAR: ANGULAR:					
NAME	SIGNATURE	DATE	TITLE: Assembly		
DRAWN: Durcan Iglesias		02/23/15	DWG NO. WS_000		
CHECK:			SCALE: 1:10		
APP'VD:			SHEET 1 OF 10		
MFG:			MATERIAL:		
Q.A.			WEIGHT:		

**SolidWorks Student Edition.
For Academic Use Only.**



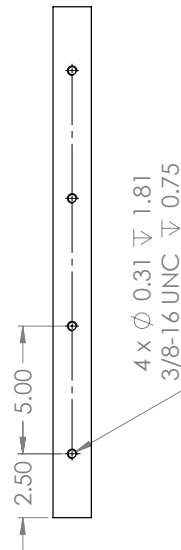
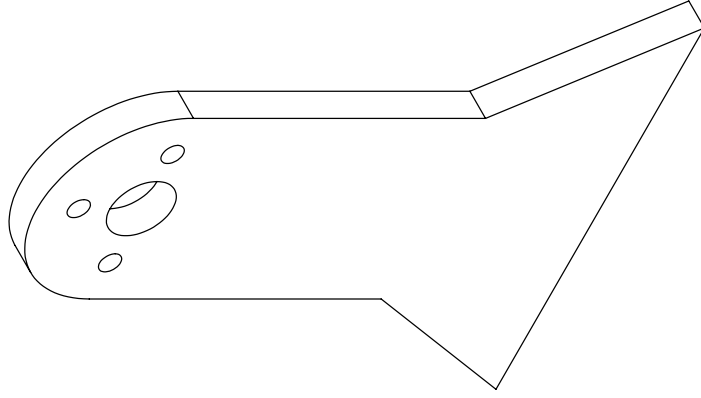
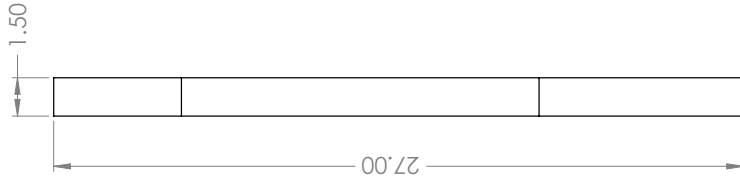
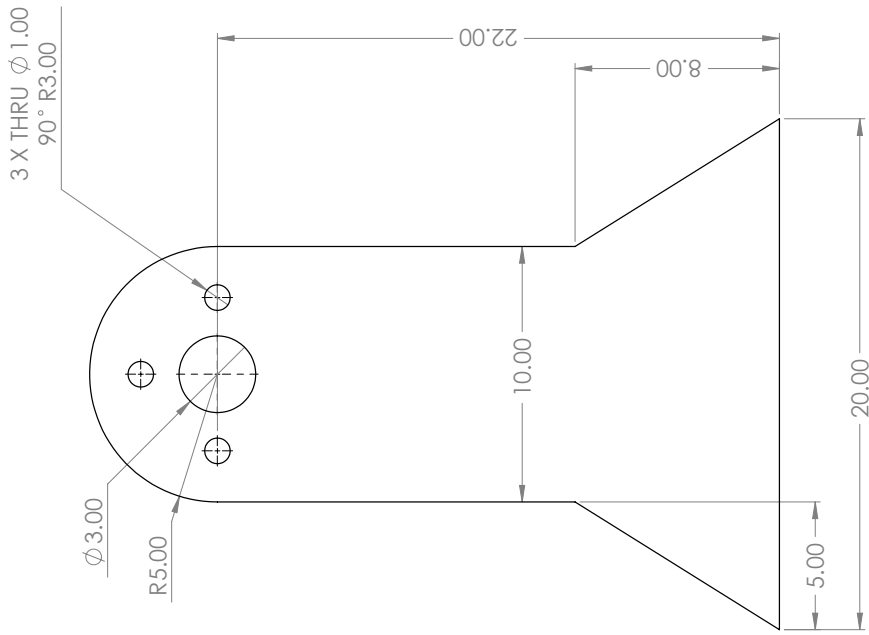
DETAIL A
SCALE 1 : 2



8 x ϕ 0.40 THRU ALL
 \square ϕ 0.88 ∇ 0.37
 ∇ ϕ 0.93 X 90°, Near Side

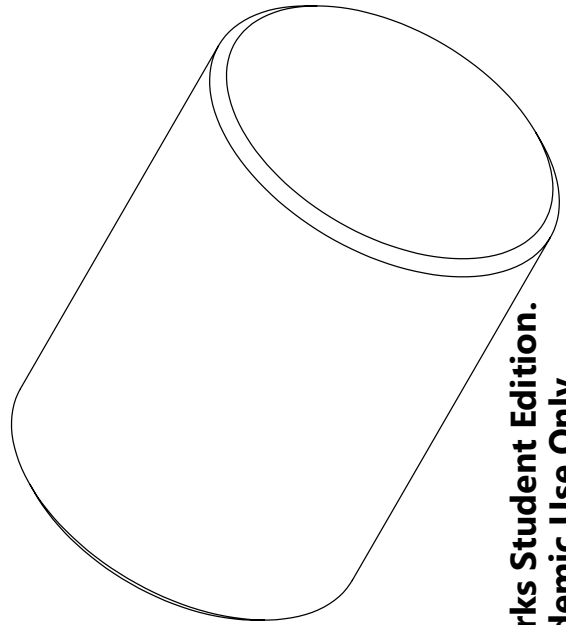
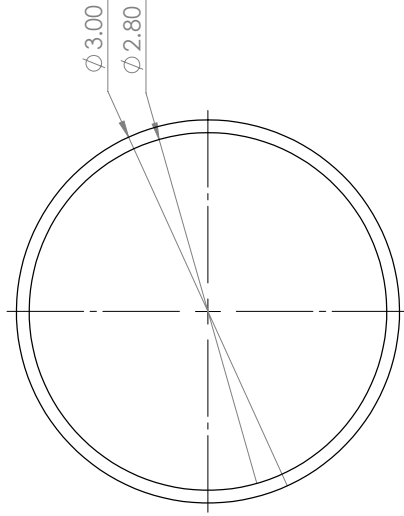
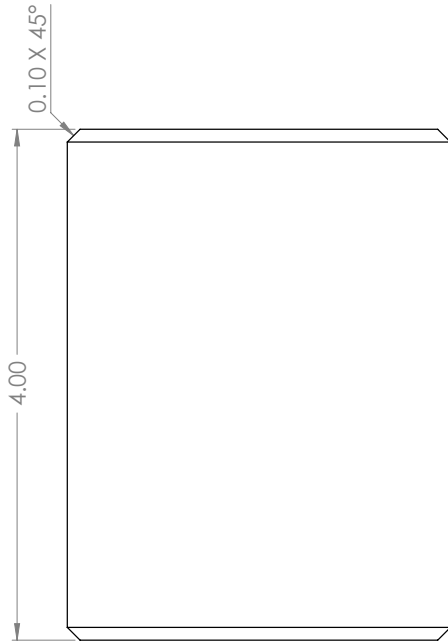
SolidWorks Student Edition.
For Academic Use Only.

UNLESS OTHERWISE SPECIFIED: DIMENSIONS ARE IN MILLIMETERS		FINISH:	DO NOT SCALE DRAWING		REVISION	V1.0
SURFACE FINISH:			DEBUR AND BREAK SHARP EDGES			
TOLERANCES:			TITLE:			
ANGULAR:			Base			
NAME	SIGNATURE	DATE	DWG. NO.	WS_001	A3	
DRAWN: Duncan Iglesias		02/23/15	SCALE: 1:10			
CHECKED:						
APPROVED:						
MFG:						
QA:						
MATERIAL: 1-1/2in Black Delrin Sheet						
WEIGHT:						



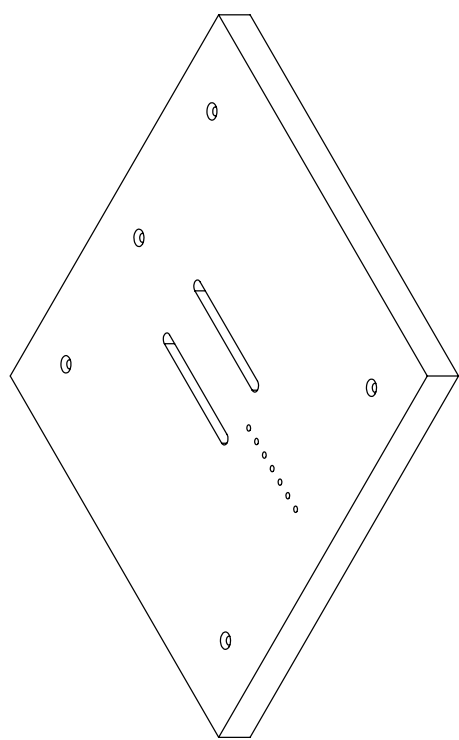
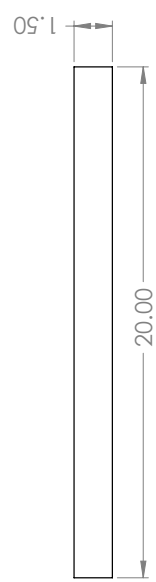
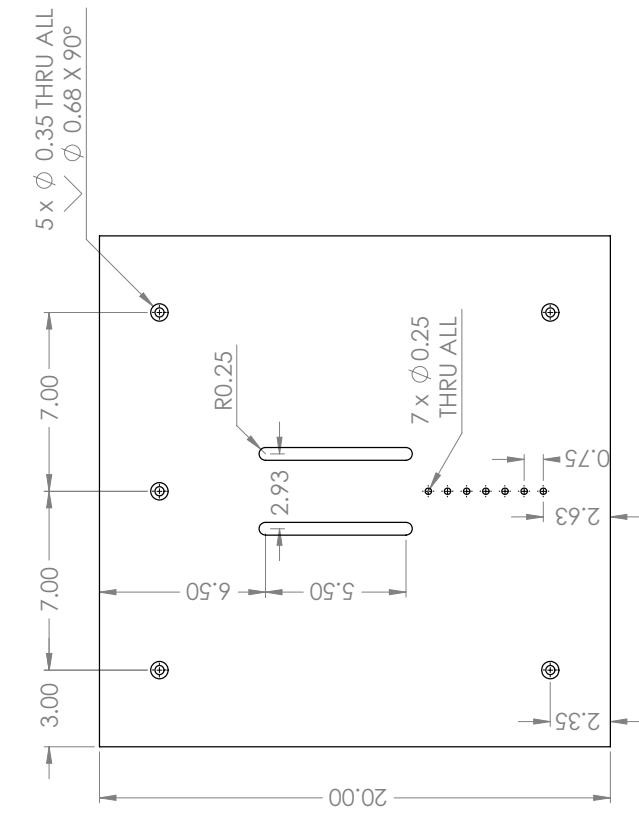
**SolidWorks Student Edition.
For Academic Use Only.**

UNLESS OTHERWISE SPECIFIED: DIMENSIONS ARE IN MILLIMETERS		FINISH:		DEBUR AND BREAK SHARP EDGES		DO NOT SCALE DRAWING		REVISION		V1.0	
SURFACE FINISH:		DRAWN		DATE		TITLE:		DWG. NO.		A3	
TOLERANCES:		CHECKED		02/23/15		Upright Support		WS_002		SHEET 3 OF 10	
LINEAR:		NAME		SIGNATURE		MATERIAL:		SCALE: 1:5		WEIGHT:	
ANGULAR:		Duncan Iglesias				1-1/2in Black Delrin Sheet					
		APPVD:									
		MFG:									
		Q.A:									



**SolidWorks Student Edition.
For Academic Use Only.**

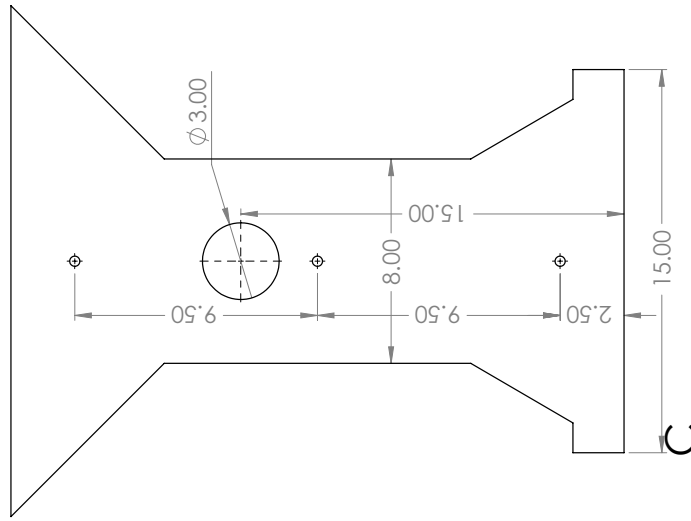
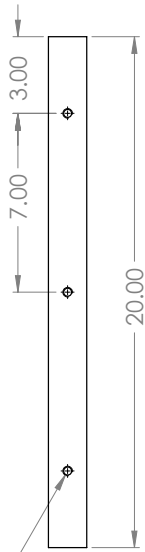
UNLESS OTHERWISE SPECIFIED: DIMENSIONS ARE IN MILLIMETERS		FINISH:	DEBUR AND BREAK SHARP EDGES		DO NOT SCALE DRAWING	REVISION	V1.0
SURFACE FINISH:							
TOLERANCES:							
LINEAR:							
ANGULAR:							
NAME	SIGNATURE	DATE	TITLE:				
DRAWN: Duncan Iglesias		02/23/15	Pivot Block				
CHECKED:			DWG. NO. WS_003				
APPVED:			SCALE: 1:1				
MFG:			SHEET 4 OF 10				
Q.A.			MATERIAL: 3.00in DIA Black Delrin Rod				
			WEIGHT:				



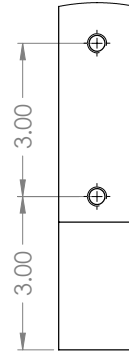
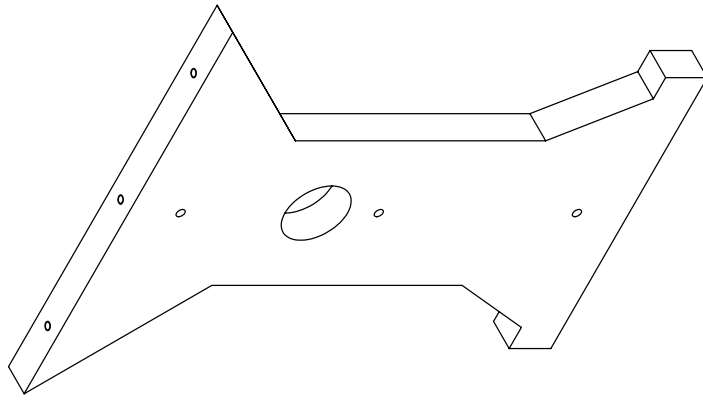
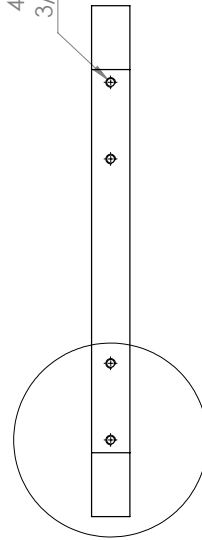
UNLESS OTHERWISE SPECIFIED: DIMENSIONS ARE IN MILLIMETERS		FINISH:		DEBUR AND BREAK SHARP EDGES		DO NOT SCALE DRAWING		REVISION		V1.0	
SURFACE FINISH:		SIGNATURE		DATE		TITLE:		Surface			
TOLERANCES:		NAME		02/23/15							
LINEAR:		DRAWN		Duncan Iglesias							
ANGULAR:		CHKD									
		APPVD									
		MFG									
		Q.A.									
										DWG NO. WS_004	
										A3	
										SCALE: 1:5	
										SHEET 5 OF 10	
										WEIGHT:	
										MATERIAL: 1-1/2in Black Delrin Sheet	

**SolidWorks Student Edition.
For Academic Use Only.**

3 x ϕ 0.31 ∇ 1.81
3/8-16 UNC ∇ 0.75



4 x ϕ 0.31 ∇ 1.00
3/8-16 UNC ∇ 0.75

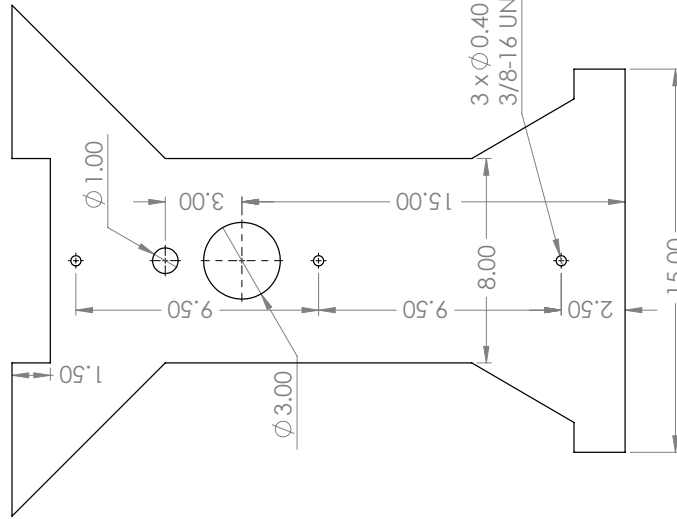
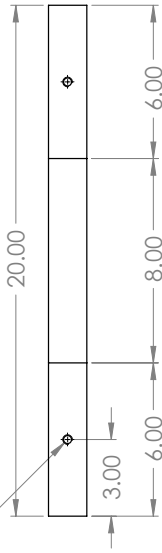


DETAIL C
SCALE 2:5

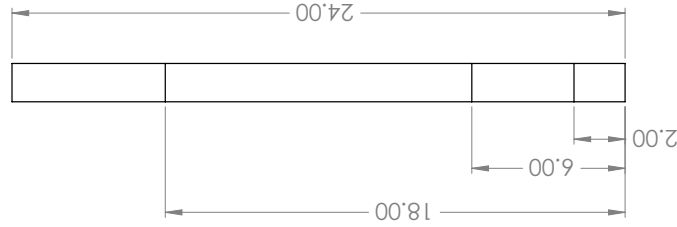
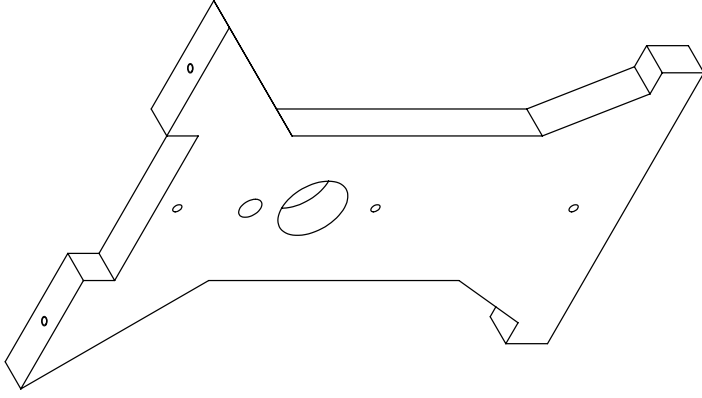
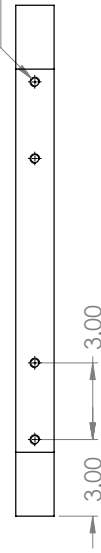
UNLESS OTHERWISE SPECIFIED: DIMENSIONS ARE IN MILLIMETERS		FINISH:	DEBUR AND BREAK SHARP EDGES		DO NOT SCALE DRAWING	REVISION	V1.0
SURFACE FINISH: TOLERANCES: LINEAR: ANGULAR:		NAME DRAWN CHECK APP'VD MFG Q.A.	SIGNATURE Duncan Iglesias	DATE 02/23/15	TITLE: Left Support		
		MATERIAL: 1-1/2in Black Delrin Sheet			DWG NO. WS_005	SHEET 6 OF 10	
					SCALE:1:5	A3	

**SolidWorks Student Edition.
For Academic Use Only.**

2 x ϕ 0.31 ∇ 1.81
 3/8-16 UNC ∇ 0.75

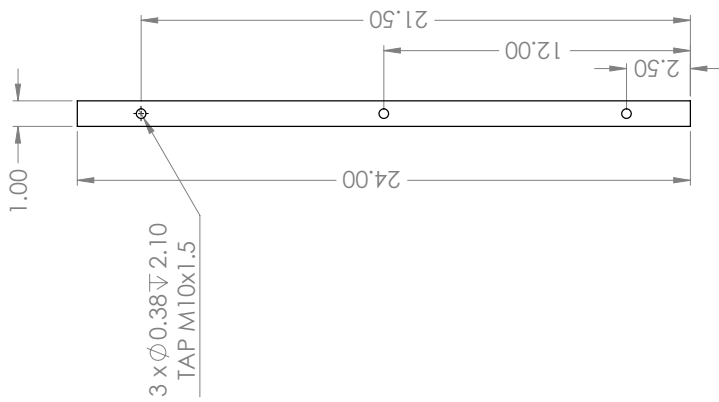
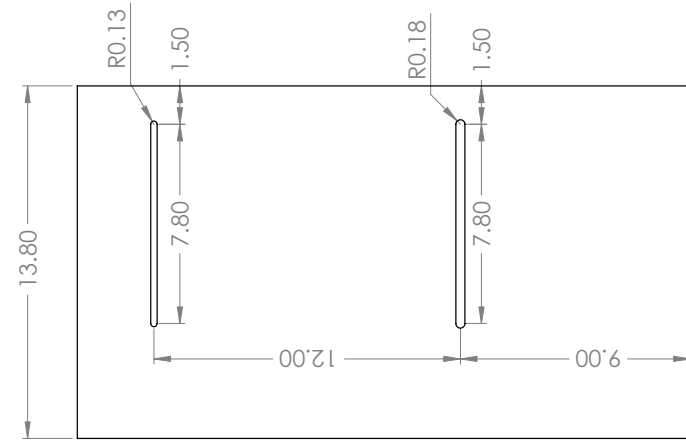
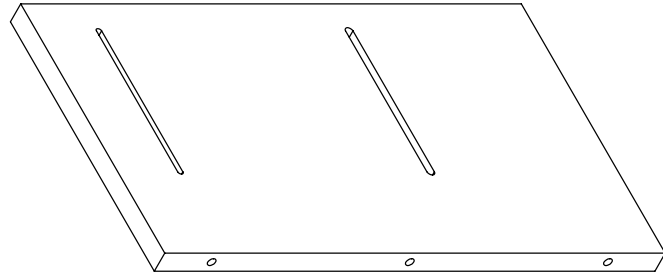


4 x ϕ 0.31 ∇ 1.06
 3/8-16 UNC ∇ 0.75



UNLESS OTHERWISE SPECIFIED: DIMENSIONS ARE IN MILLIMETERS		DATE		REVISION	
SURFACE FINISH: FRACTIONAL ANGULAR:		SIGNATURE		DO NOT SCALE DRAWING	
TOLERANCES: LINEAR: ANGULAR:		DATE		REVISION	
DRAWN: Duncan Iglesias		02/23/15		V1.0	
CHECKED:					
APPVED:					
MFG:					
QA:					
NAME		DATE		TITLE:	
DRAWN: Duncan Iglesias		02/23/15		Right Support	
CHECKED:				DWG. NO. WS_006	
APPVED:				A3	
MFG:				SCALE: 1:5	
QA:				SHEET 7 OF 10	
MATERIAL: 1-1/2in Black Delrin Sheet		WEIGHT:			

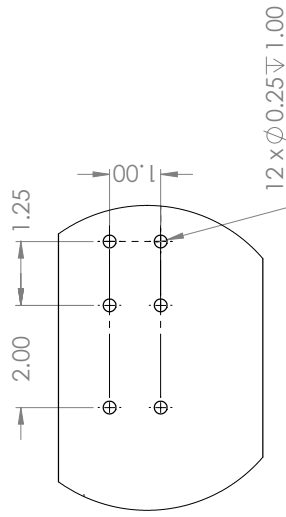
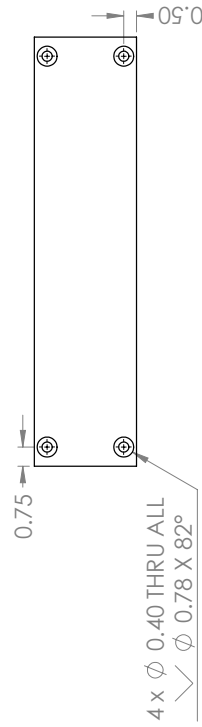
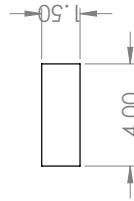
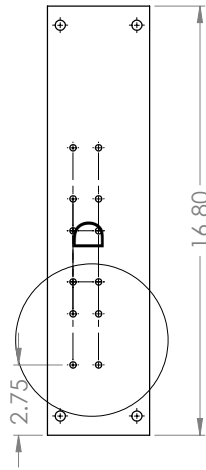
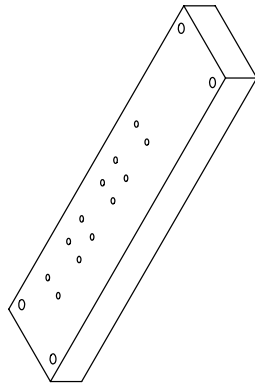
**SolidWorks Student Edition.
 For Academic Use Only.**



UNLESS OTHERWISE SPECIFIED, DIMENSIONS ARE IN MILLIMETERS		FINISH:		DEBUR AND BREAK SHARP EDGES		DO NOT SCALE DRAWING		REVISION		V1.0	
SURFACE FINISH:		TOLERANCES:		TITLE:							
LINEAR:		ANGULAR:		DRAWN		DATE					
				NAME		SIGNATURE					
				DUNCAN IGLESIA							
				CHECKED							
				APPVED							
				MFG							
				Q.A.							
				MATERIAL:		1.00in Black Delrin Sheet		DWG NO.		WS_007	
				WEIGHT:				SCALE:1:10		SHEET 8 OF 10	
										A3	

Center Support

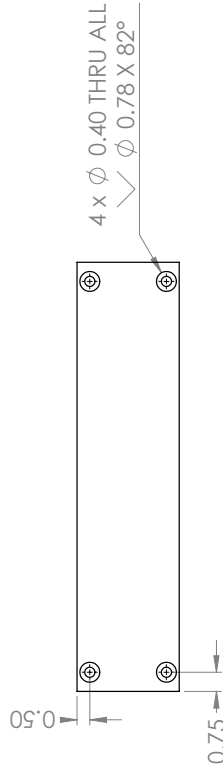
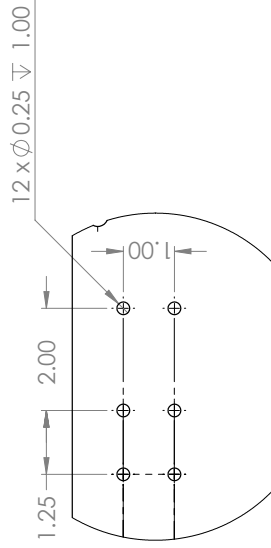
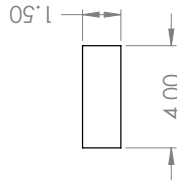
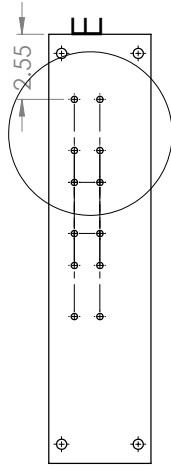
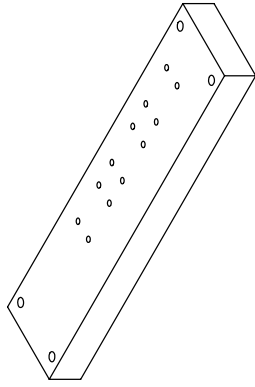
SolidWorks Student Edition.
For Academic Use Only.



DETAIL D
SCALE 2 : 5

UNLESS OTHERWISE SPECIFIED: DIMENSIONS ARE IN MILLIMETERS		FINISH:		DEBUR AND BREAK SHARP EDGES		DO NOT SCALE DRAWING		REVISION	
SURFACE FINISH:		NAME		DATE		TITLE:		V.1.0	
TOLERANCES:		SIGNATURE		DATE		Left Motor Manifold			
LINEAR:		DRAWN		02/23/15		DWG. NO.		A3	
ANGULAR:		CHKD				SCALE: 1:5		SHEET 9 OF 10	
		APPVD				MATERIAL:			
		MFG				1-1/2In Black Delrin Sheet			
		Q.A.				WEIGHT:			
			Duncan Iglesias						

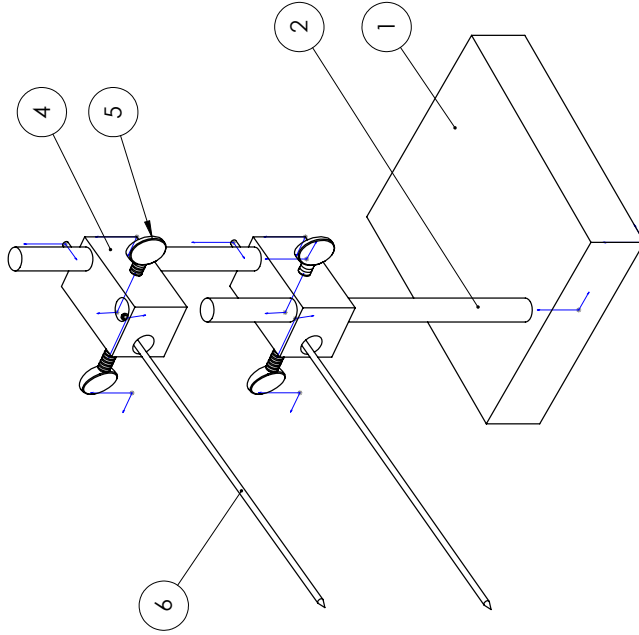
**SolidWorks Student Edition.
For Academic Use Only.**



DETAIL E
SCALE 2 : 5

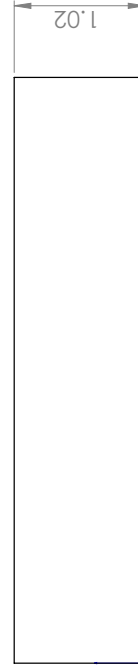
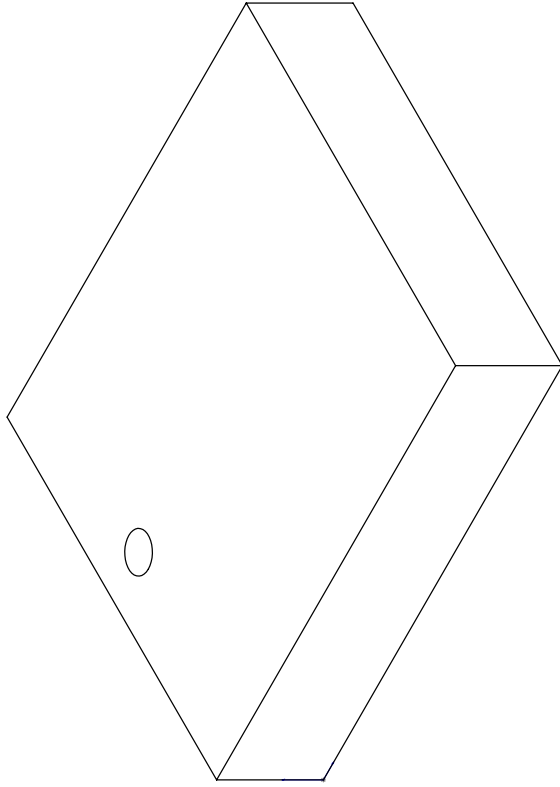
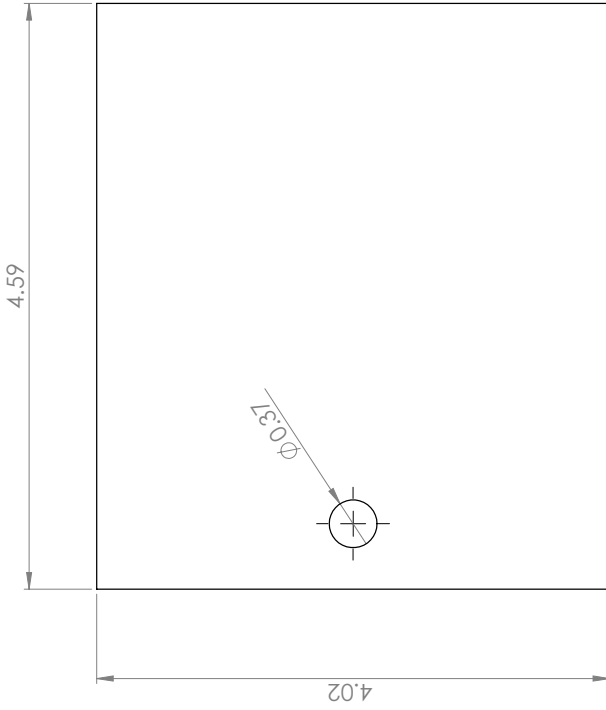
UNLESS OTHERWISE SPECIFIED: DIMENSIONS ARE IN MILLIMETERS		FINISH:		DEBUR AND BREAK SHARP EDGES		DO NOT SCALE DRAWING		REVISION	
SURFACE FINISH:		SIGNATURE						V1.0	
TOLERANCES:		DATE							
LINEAR:		02/23/15							
ANGULAR:									
DRAWN	Duncan Iglesias	NAME							
CHEK		SIGNATURE							
APPVD		DATE							
MFG									
Q.A.									
				MATERIAL:		1-1/2in Black Delrin Sheet		TITLE:	
				WEIGHT:				Right Motor Manifold	
				SCALE:1:5		SHEET 10 OF 10		DWG NO. WS_009	
								A3	

**SolidWorks Student Edition.
For Academic Use Only.**



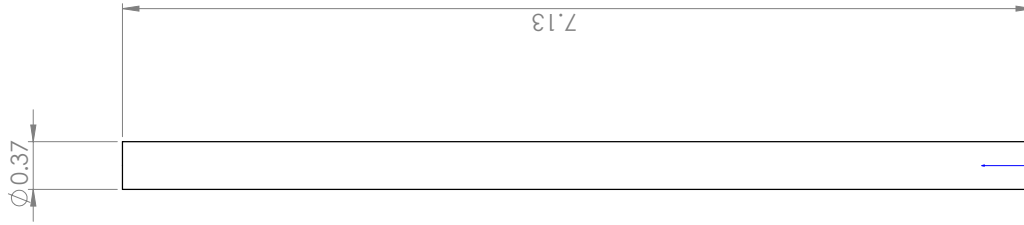
ITEM NO.	PART NUMBER	DESCRIPTION	QTY.
1	Ulna fixation base		1
2	Ulna fixation post		2
4	Ulna fixation block		2
5	Ulna fixation wing screw		4
6	2.5mm k-wire		2

UNLESS OTHERWISE SPECIFIED: DIMENSIONS ARE IN MILLIMETERS SURFACE FINISH: FRACTIONAL DECIMALS: LINEAR: ANGULAR:		FINISH:	DEBUR AND BREAK SHARP EDGES		DO NOT SCALE DRAWING	REVISION
DRAWN	NAME	SIGNATURE	DATE	TITLE: Unlar Fixation Assembly		
CHECKED	D:\lg6\st3			DWG NO. UF_000		
APP'D				SCALE: 1:5		
MFG				SHEET 1 OF 4		
Q.A.				MATERIAL:		
				WEIGHT:		



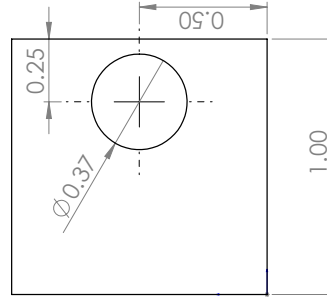
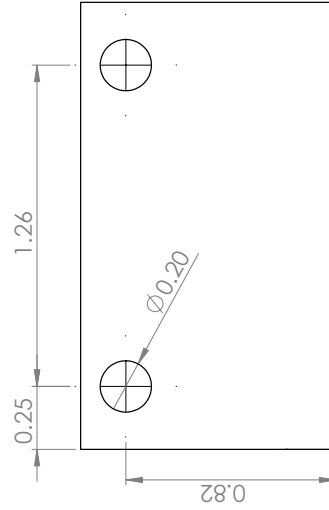
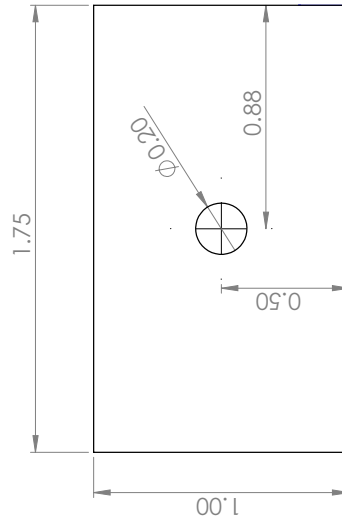
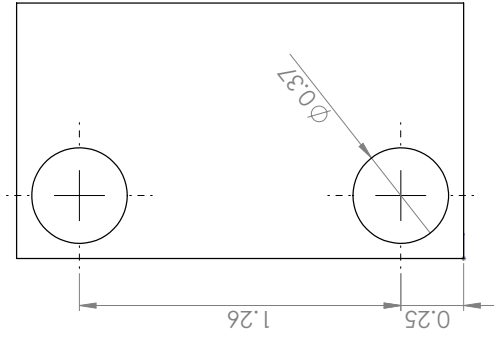
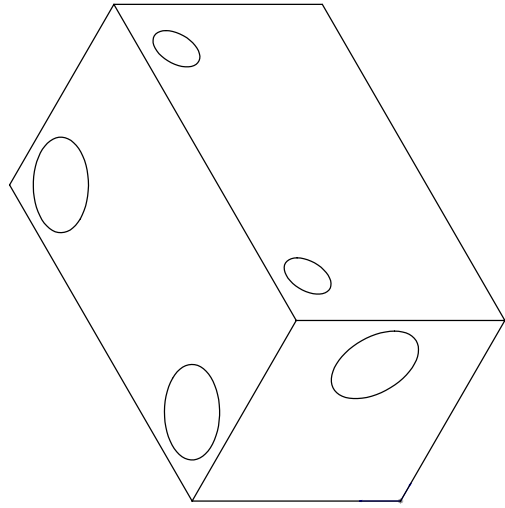
UNLESS OTHERWISE SPECIFIED, DIMENSIONS ARE IN MILLIMETERS		FINISH:		DEBUR AND BREAK SHARP EDGES		DO NOT SCALE DRAWING		REVISION	
SURFACE FINISH:		LINEAR:		ANGULAR:		TITLE:		Ulnar Fixation Base	
DRAWN		NAME		SIGNATURE		DATE		DWG. NO.	
CHECKED								UF_001	
APPVED								SCALE: 1:1	
MFG								SHEET 2 OF 4	
Q.A.								MATERIAL:	
								WEIGHT:	

**SolidWorks Student Edition.
For Academic Use Only.**



UNLESS OTHERWISE SPECIFIED, DIMENSIONS ARE IN MILLIMETERS		FINISH:	DEBUR AND BREAK SHARP EDGES	DO NOT SCALE DRAWING	REVISION
SURFACE FINISH:					
TOLERANCES:		NAME	SIGNATURE	DATE	TITLE:
LINEAR:					
ANGULAR:		DRAWN			Ulhar Fixation Rod
		CHEK			
		APPVD			
		MFG			
		Q.A.			
		MATERIAL:		DWG NO.	UF_002
		WEIGHT:		SCALE:1:2	A3
				SHEET 3 OF 4	

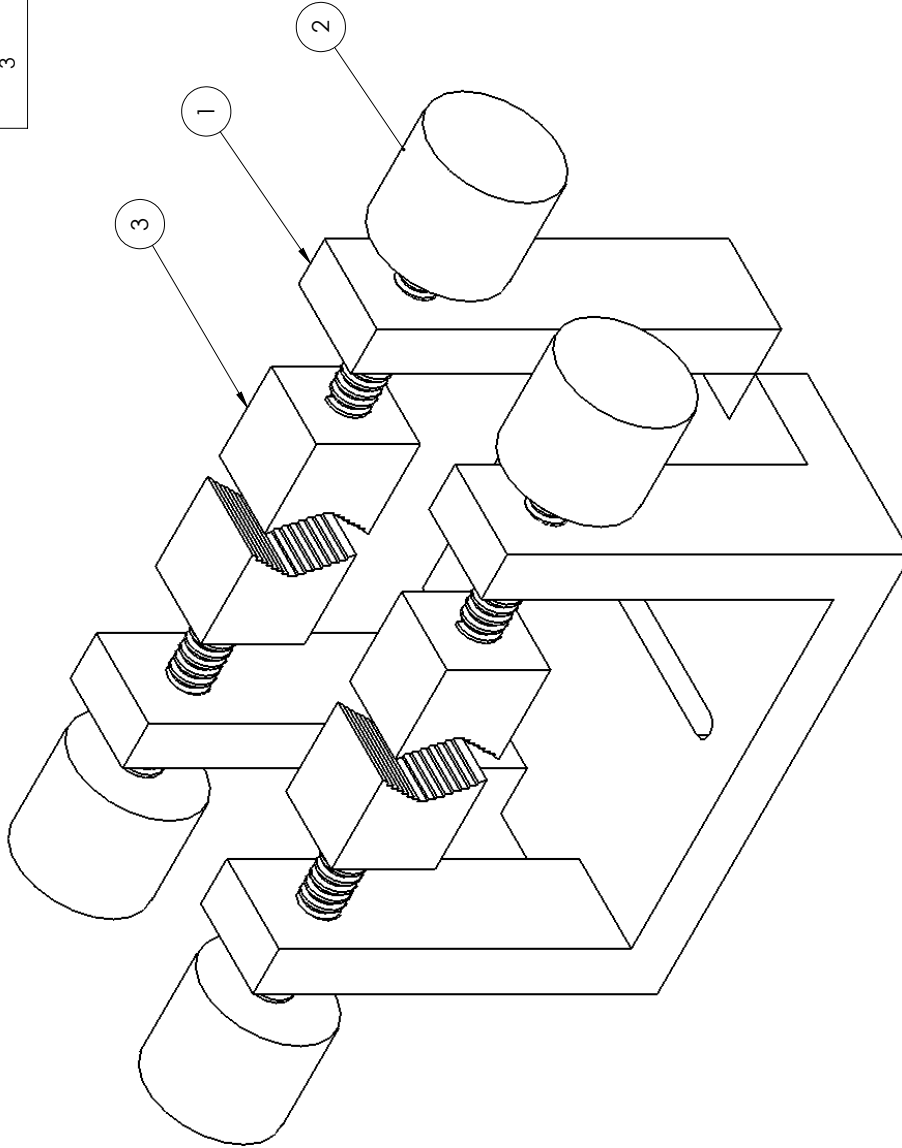
**SolidWorks Student Edition.
For Academic Use Only.**



UNLESS OTHERWISE SPECIFIED, DIMENSIONS ARE IN MILLIMETERS		FINISH:		DEBUR AND BREAK SHARP EDGES		DO NOT SCALE DRAWING		REVISION	
SURFACE FINISH:		LINEAR:		ANGULAR:		TITLE:		DWG NO.	
NAME	SIGNATURE	DATE	MATERIAL	SCALE	WEIGHT	SHEET 4 OF 4		A3	
DRAWN						Ulmar Fixation Block		UF_003	
CHEK									
APPVD									
MFG									
QA									

**SolidWorks Student Edition.
For Academic Use Only.**

ITEM NO.	PART NUMBER	DESCRIPTION	QTY.
1	humeral clamp base		1
2	humeral clamp screw		4
3	humeral clamp teeth		4



UNLESS OTHERWISE SPECIFIED: DIMENSIONS ARE IN MILLIMETERS		FINISH:		DEBUR AND BREAK SHARP EDGES		DO NOT SCALE DRAWING		REVISION	
SURFACE FINISH:		TOLERANCES:							
		LINEAR:							
		ANGULAR:							
NAME	SIGNATURE	DATE							
DRAWN	DJG/LSAS								
CHKD									
APPVD									
MFG									
Q.A.									
		MATERIAL:							
		WEIGHT:							
TITLE: Humeral Clamp Assembly								REVISION	
DWG NO.: HC_000								SCALE: 1 OF 1	
A3									

**SolidWorks Student Edition.
For Academic Use Only.**

Appendix D

Open Source Code & License Agreement

D.1 BSD License

Copyright (c) 2014, Florian Knorn,

All rights reserved.

Redistribution and use in source and binary forms, with or without modification, are permitted provided that the following conditions are met:

- 1. Redistributions of source code must retain the above copyright notice, this list of conditions and the following disclaimer.*
- 2. Redistributions in binary form must reproduce the above copyright notice, this list of conditions and the following disclaimer in the documentation and/or other materials provided with the distribution.*

THIS SOFTWARE IS PROVIDED BY THE COPYRIGHT HOLDERS AND CONTRIBUTORS "AS IS" AND ANY EXPRESS OR IMPLIED WARRANTIES, INCLUDING, BUT NOT LIMITED TO, THE IMPLIED WARRANTIES OF MERCHANTABILITY AND FITNESS FOR A PARTICULAR PURPOSE ARE DISCLAIMED. IN NO EVENT SHALL THE COPYRIGHT OWNER OR CONTRIBUTORS BE LIABLE FOR ANY DIRECT, INDIRECT, INCIDENTAL, SPECIAL, EXEMPLARY, OR CONSEQUENTIAL DAMAGES (INCLUDING, BUT NOT LIMITED TO, PROCUREMENT OF SUBSTITUTE GOODS OR SERVICES; LOSS OF USE, DATA, OR PROFITS; OR BUSINESS INTERRUPTION) HOWEVER CAUSED AND ON ANY THEORY OF LIABILITY, WHETHER IN CONTRACT, STRICT LIABILITY, OR TORT (INCLUDING NEGLIGENCE OR OTHERWISE) ARISING IN ANY WAY OUT OF THE USE OF THIS SOFTWARE, EVEN IF ADVISED OF THE POSSIBILITY OF SUCH DAMAGE.

D.2 3D Circle Fitting MATLAB Algorithm

```

function [center,rad,v1n,v2nb] = circlefit3d(p1,p2,p3)
% circlefit3d: Compute center and radii of circles in 3d which are defined
% by three points on the circumference
%
% usage: [center,rad,v1,v2] = circlefit3d(p1,p2,p3)
%
% arguments: (input)
% p1, p2, p3 - vectors of points (rowwise, size(p1) = [n 3])
%              describing the three corresponding points on the same circle.
%              p1, p2 and p3 must have the same length n.
%
% arguments: (output)
% center - (nx3) matrix of center points for each triple of points in
%          p1, p2, p3
%
% rad     - (nx1) vector of circle radii.
%          if there have been errors, radii is a negative scalar
%          (= error code)
%
% v1, v2 - (nx3) perpendicular vectors inside circle plane
%
% Example usage:
%
% (1)
%     p1 = rand(10,3);
%     p2 = rand(10,3);
%     p3 = rand(10,3);
%     [center, rad] = circlefit3d(p1,p2,p3);
%     % verification, result should be all (nearly) zero
%     result(:,1)=sqrt(sum((p1-center).^2,2))-rad;
%     result(:,2)=sqrt(sum((p2-center).^2,2))-rad;
%     result(:,3)=sqrt(sum((p3-center).^2,2))-rad;
%     if sum(sum(abs(result))) < 1e-12,
%         disp('All circles have been found correctly.');
```

```

%     else,
%         disp('There had been errors.');
```

```

%     end
%
% (2)
%     p1=rand(4,3);p2=rand(4,3);p3=rand(4,3);
%     [center,rad,v1,v2] = circlefit3d(p1,p2,p3);
%     plot3(p1(:,1),p1(:,2),p1(:,3),'bo');hold on;plot3(...
%         p2(:,1),p2(:,2),p2(:,3),'bo');plot3(p3(:,1),p3(:,2),p3(:,3),'bo');
```

```

%     for i=1:361,
%         a = i/180*pi;
%         x = center(:,1)+sin(a)*rad.*v1(:,1)+cos(a)*rad.*v2(:,1);
%         y = center(:,2)+sin(a)*rad.*v1(:,2)+cos(a)*rad.*v2(:,2);
%         z = center(:,3)+sin(a)*rad.*v1(:,3)+cos(a)*rad.*v2(:,3);
```

```

%           plot3(x,y,z,'r.');
```

```

%       end
%       axis equal;grid on;rotate3d on;
%
%
% Author: Johannes Korsawe
% E-mail: johannes.korsawe@volkswagen.de
% Release: 1.0
% Release date: 26/01/2012

% Default values
center = [];rad = 0;v1n=[];v2nb=[];

% check inputs
% check number of inputs
if nargin~=3,
    fprintf('Error: cirlefit3d\nThree input matrices are needed.\n');
    rad = -1;return;
end
% check size of inputs
if size(p1,2)~=3 || size(p2,2)~=3 || size(p3,2)~=3,
    fprintf('Error: cirlefit3d\nInput matrices must have 3 columns.\n');
    rad = -2;return;
end
n = size(p1,1);
if size(p2,1)~=n || size(p3,1)~=n,
    fprintf('Error: cirlefit3d\nAll input matrices must have the same number or rows.\n');
    rad = -3;return;
end
% more checks are to follow inside calculation

% Start calculation
% v1, v2 describe the vectors from p1 to p2 and p3, resp.
v1 = p2 - p1;v2 = p3 - p1;
% l1, l2 describe the lengths of those vectors
l1 = sqrt((v1(:,1).*v1(:,1)+v1(:,2).*v1(:,2)+v1(:,3).*v1(:,3)));
l2 = sqrt((v2(:,1).*v2(:,1)+v2(:,2).*v2(:,2)+v2(:,3).*v2(:,3)));
if find(l1==0) | find(l2==0), %#ok<OR2>
    fprintf('Error: cirlefit3d\nCorresponding input points must not be identical.\n');
    rad = -4;return;
end
% v1n, v2n describe the normalized vectors v1 and v2
v1n = v1;for i=1:3, v1n(:,i) = v1n(:,i)./l1;end
v2n = v2;for i=1:3, v2n(:,i) = v2n(:,i)./l2;end
% nv describes the normal vector on the plane of the circle
nv = [v1n(:,2).*v2n(:,3) - v1n(:,3).*v2n(:,2) , v1n(:,3).*v2n(:,1)...
      - v1n(:,1).*v2n(:,3) , v1n(:,1).*v2n(:,2) - v1n(:,2).*v2n(:,1)];
if find(sum(abs(nv),2)<1e-5),
    fprintf('Warning: cirlefit3d\nSome corresponding input points are nearly collinear.\n');
end
% v2nb: orthogonalization of v2n against v1n
dotp = v2n(:,1).*v1n(:,1) + v2n(:,2).*v1n(:,2) + v2n(:,3).*v1n(:,3);
v2nb = v2n;for i=1:3,v2nb(:,i) = v2nb(:,i) - dotp.*v1n(:,i);end
% normalize v2nb

```

```

l2nb = sqrt((v2nb(:,1).*v2nb(:,1)+v2nb(:,2).*v2nb(:,2)+v2nb(:,3).*v2nb(:,3)));
for i=1:3, v2nb(:,i) = v2nb(:,i)./l2nb;end

% remark: the circle plane will now be discretized as follows
%
% origin: p1                normal vector on plane: nv
% first coordinate vector: v1n  second coordinate vector: v2nb

% calculate 2d coordinates of points in each plane
% p1_2d = zeros(n,2); % set per construction
% p2_2d = zeros(n,2);p2_2d(:,1) = l1; % set per construction
p3_2d = zeros(n,2); % has to be calculated
for i = 1:3,
    p3_2d(:,1) = p3_2d(:,1) + v2(:,i).*v1n(:,i);
    p3_2d(:,2) = p3_2d(:,2) + v2(:,i).*v2nb(:,i);
end

% calculate the fitting circle
% due to the special construction of the 2d system this boils down to solving
% q1 = [0,0], q2 = [a,0], q3 = [b,c] (points on 2d circle)
% crossing perpendicular bisectors, s and t running indices:
% solve [a/2,s] = [b/2 + c*t, c/2 - b*t]
% solution t = (a-b)/(2*c)

a = l1;b = p3_2d(:,1);c = p3_2d(:,2);
t = 0.5*(a-b)./c;
scale1 = b/2 + c.*t;scale2 = c/2 - b.*t;

% centers
center = zeros(n,3);
for i=1:3,
    center(:,i) = p1(:,i) + scale1.*v1n(:,i) + scale2.*v2nb(:,i);
end

% radii
rad = sqrt((center(:,1)-p1(:,1)).^2+(center(:,2)-p1(:,2)).^2+(center(:,3)-p1(:,3)).^2);

```

D.3 3D Sphere Fitting MATLAB Algorithm

```

function [center,radius,residuals] = spherefit(x,y,z)
% Fit a sphere to data using the least squares approach.
%
% Fits the equation of a sphere in Cartesian coordinates to a set of xyz
% data points by solving the overdetermined system of normal equations, i.e.
%  $x^2 + y^2 + z^2 + a*x + b*y + c*z + d = 0$ 
% The least squares sphere has radius  $R = \sqrt{(a^2+b^2+c^2)/4-d}$  and
% center coordinates  $(x,y,z) = (-a/2,-b/2,-c/2)$ .
%
% Input arguments:
% x,y,z:
%   Cartesian coordinates of noisy data points
%
% Output arguments:
% center:
%   coordinates of the least-squares fit sphere center
% radius:
%   least-squares fit sphere radius
% residuals:
%   residuals in the radial direction
%
% Examples:
% [center,radius,residuals] = shpherefit(X)
% [center,radius,residuals] = spherefit(x,y,z);

% Copyright 2010 Levente Hunyadi

marginchk(1,3);
n = size(x,1);
switch nargin % n x 3 matrix
    case 1
        validateattributes(x, {'numeric'}, {'2d','real','size',[n,3]});
        z = x(:,3);
        y = x(:,2);
        x = x(:,1);
    otherwise % three x,y,z vectors
        validateattributes(x, {'numeric'}, {'real','vector'});
        validateattributes(y, {'numeric'}, {'real','vector'});
        validateattributes(z, {'numeric'}, {'real','vector'});
        x = x(:); % force into columns
        y = y(:);
        z = z(:);
        validateattributes(x, {'numeric'}, {'size',[n,1]});
        validateattributes(y, {'numeric'}, {'size',[n,1]});
        validateattributes(z, {'numeric'}, {'size',[n,1]});
end

% need four or more data points
if n < 4

```



```
error('spherefit:InsufficientData', ...
      'At least four points are required to fit a unique sphere.');
```

```
end

% solve linear system of normal equations
A = [x, y, z, ones(size(x))];
b = -(x.^2 + y.^2 + z.^2);
a = A \ b;

% return center coordinates and sphere radius
center = -a(1:3)./2;
radius = realsqrt(sum(center.^2)-a(4));

if nargin > 2
    % calculate residuals
    residuals = radius - sqrt(sum(bsxfun(@minus,[x y z],center).^2,2));
elseif nargin > 1
    % skip
else
    % plot sphere
    hold all;
    sphere_gd(6,radius,center);
    hold off;
end
```

Appendix E

The Effects of Tissue Degradation on System Performance: An 18 Hour Test

Investigations discussed in this thesis generally ran longer than 18 hours due to the large amount data that had to be collected and debugging required as this was the first series of tests undertaken. A paper published by King *et al.* reported significant degradation of cyclic peak loads in dense connective tissues of $8.6 \pm 4.6\%$ over an 18 hour period ($p < 0.0001$) at room temperature ($23 \pm 2^\circ\text{C}$) which raises a concern with the validity of data collected in this thesis. To determine whether there was a significant difference in the repeatability over time a specimen was tested in a gravity neutral position through a range of FEM (5 cycles) immediately after specimen preparation was complete (t-0) and then remained room temperature for an 18 hour period (undergoing testing) before testing again at the end of the 18 hour period (t-18).

The average standard deviation (ASD) for flexion-extension motions at t-0 and t-18 were 0.14° and 0.18° with average error never exceeding 0.24° and 0.29° respectively. A one-way (time) repeated measures (RM) ANOVA was performed on the average error of each trail set to identify differences between samples, however no significant difference was present ($p < 0.05$). Therefore, regardless of the degradation of dense connective tissues over an 18 hour period in standard room temperature there is no effect on the ability of the simulator to perform repeatable trials. However, attention should be paid to studies that investigate articulations of the joint as they could very well be an effect present there.

Appendix F

Bone Tracker Design

For the purpose of this thesis optical triad-cluster trackers (Certus Optotrak, Northern Digital Inc., VT) were mounted to the third metacarpal, radius, and ulna using custom designed mounts. The parts were designed using a 3D CAD program (SolidWorks, Dassault Systemes, MA) and fabricated using 3D printing rapid prototyping methods (Replicator, MakerBot, NY) using *polylactic acid* (PLA) filament which allowed for unique geometries and properties unavailable by conventional fabrication methods. Each part was printed using a 10% infill option that builds with a honeycomb structure on inside of the component to effectively reduce weight by approximately 90%. This reduction in weight was intended to reduce the overall effect of the trackers on the center of mass of the bones they were attached to. The benefits of using 3D printed parts arise from the ability to rapid prototype a series of components, each with minor modifications to the rest, in a short amount of time for extremely low costs when compared to prices charged by machine shops. Multiple parts may be printed in a single batch and can have unique geometries that involve splines and curves that would require complicated CNC mills to reproduce. Not to mention that 3D printing is totally awesome. Although each tracker was unique, there were two similarities between them; the first being the mounting holes for the optical tracker to mount to, and the second being the V-notch where the mount attaches to the bone to maximize the amount of surface area in contact with the bone. Care was taken to ensure that the tracker was mounted at an appropriate angle to the camera throughout the motion trials in the investigation. Figures F.1 displays the design and positioning of the optical tracker mounts.

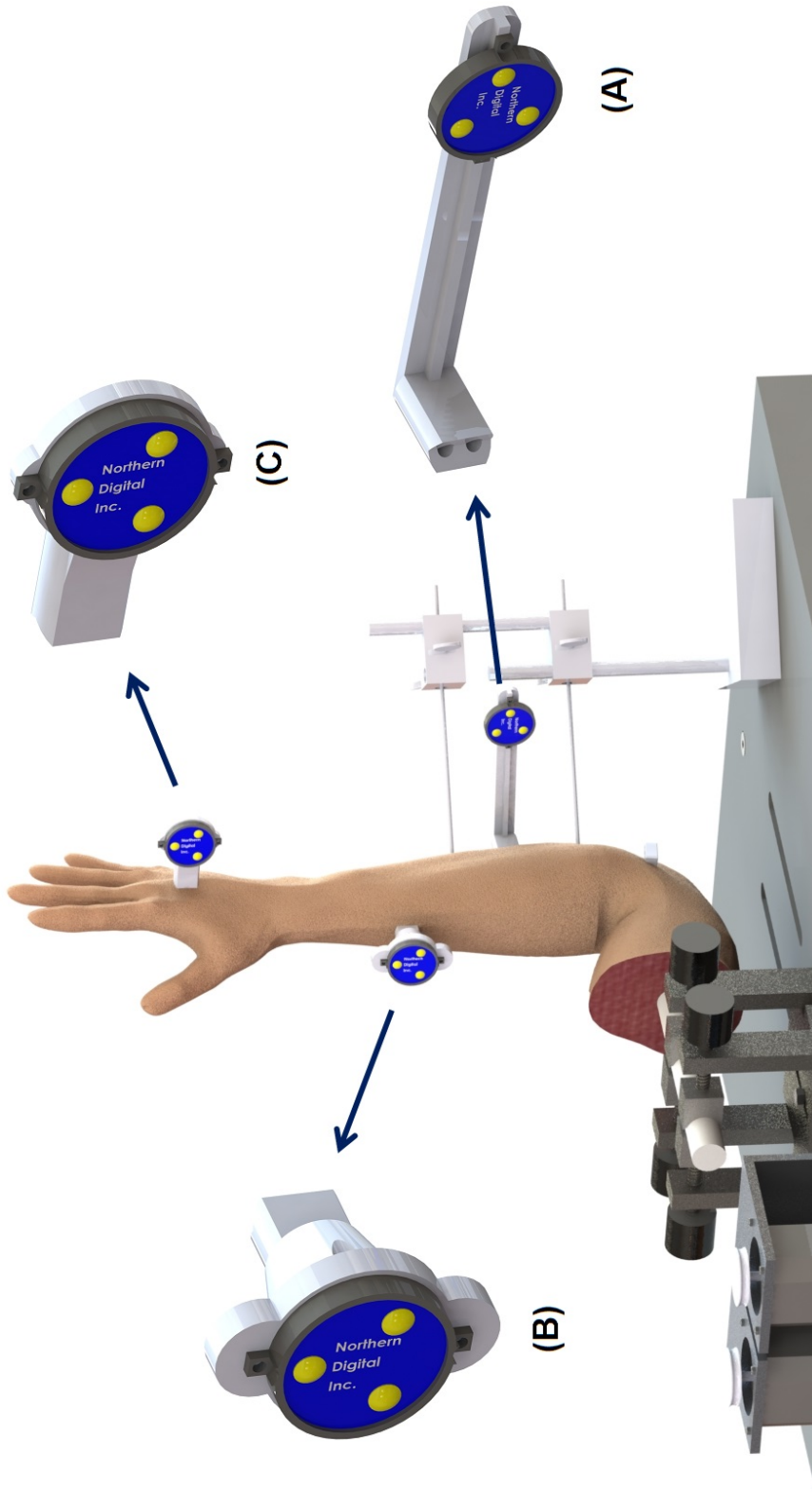


Figure F.1: This image shows the position of the three optical tracker mounts with and the direction of the triad-cluster with respect to one another with a tracker attached to the proximal ulna [A], mid-shaft of the radius [B], and the dorsal mid-shaft of the third metacarpal [C]. Each mount used a V-notch at the base to increase the contact area with the shaft of the bone and had two channels for 2.7 mm bone screws to rigidly attach the mount to the bone.

Appendix G

Curriculum Vitae

DUNCAN J. IGLESIAS

EDUCATION

- 2015-PRESENT BACHELOR OF COMPUTER SCIENCE (BSC), SPECIALIZATION IN COMPUTER SCIENCE
University of Western Ontario, London, Ontario
- 2013-2015 MASTER OF BIOMEDICAL ENGINEERING (MESC), BIOMECHANICS WITH COLLABORATION IN
MUSCULOSKELETAL HEALTH RESEARCH (CMHR)
University of Western Ontario, London, Ontario
Focus: Mechatronics, Wrist Kinematics & Biomechanics
- 2008-2013 BACHELOR OF APPLIED SCIENCE (BSC), MECHANICAL ENGINEERING (OPT. BIOMECHANICS)
WITH PROFESSIONAL INTERNSHIP
Queen's University, Kingston, Ontario
Focus: Mechatronics, Biomechanics, Robotics, Computer-Aided Design, FEA
Internship: Reliability Intern - INVISTA Canada Kingston Site (Kingston, Ontario)

RESEARCH INTERESTS

- BIOMEDICAL - BIOMECHANICS AND KINEMATICS OF HUMAN JOINTS
- *IN-VITRO* ASSESSMENTS OF STANDARD/NOVEL SURGICAL TECHNIQUES
- MECHATRONIC SYSTEM DEVELOPMENT AND THIRD PARTY SOFTWARE INTERFACING
- JOINT ARTHROPLASTY ASSESSMENT AND PROTOTYPE DEVELOPMENT
- AERO SPACE - UNMANNED AERIAL VEHICLE (UAV) DESIGN & DEVELOPMENT
- AUTONOMOUS NAVIGATION & STABILIZATION OF MULTIROTOR VEHICLES

RESEARCH EXPERIENCE

- 2013-PRESENT GRADUATE RESEARCH PROJECT (THESIS) – ACTIVE WRIST MOTION SIMULATOR
University of Western Ontario, London, Ontario
Designed & Developed a Simulator to Reanimate Cadaver Upper Limbs for the
Investigation of Wrist Kinematics using LABVIEW and NDI Optical Tracking
- 2012-2013 DESIGN & IMPLEMENT CAPSTONE PROJECT – NIAGARA PROSTHETICS & ORTHOTICS
Queen's University, Kingston, Ontario
Further Developed & Tested a Load Dispersal Implant for Transfemoral
Amputees to Increase the Functionality of Lower Limb Prosthetics
- 2013 UNDERGRADUATE RESEARCH PROJECT (THESIS) – WALKING GAIT FOOT MONITOR
Queen's University, Kingston, Ontario
Designed & Developed a Wireless Wearable Mechatronic Device to Monitor Toe
Clearance during Walking Gait and Report the Patient's Likelihood of Tripping
- 2013 ROBOTIC SYSTEMS - FINAL PROJECT
Queen's University, Kingston, Ontario
Focus: Multi-Link Systems, Hazardous Environment, Kinematics

- 2012 HUMAN BIOMECHANICS - FINAL PROJECT
Queen's University, Kingston, Ontario
Assessed the Differences in Knee Motion during Squatting With and Without Shoes using NDI Optical Tracking and a Custom MATLAB Point Filter
- 2012 COMPUTER AIDED DESIGN - FINAL PROJECT
Queen's University, Kingston, Ontario
Optimized the Geometry of a Commercial DJI Quadcopter Arm for Inflight Parameters Using ANSYS with the Input Point Script Built using MATLAB

TEACHING EXPERIENCE

- 2015 GRADUATE TEACHING ASSISTANT, UNIVERSITY OF WESTERN ONTARIO
Mechanical Component Design - MME 3380
Focus: 3 Axis CNC Milling, Pump Assembly, Component Identification, Strain
- 2014 GRADUATE TEACHING ASSISTANT, UNIVERSITY OF WESTERN ONTARIO
Modern Control Systems - MME 4450
Focus: Simulation of Response, PID Control, SIMULINK, PID, LabVIEW
- 2014 SUMMER ENGINEERING ACADEMY, UNIVERSITY OF WESTERN ONTARIO
Applications of 3D Printing in Biomedical Engineering Research
Focus: Rapid Prototyping, 3D Printing, Joint Modelling
- 2014 GRADUATE TEACHING ASSISTANT, UNIVERSITY OF WESTERN ONTARIO
Mechanical Component Design - MME 3380
Focus: 3 Axis CNC Milling, Pump Assembly, Component Identification, Strain
- 2013 GRADUATE TEACHING ASSISTANT, UNIVERSITY OF WESTERN ONTARIO
Engineering Design Studio - ES 1050
Focus: Engineering Design, Brain Storming, Constructive Feedback
Presentation: Post Graduate Opportunities and How to Work Towards Them
- 2012-2013 UNDERGRADUATE TEACHING ASSISTANT, QUEEN'S UNIVERSITY
Engineering Design Studio - APSC 100
Focus: Professional Communication, Project Management, Design Process

PROFESSIONAL EXPERIENCE

- 2015-PRESENT RESEARCH ENGINEER – HAND & UPPER LIMB CENTRE, ST. JOSEPH'S HOSPITAL
London, Ontario
Responsible for developing laboratory apparatus/software for obtaining data from cadaveric specimens to further our understand of wrist kinematics
- 2013 MUSCULOSKELETAL BIOMECHANICS INTERN (4 MONTH CO-OP)
Queen's University, Kingston, Ontario
Designed & Developed a Lower Limb Inertial Data Collection Laboratory and Apparatus using Arduino Microcontrollers with a MATLAB User Interface

2011-2012 MECHANICAL RELIABILITY ENGINEERING INTERN (16 MONTH CO-OP)
INVISTA Canada, Kingston, Ontario
Focus: Reverse Engineering, Failure Analysis, Update P&ID's, Maintenance Plans

ACADEMIC INVOLVEMENT

2013-2015 SOCIAL COORDINATOR – ROTH|MCFARLANE HAND & UPPER LIMB CENTRE (HULC)
University of Western Ontario, London, Ontario

2013-PRESENT AERO DESIGN TEAM – TEAM MANAGER & CONTROL SYSTEMS LEAD
University of Western Ontario, London, Ontario

2013-2015 SPORTS FACILITATOR – FACULTY OF BIOMEDICAL ENGINEERING
University of Western Ontario, London, Ontario

2012 QUEEN'S UNIVERSITY REPRESENTATIVE – ONTARIO UNIVERSITY FAIR
Toronto, Ontario

2011-2012 QUEEN'S SPACE ENGINEERING TEAM (QSET) – CONTROL SYSTEMS TEAM
Queen's University, Kingston, Ontario

2009-2013 APPLIED SCIENCE 2012 YEAR EXECUTIVE – MERCHANDISE/EVENTS/PRESIDENT
Queen's University, Kingston, Ontario

PRESENTATIONS & CONFERENCES

2015 CANADIAN ORTHOPAEDIC RESEARCH ASSOCIATION (CORS) 2015 CONFERENCE
Vancouver, British Columbia
Title: *"Design & Development of an In-Vitro Active Motion Wrist Simulator for the Investigation of Wrist Kinematics in Multiple Gravity Loaded Positions"*

2014 BONE & JOINT SEMINAR SERIES
London, Ontario

2015 TALKS ON FRIDAYS (TOFS) – LAWSON HEALTH RESEARCH INSTITUTE
London, Ontario
Title: *"Design & Development of an In-Vitro Active Motion Wrist Simulator for the Investigation of Wrist Kinematics"*

2014 BME SEMINAR – UNIVERSITY OF WESTERN ONTARIO
London, Ontario
Title: *"Repeatability of an Active Motion Simulator in Pure Flexion/Extension"*

2014 CANADIAN ORTHOPAEDIC RESEARCH ASSOCIATION (CORS) 2014 CONFERENCE
Montreal, Quebec

AWARDS

2015 1ST PLACE (DESIGN) - SAE AERO DESIGN COMPETITION EAST ADVANCED CLASS (FLORIDA)

2014 1ST PLACE (DESIGN) - SAE AERO DESIGN COMPETITION EAST ADVANCED CLASS (TEXAS)

2014 2ND PLACE (OVERALL) - SAE AERO DESIGN COMPETITION EAST ADVANCED CLASS (TEXAS)

2013 GRADUATE RESEARCH ASSISTANTSHIP DEPARTMENT OF BIOMEDICAL ENGINEERING (2 YEAR)

2013 DEAN'S HONOUR LIST – ACHIEVED A GPA GREATER THAN 3.5 FOR AN ACADEMIC YEAR

COMPUTER SKILLS

Operating Systems: Windows, Linux

Core Languages: C/C++, Java

Mechanical Engineering: LabVIEW, SolidWorks, MATLAB, 3D Printing, AutoCAD, ANSYS

PERSONAL PROJECTS

UAV DESIGN

SAE AERO DESIGN COMPETITION EAST 2015 (ADVANCED CLASS)

- Designed & Developed the Onboard Telemetry Circuitry using an Arduino Microcontroller for Remote Payload Release using a Mobile Android App

Past: FPV Quadcopter (Go Pro Hero 3), SAE Aero Design Competition West 2014

ANDROID APPS

PREDICTIVE TIME TO DROP

- Enabled Position Tracking of an RC Plane From an Android Mobile Phone
- Designed & Implemented an Estimated Time to Drop Algorithm to Assist in the Release of a Payload to Hit Target to Increase Accuracy of Impact

NATO Phonetic Alphabet Learner

- Created an Interactive Learning Tool to Learn & Practice the NATO Alphabet
- Implemented Text to Speech for Teaching & Speech to Text for Practicing
- Intended for Use by Pilots/Military/Vigilante

3D PRINTING

NEXUS 5 MOBILE PHONE CASE

- 3D Scanned a Nexus 5 Mobile Phone and Imported the Point Cloud into SolidWorks to Customize into a Case with the Western Engineering Logo
- Completed the Print using a MakerBot Replicator with Flexible Filament

3D PRINTING IN BIOMEDICAL ENGINEERING

- Designed a Workshop for a Western's Summer Engineering Academy
- Focused on Hemi & Total Radiohumeral Arthroplasty of the Elbow
- Instructed Students on SolidWorks to Explore Various Implant Properties

Past: Hand Phone Charger, Quadcopter Frame, Wearable Devices, Cases, Bones

ARDUINO & PI

PRINT TO PEER HOME 3D PRINTING & MONITORING

- Modified a Power Bar with a Relay Shield Controllable by the PI's I/O Pins
- Developed a Python Script to Toggle Power States of Lights and Printer through an SSH Connection and Monitor Print Status via Webcam

MISCELLANEOUS

[MIG Welding, SolidWorks, FEA Study], [HTML&CSS, WordPress], [Python, GitHub]

Squat Rack: Designed & Built a Modular Exercise Cage Rated for +300lb

Personal Website: WordPress Platform for Displaying UAV Projects

METAR Converter: Scraps a Website using Beautiful Soup for Aviation Data

Custom PC Build: i5 3570K, 16.0GB RAM, 120GB SSD

MISCELLANEOUS

Just for a conversation starter I am currently working towards my recreational pilot's license, while tackling small side projects in my basement such as developing a prototype drone platform for next years Unmanned Systems Canadian Competition (USCC), a universal remote that communicates with your SmartPhone via Bluetooth, and creating a low-cost robotic manipulator with a feedback system for small tasks.